THE DEVELOPMENT AND APPLICATION OF AN ARTHROKINEMATIC BIOMARKER FOR THE EARLY DETECTION OF OSTEOARTHRITIS

by

Chelsea Anne Marsh

B.S. in Chemical Engineering and Biomedical Engineering, Carnegie Mellon University, 2009

M.S. in Biomedical Engineering, University of Pennsylvania, 2010

Submitted to the Graduate Faculty of

the Swanson School of Engineering in partial fulfillment

of the requirements for the degree of

Doctor of Philosophy

University of Pittsburgh

2014

UNIVERSITY OF PITTSBURGH

SWANSON SCHOOL OF ENGINEERING

This dissertation was presented

by

Chelsea Anne Marsh

It was defended on

June 20th, 2014

and approved by

Rakié Cham, Ph.D., Associate Professor, Department of Bioengineering

Volker Musahl, M.D., Associate Professor, Department of Orthopaedic Surgery

Xudong Zhang, Ph.D., Associate Professor, Department of Mechanical Engineering

Scott Tashman, M.D., Associate Professor, Department of Orthopaedic Surgery

THE DEVELOPMENT AND APPLICATION OF AN ARTHROKINEMATIC BIOMARKER FOR THE EARLY DETECTION OF OSTEOARTHRITIS

Chelsea Marsh, Ph.D.

University of Pittsburgh, 2014

Osteoarthritis (OA) is a progressive disease characterized by the deterioration of articular cartilage. Although most commonly reported in older patients, musculoskeletal injury is a major risk factor for the development and early onset of OA. Individuals typically present in the orthopaedic clinic when they experience symptoms of OA, however at this point the disease has irreversibly progressed through much of the cartilage. The inability to reliably detect cartilage damage noninvasively before it advances into OA hinders the development and/or use of chondroprotective and OA-modifying treatments. Therefore, we aim to functionally detect and model early cartilage damage in asymptomatic individuals, and translate this method into a clinical diagnostic for use in the orthopaedic clinic.

We assessed joint spacing and kinematics during static and dynamic activities in subjects who underwent partial medial meniscectomy (PM) and in age/sex-matched uninjured controls. All surgical subjects were classified during arthroscopy as having either intact or softened cartilage. Subjects performed a static step-loading task and level running within the dynamic stereo X-ray (DSX) system, and biplane X-ray images were taken at sequential times during the activities. During the step-loading task, PM subjects with softened cartilage demonstrated greater tibiofemoral joint space compression than subjects with healthy cartilage. A Voigt model was used to derive qualitative material properties that can distinguish joints with softened cartilage

from joints with healthy cartilage. Mirroring *in vitro* findings, joints with softened cartilage were found to have lower stiffness values than joints with healthy cartilage.

We then simplified the step-loading protocol in order to translate our findings into a clinical diagnostic. Subjects underwent ACL reconstruction and were classified intraoperatively as having healthy or softened articular cartilage. After resting for 30 minutes, subjects stood for 3 minutes and biplane X-rays were captured at 5 points during the test. We analyzed the change in joint space using CT-derived bone models, single-plane measurements, and Voigt modeling. Subjects with softened cartilage again underwent significantly more joint compression, and modeling indicated that these joints exhibited lowered stiffness values. These results represent a novel, functional method of detecting early cartilage damage in asymptomatic subjects.

TABLE OF CONTENTS

LIST OF TABLES

LIST OF FIGURES

PREFACE

I would like to dedicate this thesis to my wonderful friends, my beloved family, and my beautiful city.

1.0 BACKGROUND

Osteoarthritis, or OA, is a degenerative joint disorder characterized by the degradation of the articular cartilage that lines the bones of joints. It is commonly characterized by pain and lack of joint mobility, can affect any synovial joint. OA impacts over 20 million Americans[1] and an estimated 10% of the world's population over 60[2]. Prevalence of the disease increases with age (Figure 1), and is more often reported in females than in males[3]. Because of the prevalence of the disease, the economic burden of OA is staggering. It's been estimated that OA costs over $60 billion per year in the US[4], and is a leading cause of work disability in men over 50 years old[1]. There are no preventative measures that can be taken to slow or halt the progression of OA. The lack of available prevention, combined with growing world populations, the obesity rate, and the rising activity levels of older adults, translate to an ever-increasing number of OA sufferers worldwide.

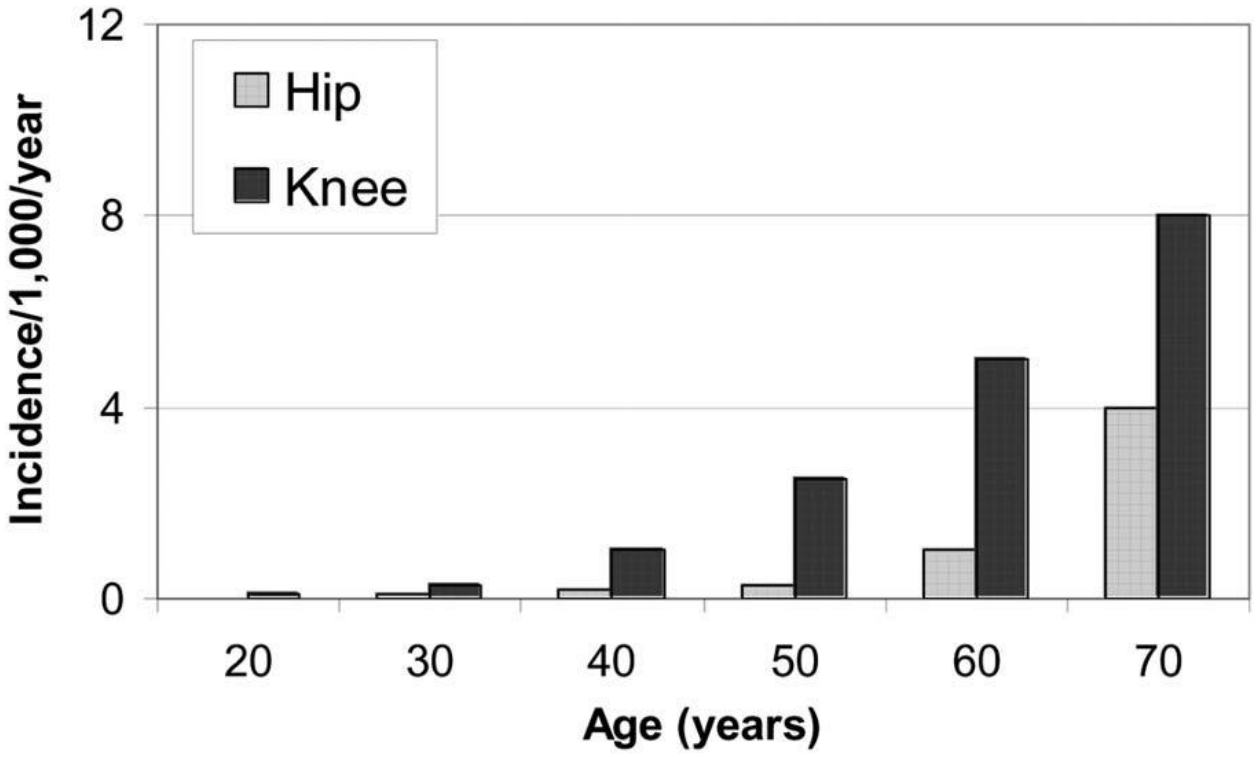

Figure 1. Incidence of OA in the knee and hip as a function of age [5,6]

While reported in most joints, OA is most commonly observed in the knee. An estimated 6.1% of all adults over the age of 30 report OA symptoms in the knee[7]. Consequences of knee OA are similar to those seen in most joints, though knee OA is particularly detrimental to the patient's quality of life. The lack of mobility and constant pain upon walking leaves many patients to leave sedentary lives, and the disease only progresses with time to leave the patients in more pain. Eventually the only course of action to cure a patient of OA-related pain is to pursue a total knee replacement.

1.1 OSTEOARTHRITIS DEVELOPMENT

To understand how OA initiates and progresses, it is important to examine the composition of healthy articular cartilage. Articular cartilage is comprised of four major components, namely a type II collagen matrix, in which water, proteoglycans, and chondroctyes reside[8]. The collagen network comprises of approximately 60% of the dry weight of articular cartilage[9], while interstitial fluid makes up 65-80% of the wet weight of healthy articular cartilage[10]. The percentage of water has been found to increase in OA patients[11]. Proteoglycans are approximately 10-15% of the wet weight of articular cartilage[9], and though there are few cells in cartilage relative to other tissues, chondrocytes make up 2% of articular cartilage's volume[12]. These cells maintain the tissue's infrastructure.

Articular cartilage is comprised of 4 major zones – the superficial zone, transitional zone, deep zone, and calcified cartilage zone. Each of these areas is characterized by a unique structure that differentiates one from the other. Specifically, the fibers of the collagen matrix have varied directionality depending on their location within articular cartilage (Figure 2). Collagen fibers closest to the articulating surface in the superficial zone are oriented longitudinally. Because of the rope-like structure of collagen, it only acts in tension. Therefore during joint compression, the longitudinal fibers absorb the force by stretching and imparting strength on the tissue. That being said, the superficial zone is able to undergo shear, tension, and compression[13,14].

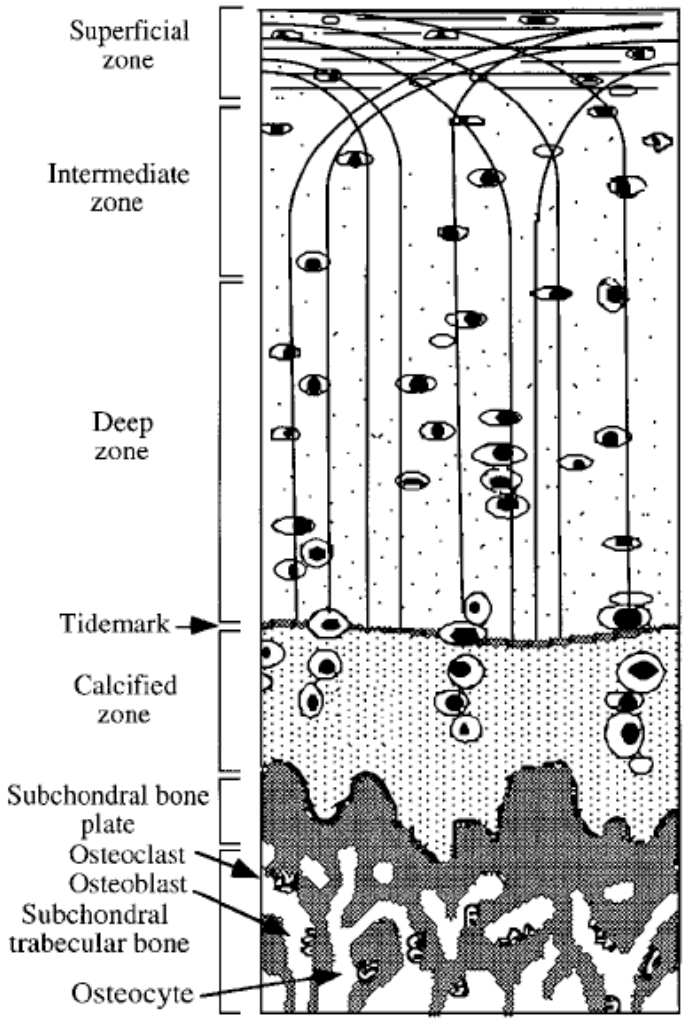

Figure 2. Diagram of microscopic structure of articular cartilage [15]

The transitional, deep, and calcified cartilage zones feature fiber directionalities that are less suited to handle compressive loads. In these zones, the collagen fibers take on an arched, perpendicular, and sometimes random alignment. Unlike the collagen fibers of the superficial zone, they are not forced into tension during a compressive load. The compressed collagen fibers donate little mechanical strength to the tissue in these deeper areas. Mechanical strength is instead derived from the relatively high concentration of aggrecan[16], which has been shown to contribute to compressive strength of cartilage via swelling within the collagen matrix[8].

The relationship between the collagen matrix, interstitial water, and proteoglycans dictates the mechanical behavior of the tissue. The solid collagen matrix imparts strength on the articular cartilage, while the proteoglycans allow for the tissue to maintain elastic properties. The flow the interstitial water through the pores of the matrix allow for the tissue to compress and swell. Lai, et al, developed a triphasic model of articular cartilage that nicely describes the relationship between the three phases[17]. The positive charge of the proteoglycans attracts the negatively-charged water to the matrix, which allows for force dissipation. Compression loading acts to pressurize the fluid phase, thereby elongating the collagen fibers and imparting mechanical strength to the articular cartilage. Therefore, the electrostatic interactions between proteoglycans and water contained within the solid matrix generate a swelling pressure designed to withstand "normal loading". Additionally, the solid matrix has a very low permeability, and combined with the incompressibility of water, the structure of articular cartilage allows for efficient pressurization and support of the large loads seen during dynamic activities.

Researchers have found that early signs of arthritic damage in articular cartilage include decreased concentration of proteoglycans, increased water content, and increased collagen matrix disorganization[15]. These patterns suggest an imbalance between the components of articular cartilage, and a disruption of its function. It's been hypothesized that OA begins in the superficial zone[18], where damage to the collagen matrix will greatly decrease the tissue's ability to handle tension, compression, and shear. Damage to the collagen matrix increases the structure's permeability, and water is able to enter and escape from the interstitial space more rapidly. Without retention of water, the tissue is unable to pressurize in response to compressive loads, the cartilage loses much of its stiffness, and deforms more rapidly. Matrix defects in the superficial zone leave the deeper zones to experience elevated stresses and strains, and the

unsuitable collagen matrix directionality in these areas of the articular cartilage leads to OA progression. Damage is then able to spread through all zones of the tissue and eventually leave the subchondral bone exposed. Therefore once OA is initiated in the superficial zone, the disease is able to progress quickly and leave patients with little time for intervention.

1.2 VISCOELASTIC MODELING OF ARTICULAR CARTILAGE

By definition, viscoelastic materials exhibit both viscous and elastic characteristics during mechanical loading. Viscoelastic materials are unique in that they exhibit a few unique responses to loading, namely creep, relaxation, and hysteresis (Figure 3). These materials demonstrate a creep response to a sustained force, or a slow increase in strain, and a relaxation response to a sustained displacement, or a slow decrease in stress. Additionally, unlike elastic materials, viscoelastic materials are unable to conserve energy during cyclic loading, resulting in the dissipation of mechanical energy, or hysteresis. These characteristics of viscoelastic materials have led many researchers to attempt to model the unique mechanical behavior.

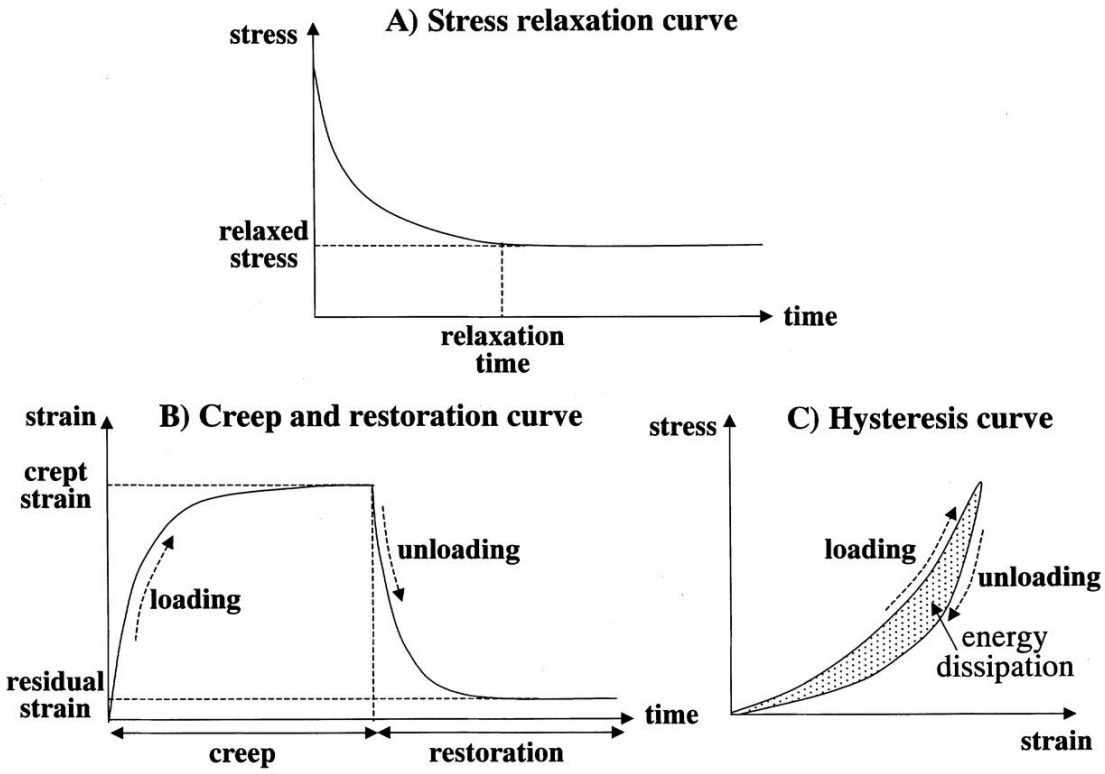

Figure 3. Unique mechanical behaviors of viscoelastic materials, namely A) stress relaxation, B) creep, and C) hysteresis[19]

1.2.1 Spring-Dashpot Modeling

The simplest viscoelastic models attempt to replicate the mechanical behavior of tissue with a series of spring and dashpot elements. The spring elements aim to capture the elastic characteristics of the viscoelastic tissue, while the dashpot attempts to replicate its viscous nature. The spring elements are able to deform instantaneously to a magnitude that is proportional to an applied stress, and are responsible for determining the stiffness of the specimen. The dashpot elements, however, are able to produce a velocity that is proportional to an applied stress, and are responsible for the viscosity of the specimen. The configuration of the different elements relative to each other attempts to characterize the tissue under different

loading conditions. There are three major types of spring-dashpot models – the Maxwell model, the Voigt model, and the Kelvin model (Figure 4).

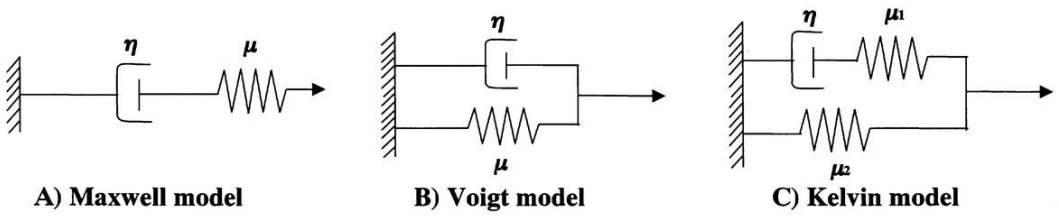

Figure 4. Illustrations of the different types of spring-dashpot models – A) Maxwell model, B) Voigt model, and C) Kelvin, or standard linear solid model[19]

All of the spring-dashpot models follow 2 equations for tensile stress and strain. By inserting the relations into the governing equations for each model and solving the resulting differential equation for strain, it is possible to model creep and stress relaxation.

$$\sigma_{spring} = E(\varepsilon)$$

Equation 1. Relationship between stress and strain in the spring element

$$\sigma_{dashpot} = \mu(\dot{\varepsilon})$$

Equation 2. Relationship between stress and strain in the dashpot element

The Maxwell model is the most basic of the spring and dashpot models, and aligns a spring and dashpot element in series. This model is able to accurately capture stress relaxation behavior, but unable to fully characterize creep. This model is defined by the following stress (equation 2) and strain (equation 3) equations.

$$\sigma_{total} = \sigma_{dashpot} + \sigma_{spring}$$

Equation 3. Governing equation of stress in Maxwell model

$$\varepsilon_{total} = \varepsilon_{dashpot} + \varepsilon_{spring}$$

Equation 4. Governing equation of strain in Maxwell model

During a sustained strain, the Maxwell model is extended to a set displacement and the dashpot element allows for the stress of the model to slowly dissipate, much like what is seen in viscoelastic materials. During creep, however, the sustained stress results in a sudden increase in deformation from the spring element, followed by a linear increase in deformation resulting from the dashpot until the dashpot has deformed to its limit. This does not mimic the actual viscoelastic behavior of materials, as viscoelastic creep is characterized by a time-dependent increase in deformation. Therefore while the Maxwell model may adequately depict stress relaxation, another arrangement of the elements will need to be explored for the correct characterization of creep.

The Voigt model is similar to the Maxwell model in that it has a single dashpot and spring element, but instead aligns them in parallel. This configuration allows for the model to accurately characterize creep, but incorrectly depict stress relaxation. Equations 5 and 6 define the model's governing stress and strain equations.

$$\sigma_{total} = \sigma_{dashpot} + \sigma_{spring}$$

Equation 5. Governing equation of stress in Voigt model

$$\varepsilon_{total} = \varepsilon_{dashpot} = \varepsilon_{spring}$$

Equation 6. Governing equation of strain in Voigt model

During a sustained stress, the dashpot and spring deform equally and in a time-dependent manner. The Voigt model's response to an applied strain, however, is minimal. The parallel configuration of the elements does not allow for the slow dissipation of stress that is characteristic of viscoelastic stress relaxation. The successes and pitfalls of the Voigt and Maxwell models indicate that another element may be needed in the spring and dashpot model for the correct depiction of the stress relaxation and creep behavior of viscoelastic materials.

The Kelvin model, or standard linear solid (SLS) model, is a bit more complex than the previous two and attempts to combine the Maxwell and Voigt models to optimally characterize both stress relaxation and creep. It contains 2 spring elements and a single dashpot, and aligns them as a Maxwell model with a spring in parallel. The governing equations of stress (equation 7) and strain (equation 8) are as follows.

$$\sigma_{total} = \sigma_{Maxwell} + \sigma_{spring}$$

Equation 7. Governing equation of stress in Kelvin (SLS) model

$$\varepsilon_{total} = \varepsilon_{Maxwell} = \varepsilon_{spring}$$

Equation 8. Governing equation of strain in Kelvin (SLS) model

The inclusion of the additional spring term allows for the Kelvin model to adequately depict both stress relaxation and creep responses. The extra spring induces a quicker initial creep response to a sustained force when compared to Voigt modeling, and may be better for modeling certain viscoelastic materials that exhibit large initial deformations. All of the spring and dashpot models are generalized and may apply to various viscoelastic materials. Some researchers, however, prefer to pursue alternate models that may be further tailored to the biology and physiology of articular cartilage.

1.2.2 Multi-Phase and Mixture Modeling

Articular cartilage may be modeled as a tissue comprised of two or three phases. These models are based on the viscoelastic behavior of cartilage, as well as the known physiology of the tissue. Biphasic and triphasic theory, as they are known, break the tissue into solid and liquid phases, and triphasic theory adds an additional term to account for electrostatic interactions. They are much more complex that the spring and dashpot models, and have been validated using cartilage plugs in vitro.

Biphasic theory models the behavior of articular cartilage with solid (collagen) and liquid (interstitial water) components (Figure 5). Instead of electrostatic interactions, the theory attributes the interactions between the solid and fluid phases to frictional drag[20]. During short loading conditions, such as running, the fluid phase of articular cartilage bears most of the load. Rapid, repetitive loading does not allow time for the fluid to flow out of the solid collagen/proteoglycan matrix, and during these instances the articular cartilage is often regarded as an incompressible, elastic solid[21]. During prolonged compression, however, the interstitial fluid is allowed to flow through the solid matrix, yielding a creep behavior. Once fluid flow ceases, an equilibrium deformation is reached and the solid matrix supports the compressive load. Biphasic modeling is commonly used to model compression[22], and typically models experimental data from plugs of articular cartilage *in vitro*.

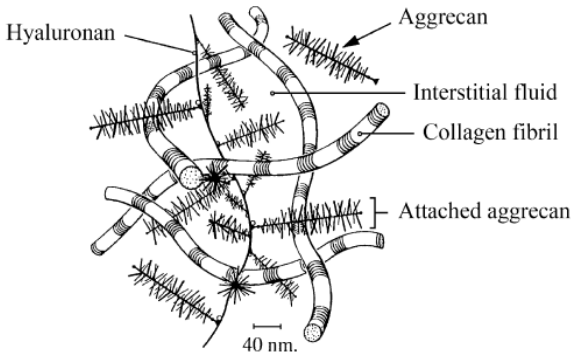

Figure 5. Visual representation of biphasic theory[23]

As previously described, an alternate theory to describe the behavior of articular cartilage is triphasic theory. Triphasic theory accounts for the electrostatic interactions between positively-charged proteoglycans and negatively-charged water[17]. The interaction between these two charged components leads to pressurization within the collagen matrix and force dissipation when the knee is loaded. While this model accurately captures the physiology of articular cartilage, it is more computationally intensive than other models.

Poroelastic and linearly elastic models are two commonly-used alternatives to biphasic and triphasic theory. These models are often used to replicate the behavior of cartilage with finite element modeling. Many studies that attempt to model articular cartilage regard the tissue as a linearly elastic material[24-26], citing the limited mechanical response of cartilage to short-duration loads. These studies often accurately simulate articular cartilage during gait, though fail to capture the creep behavior of articular cartilage during sustained compression. Other mixture theories exist, such as poroelastic, poro-viscoelastic, and fiber-reinforced poroelastic models[27-29]. Poroelastic models regard the collagen matrix as "porous", and the interaction between the porous elastic matrix and viscous water lends to stress relaxation and creep behaviors. These theories are similar to biphasic theory in that they regard articular cartilage as a material with a

solid and fluid phase, though biphasic theory has been utilized and developed the most for articular cartilage analysis.

1.3 MUSCULOSKELETAL INJURY AND OSTEOARTHRITIS

OA most commonly results joint degeneration that is unrelated to a known cause[30], and is referred to as primary OA. The risk for primary OA rises with age[31], and is relatively rare in younger patients. Secondary OA, however, is when the disease arises as a result of traumatic injury or a known genetic or inflammatory disorder[32]. While secondary is rarer than primary OA, it is more frequently observed in younger patients as a result of musculoskeletal injury. Although there are a variety of musculoskeletal injuries that may trigger the OA pathway, this proposal will focus on meniscal injury and anterior cruciate ligament (ACL) reconstruction.

1.3.1 Meniscal Injury

The meniscus is a fibrocartilage structure that is situated on the tibial plateau within the knee joint (Figure 6). It has both medial and lateral semi-lunar components, and acts to dissipate load between the femur and tibia. These wedge-shaped tissues have been found to transmit between 40-70% of total body weight[33], and both the medial and lateral menisci are secured to the tibial plateau with an anterior and posterior root[34]. The medial tibial plateau is larger than the lateral plateau, and for this reason the medial meniscus is larger and transmits more load that the lateral meniscus. Additionally, the medial meniscus is more firmly attached to the tibial plateau than the lateral meniscus and is therefore less mobile[35].

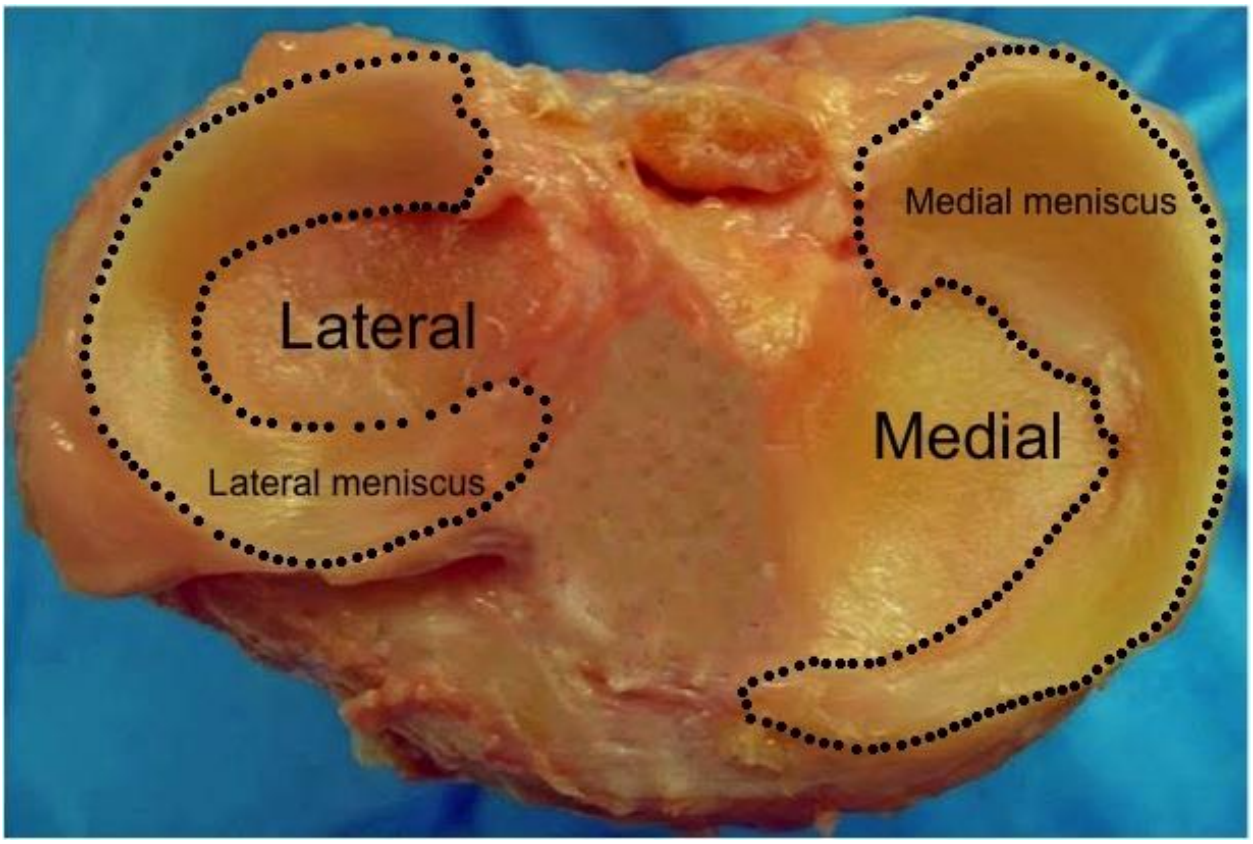

Figure 6. Axial view of the tibial plateau and menisci (photo courtesy of Monica Linde-Rosen)

The meniscus has a composition similar to articular cartilage, with some differences that lend themselves to their different functions. The meniscus has a higher collagen content than articular cartilage[36], and is comprised primarily of type I collagen[37]. There is a significantly lower proteoglycan content in both menisci[38], and both tissues are approximately 74% water by wet weight[39]. In vitro studies have shown that the meniscus has relatively low compressive stiffness and permeability[20], implying that the tissue is able to easily deform and absorb load. These properties make the meniscus effective shock absorbers, and able to transmit 50-90% of the load experiences by the knee[40].

In addition to force dissipation, the menisci have been found to guide femoral condyle motion and translate around the tibial plateau during joint motion[35,41]. After ACL injury, the medial meniscus acts as a primary restraint to anterior tibial translation[42], and is likely a secondary restraint to such movements in the ACL-intact knee. As previously discussed, the menisci are attached to the tibial plateau by anterior and posterior roots. During flexion, the menisci follow the natural backwards-roll of the femoral condyles on the tibial plateau. The lateral meniscus is substantially more mobile than the medial meniscus, and translates twice as much as the medial meniscus in the posterior direction[35].

The meniscus is frequently injured, either by traumatic or degenerative means. Injury to the meniscus is a known risk factor for the development of OA and can trigger early onset of the disease[43,44]. These injuries most frequently occur in the main body of the tissue, specifically in the central and/or posterior regions, and are more common in the medial meniscus. Although some tears are deemed stable and are undetected by patients, symptoms of this injury can include pain, locking, and decreased stability in the injured joint. Though less common, tears to the posterior root are becoming increasingly recognized in orthopaedic practice[45,46]. Patients presenting with this injury have been found to exhibit a rapid progression of osteoarthritis in the injured knee[47-49], and posterior medial meniscal root tears are frequently misdiagnosed and left untreated[46].

Arthroscopic meniscal surgery (CPT 29881, 29880) is the most common procedure reported in the orthopaedic literature[50-52], and is performed to address the symptoms of meniscal injury. Either partial meniscectomy or meniscal repair is typically performed to treat a meniscal tear to the main body of the tissue. Partial meniscectomy is an arthroscopic surgery that involves trimming and shaving away the damaged tissue from the intact meniscus, while meniscal repair

involves suturing the torn ends of the meniscus together. Surgeons decide between the two surgical options by locating the tear in the meniscus and assessing the tissue's ability to heal. If the tear occurs on the periphery of the tissue and is located in a vascularized region, surgeons will typically opt to repair the meniscus rather than shave it. Treatment for a meniscal root tear is also performed arthroscopically, and involves suturing the injured meniscus back to the posterior region of the tibial plateau[53]. While these procedures adequately treat the symptoms of meniscal injury, the risk of OA development persists. Patients who undergo partial meniscectomy have a 50% risk of later developing OA[54].

1.3.2 Anterior Cruciate Ligament Injury

The anterior cruciate ligament, or ACL, is a ligament that crosses the knee from the posterior inner surface of the lateral femoral condyle to an area of the tibia that is anterior and lateral to the medial tibial spine[55] (Figure 7). This structure is comprised of two major "bundles", the anteromedial (AM) and posterolateral (PL) bundles, which correspond with their respective location within the ACL complex. The AM bundle is forced into tension during knee flexion, while the PL bundle has been found to tighten during knee extension[56]. The ACL acts to restrain excessive anterior tibial translation and tibial rotation [57,58], and is commonly injured during sporting or traumatic events. Tearing of the ACL can affect only a single bundle, or can rupture the entire ligament.

Figure 7. Intact ACL, with both the AM and PL bundles visible[59]

Upon injury to the ACL, patients must choose between non-operative, conservative treatment and surgical reconstruction. If a patient is deemed too unstable for conservative treatment or would prefer to quickly return to sport, he/she is often recommended to undergo ACL reconstruction (ACLr). Over 100,000 ACLr surgeries are performed each year in the US[60], and while it often allows patients to return to function, it has been indicated as a major risk factor for the development of OA[61-63]. In fact, regardless of treatment, injury to the ACL has been implicated as a risk factor for the development of OA[64]. While it is unknown what exactly causes the onset of OA after ACL injury, it has been found that knee kinematics are altered after conservative[65] and surgical[66,67] treatments.

Concomitant injury of the meniscus is very common in individuals who tear their ACL, and 40-60% of patients who sustain an ACL injury also tear their meniscus[68]. Meniscal tears are often addressed during arthroscopic ACL reconstruction, and surgeons must choose which intervention will be the most successful. It's been found that of concomitant injuries to the medial meniscus, 63% of the tears are treated by partial meniscectomy, 27% are repaired, and 9% of the injuries are left *in situ* [69]. While there are many factors that contribute to the surgeon's decision of how to address concomitant meniscal injury, age often dictates the course of treatment. Meniscal repair is more often performed in younger subjects as compared to older

subjects [70], likely because of their enhanced healing capabilities. Although meniscal repair helps to lessen the risk of later developing OA, concomitant meniscal injury significantly increases the patient's risk of later developing the disease [71].

1.4 ARTICULAR CARTILAGE GRADING

Articular cartilage is often graded during arthroscopic surgery as a measure of the tissue's integrity and health. Surgeons often perform this diagnostic of the articular cartilage while assessing the total joint health at the beginning of the arthroscopic procedure. To grade the cartilage, surgeons insert a metal probe through one of the arthroscopic portals and apply pressure to the tissue to assess its behavior in response to the small load (Figure 8). Surgeons also note the location and presence of any lesions and tears, and measure the size of any defects. This assessment is performed for the cartilage covering the tibial plateau, femoral condyles, patella, and trochlea. It is during this assessment that surgeons also note the present of meniscal tears and any foreign bodies present in the joint.

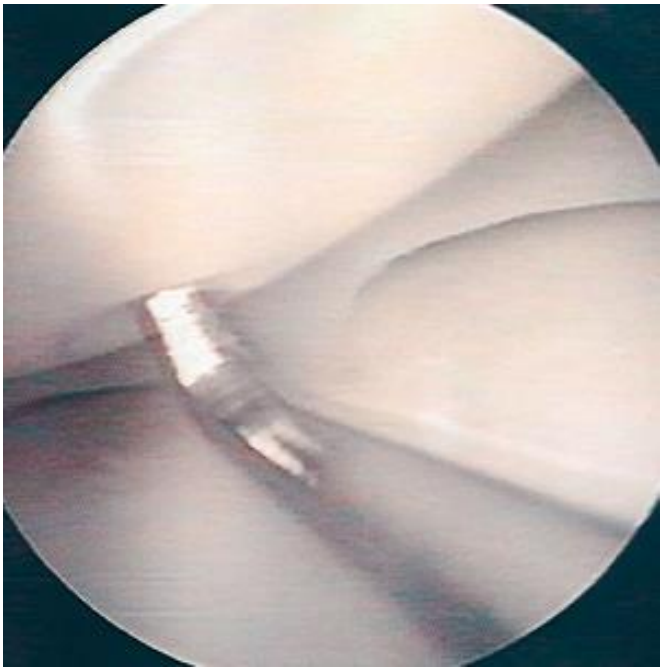

Figure 8. Arthroscopically probing the articular cartilage of the medial femoral condyle[72]

Several scales exist to quantify the integrity of articular cartilage, including the Outerbridge Scale and the International Cartilage Repair Society (ICRS) grading system. In the present studies, the ICRS scale is used because of its familiarity among the surgeons at the University of Pittsburgh Medical Center. Both scales, however, operate on the same principal that grade 0 corresponds with completely healthy articular cartilage, and the amount of cartilage damage increases with the assigned grade. In ICRS grading, articular cartilage is graded on a scale from 0-4 as follows in Table 1 [73]. Subjects with grade 0-2 cartilage are often viewed as having "normal" cartilage, while subjects with grade 3-4 cartilage are classified as having abnormal cartilage[74].

Table 1. Description of articular cartilage grades assigned using the ICRS grading system

Grade	Description
0	"Normal" – healthy articular cartilage
1	"Nearly normal" – cartilage features slight softening and/or superficial lesions
2	"Abnormal" – Lesions in the cartilage that extend to <50% of the tissue's depth
3	"Severely Abnormal" – lesions that extend >50% of the tissue's depth, but not through the subchondral bone
4	"Severely Abnormal" – lesions that extend to the subchondral bone

During a surgeon's diagnostic probing of the articular cartilage, he/she often finds areas of articular cartilage that are not normal and may or may not correlate with subject pain. Unfortunately, however, there is little the surgeon can do to address most cartilage lesions. If the damage is extensive enough, some surgeons may opt for microfracture or autologous chondrocyte implantation (ACI). Microfracture is a procedure that involves puncturing the subchondral bone, which allows for the natural formation of a fibrocartilage[75]. ACI, on the other hand, involves implanting autologous cartilage plugs to allow for articular cartilage that is more similar to the natural tissue[76]. Both methods are able to address high grades of cartilage damage, but are ineffective against lower grades of cartilage damage. These lower grades of cartilage damage have been associated with altered mechanical properties[77], which reflects the softening seen during arthroscopy.

1.5 CURRENT PREDICTORS OF OSTEOARTHRITIS

1.5.1 Plain Radiograph

The most common method of clinically detecting OA is using plain radiographs to assess the presence of joint space narrowing and osteophytes. This method has been used for over 60 years to analyze the effects of musculoskeletal injury on the development of osteoarthritis[78]. More recently, scales and grading systems have emerged to better quantify these degenerative changes in the joint. This method is popular among surgeons because of its relative ease and low cost. Although many surgeons admit to using their clinical experience as their guide when analyzing joint space changes, the Fairbank[79] and Kellgren[80] scales attempt to quantify these changes into comparable grades. Similar to the ICRS grading system, both scales operate on a 1-4 scale, where increasing grade represents more significant changes present in the radiograph. Many clinicians and researchers classify the radiographic presence of OA as a Kellgren score of 2 or greater[7].

Figure 9. Kellgren scale of OA-related changes present via plain radiograph[81]

While the use of plain radiographs to quantify arthritic changes in the knee is a useful method to compare patients, it is still rather subjective and patient-dependent. Studies have attempted to link arthroscopic cartilage changes with radiographic evidence of OA and have found mixed results [82,83]. The studies that have been able to find a link between cartilage damage and radiographic evidence have only been able to do so with high grades of cartilage damage (grade 3 or 4). It's possible that inconsistencies among the literature are a function of the subjective nature of scoring. Additionally, radiographic signs of OA do not always correlate with patient pain or other symptoms of the disease[84]. While this may again reflect the subjective nature of scoring, it is also possible that such a technique is difficult to generalize to the entire population. Another method of OA detection may help clinicians to diagnose and treat OA earlier than by using plain radiographs alone.

1.5.2 Magnetic Resonance Imaging

Magnetic resonance imaging (MRI) is emerging as a potentially promising method of detecting early cartilage damage in vivo. MRI is able to image soft tissues such as articular cartilage, and researchers are modifying and creating sequences that are able to discern damaged cartilage from healthy tissue. Many researchers and clinicians are attracted to the methodology because it is noninvasive and able to detect differences in both physical cartilage morphology and biology. These early changes in cartilage biology and structure are not yet visible using plain radiographs. MRI is therefore able to detect changes in the early or pre-stages of osteoarthritis, and is thus a potentially very powerful diagnostic.

Early use of MRI to assess the integrity of articular cartilage used various T1-weighted sequences with frequency-selective spectral fat-suppression or frequency-selective water

excitation[85-87]. These early techniques aimed to provide ample contrast between the cartilage and surrounding tissues in the knee. The ability to identify the articulating and subchondral boundaries of cartilage allows researchers to determine the volume and thickness of the tissue, and pinpoint the location of morphological abnormalities via segmentation (Figure 10). T1-weighted sequences can be used on scanners of varying strength, and as the magnetic field strength increases, the resolution and precision of the images also increase[88]. A con of this technique, however, is that it is only able to detect changes after lesions in the articular cartilage are present, corresponding with ICRS grades >2. Although many patients remain asymptomatic at this point of cartilage damage, much of the deterioration is irreversible and it is only a matter of time until the damage spreads deeper into the tissue.

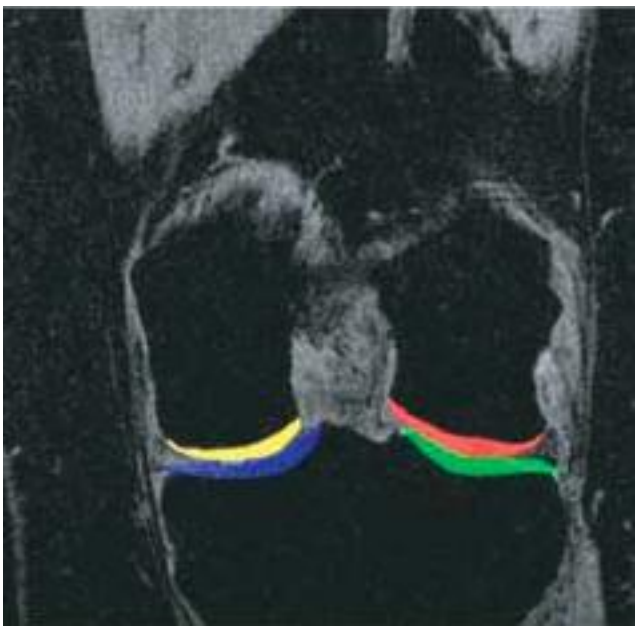

Figure 10. Segmentation of femoral and tibial articular cartilage using a T1-weighted MRI sequence[88]

An alternate technique being used to exploit the biological differences of damaged articular cartilage is transverse relaxation time, or T2, mapping (Figure 11). T2 mapping assesses

the presence of water in the tissue[89], and a linear inverse relationship has been established between water content and T2 times[90]. Since damaged cartilage has a higher water content than healthy cartilage, this technique is able to detect subtle abnormalities in articular cartilage. Much of the previous work using T2 mapping has assessed elevated water content in vivo resulting from age and/or OA[91-93]. Some postulate, however, that T2 mapping can be used to assess the presence of pre-OA cartilage damage[94]. Although some studies have been able to correlate low ICRS grades of cartilage damage with changes in T2 mapping[95], the results are largely dependent on the quality of MRI hardware and have varying degrees of accuracy[96]. Additionally, the use of an MRI scan as a diagnostic is burdensome to clinicians and patients in terms of time, money, and ease of processing. Finally, while cartilage abnormalities may be present via MRI, these do not always correlate with functional, mechanical changes in the tissue. Therefore, while MRI is able to noninvasively detect lesions before they are present in plain radiograph, there is room for improvement.

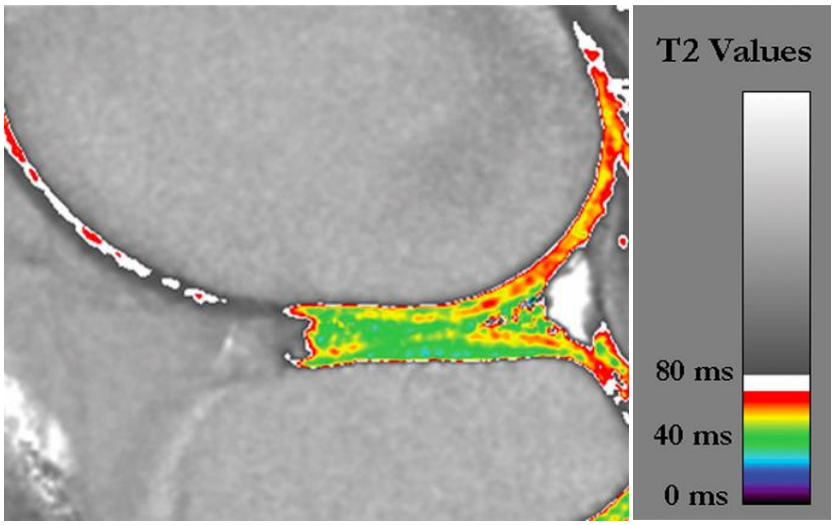

Figure 11. T2 mapping of tibial and femoral cartilage to assess water content[93]

1.5.3 Laboratory-Based Measurements

Though not always applicable in the clinic, there are many laboratory-based measurements that attempt to non-invasively quantify or detect OA. These measurements may help to physiologically explain OA symptoms. These techniques are often based on the different factors that are believed to contribute to the development of OA, namely mechanical and biological factors.

Many researchers have examined the kinematic patterns associated with knee OA, in an attempt to explain the mechanical progression of the disease. Clinically, knee osteoarthritis is more prevalent in the medial compartment[97], and medial compartment OA has been associated with varus static knee alignment[98]. Unsurprisingly, studies examining the dynamic knee kinematics of subjects with OA have found increased adduction moments[99,100], as well as increased flexion angle[100,101]. It is unknown, however, when these patterns appear during the progression of OA. Increased adduction is also associated with ACLr[66] and medial meniscal injury[102], which indicates that the medial compartment of the affected limb is loaded differently than control limbs. Some point to these kinematic similarities as a possible mechanism of OA progression after certain musculoskeletal injuries.

Studies focused on the biological initiation and progression of OA have developed certain biological biomarkers that may indicate the presence of the disease. These biomarkers typically examine different aspects of cartilage and collagen health, and are often detected during analysis of synovial fluid[103], blood[104], or urine[105]. The biomarkers are then validated against traditional MRI measurements of OA development[106]. These noninvasive biomarkers of OA are attractive to many researchers and clinicians because of the ease of collection and minimal patient burden. Currently, however, they only address the biological aspects of OA. The multifactorial-nature of

OA development necessitates a biomarker that can examine the mechanical and functional changes present in joints with cartilage damage.

1.6 CONCLUSIONS

OA is a multifactorial, progressive disease that affects millions of people worldwide. Characterized by cartilage deterioration, OA progresses from the articulating surface to the subchondral bone. Although it is more common in older individuals, a known risk factor for the early development of OA is musculoskeletal injury.

Studies have characterized the biology and mechanical behavior of arthritic and damaged cartilage *in vitro*. Additional work has been done to exploit these known differences in biology to develop imaging and biological biomarkers that will indicate the presence of early cartilage damage. While there is no cure for OA, the early detection of cartilage damage may allow clinicians to stave off the disease and better manage its symptoms. In doing so, sufferers of OA will be able to maintain functionality and mobility of their knees, thus improving the quality of life for many.

1.7 SPECIFIC AIMS

The purpose of this work is to detect softened articular cartilage *in vivo*, and translate this method into a clinical diagnostic. This project is broken into three interrelated specific aims that focus on (1) detection, (2) modeling, and (3) translation.

Aim 1: Detect an arthrokinematic biomarker for osteoarthritis in the *in vivo* biomechanical response of healthy and softened articular cartilage after partial meniscectomy

Aim 1a: Determine the effect of healthy vs softened articular cartilage on changes in joint space during static and dynamic activities.

Hypothesis 1: Partial meniscectomy patients with grade 0, healthy articular cartilage will exhibit different joint space deformation patterns than patients with grade 1, softened cartilage over a duration of compression.

Hypothesis 2: Partial meniscectomy patients with grade 0, healthy articular cartilage will exhibit different joint space deformation patterns than uninjured control patients over a duration of compression.

Aim 1b: Analyze the effect of softened articular cartilage and meniscal injury on gait kinematics.

Hypothesis 1: Partial meniscectomy subjects with softened articular cartilage will exhibit similar gait kinematics to subjects with healthy articular cartilage.

Hypothesis 2: Medial meniscal root tear will result in significantly more lateral tibial translation and adduction than the uninjured knee during all three activities. Additionally, we hypothesize that the medial compartment will exhibit significantly different arthrokinematics than the lateral compartment in the affected limb.

Aim 2: Modeling of in vivo joint deformation to determine material properties of softened cartilage

Aim 2a: Spring-dashpot viscoelastic modeling will be used to identify and estimate the material properties that will best distinguish softened from healthy articular cartilage.

Hypothesis: The simplicity of the spring-dashpot models will adequately characterize *in vivo* creep behavior. Additionally, we hypothesize that subjects with softened articular cartilage will have smaller elastic moduli than subjects with healthy cartilage.

Aim 2b: Determine the optimal time points from modeling results at which the total joint deformation is different between patients with softened and healthy articular cartilage.

Hypothesis: Different load-response curves of healthy and softened articular cartilage will yield specific time points at which deformation patterns of softened cartilage are able to be distinguished from healthy cartilage.

Aim 3: Development of a clinical diagnostic using X-rays to detect softened articular cartilage *in vivo*

Aim 3: Conduct pilot study in Biodynamics Laboratory using minimal X-ray images to detect differences in joint space deformation during standing between patients with healthy and softened articular cartilage using both biplane and single-plane analyses, as well as modeling.

Hypothesis: Joints with softened cartilage will exhibit significantly more medial compartment joint compression than joints with healthy cartilage using both biplane and single plane analyses. Additionally, we hypothesize that Voigt modeling of the results will again show that that the joints with softened cartilage exhibit a lowered elastic modulus than joints with healthy cartilage.

2.0 A NOVEL TECHNIQUE USING DYNAMIC TIBIOFEMORAL JOINT SPACE AS AN INDICATOR OF EARLY CARTILAGE DAMAGE

As previously discussed, the detection of early cartilage damage has the potential to help millions of people who will suffer from OA. While research is being done to detect early biological and imaging biomarkers that may indicate the presence of cartilage deterioration, these methods ignore the tissue's functionality. Upon arthroscopic examination, surgeons are able to identify early cartilage damage by assessing the tissue's response to probing. Damaged cartilage is slightly softened cartilage and has a lowered resistance to the load of the probe. The softness of the damaged cartilage indicates that the mechanical behavior of the tissue is altered. These altered mechanics should translate to changes in functionality of the cartilage under loading conditions.

The purpose of the present study is to detect these functional differences between softened and healthy articular cartilage *in vivo* under static and dynamic loading conditions. Various biomechanical measurements, including joint space and joint kinematics, will be used to detect any differences between subjects with known healthy cartilage and subjects with known softened cartilage. If able to differentiate healthy from softened articular cartilage, this method could represent a new technique to detect early cartilage damage and OA.

2.1 INTRODUCTION

Osteoarthritis (OA) is the most common joint disorder in the world[107], and an estimated 6.1% of all adults in the US over the age of 30 report symptoms in the knee[7]. While OA is often reported in older patients, studies have shown that injury to the meniscus and subsequent partial meniscectomy may trigger early onset of the disease[43,44]. Arthroscopic meniscal surgery is among the most common orthopaedic procedures [50-52], and partial meniscectomy patients have a 50% risk for the development of OA[54]. Unfortunately, these patients typically do not recognize the symptoms of OA until the disease has progressed to an irreversible state.

Often during partial meniscectomy, surgeons arthroscopically probe the cartilage to assess the tissue's health and identify areas of "softened" articular cartilage[108]. Using the International Cartilage Repair Society (ICRS) scale, these areas of softened cartilage are characterized by superficial lesions and a lowered resistance to arthroscopic probing. These areas do not correlate with radiographic signs of OA and have few visible signs of cartilage damage, but are softer than healthy articular cartilage when arthroscopically probed. Research has shown that softening is related to changes in the collagen matrix of articular cartilage[109]. These alterations could represent early structural damage[77] that can lead to irreversible cartilage damage and OA.

Many studies have characterized the response of healthy tibiofemoral articular cartilage to various loading conditions *in vivo*. The thickness distributions of articular cartilage have been linked to areas of closest contact[110] and kinematics[111]. Researchers examining the strain of articular cartilage during static loading have found that cartilage from both the medial and lateral plateaus undergo the most change in the initial seconds of loading[112,113]. In terms of dynamic activities, the cartilage of the medial tibial plateau has been found to deform significantly more

than the lateral plateau during walking[114] and lunging[115], though the most tibial cartilage deformation is observed during running[116]. Subjects with OA demonstrate significantly more deformation in their medial tibial cartilage than uninjured controls during static loading[117]. It is unknown, however, when these patterns of increased medial tibial deformation present in the progression of OA.

Clinicians and researchers have developed various tools to noninvasively detect the presence of knee OA. Health professionals most often use joint space radiographs or MRI[118,119], while biomechanists have found certain variations in gait that are characteristic of the presence of OA[100,120]. While these tools can reliably distinguish between early and late-stage OA, they are currently unable to reliably predict the disease prior to the development of significant cartilage lesions[121]. There are some methods using plain radiographs to assess the change in joint space width over time as an indicator of cartilage health, though they require multiple visits over years[122]. Some researchers have postulated MRI-based methods to detect OA before it progresses, citing the elevated water content as a possible MRI-visible marker[94,95]. Although these techniques are not invasive, they assess the biology of early cartilage damage and softening rather than the mechanics. Thus they are unable to detect differences in function resulting from cartilage softening. Gait kinematics represent an interesting method of OA detection that can be further developed, though extensive post-testing processing is currently necessary and it is unknown when these altered gait patterns emerge in the course of the disease. The inability to easily and reliably detect cartilage damage before it advances into OA hinders the development and/or use of chondroprotective and OA-modifying treatments. Thus, the detection of OA before the appearance of significant cartilage damage could potentially aid in treating and possibly reversing the disease.

The purpose of this study was to develop a technique using dynamic stereo radiography to detect functional differences between subjects with ICRS grade 0 and grade 1 articular cartilage following partial medial meniscectomy. We hypothesized that the meniscal-injured subjects with grade 1 articular cartilage would have different load-response curves than meniscal-injured subjects with grade 0 cartilage, and that both groups would have different load-response curves than uninjured, healthy controls. We hypothesized that these cartilage-dependent differences would not, however, be evident in running kinematics.

2.2 METHODS

2.2.1 Subjects

19 subjects participated in this University of Pittsburgh IRB-approved study and were separated into 3 groups – partial medial meniscectomy (PMM) subjects with softened articular cartilage (n=5, 4M, 1F), PMM subjects with healthy articular cartilage (n=4, 2M, 2F), and age/sex matched healthy controls (n=10, 6M, 4F). Articular cartilage status was graded during arthroscopy using the ICRS scale, where grade 0 represents healthy cartilage and grade 1 represents softened cartilage. Surgeons probed both the medial and lateral compartments of the tibial plateau, as well as the femoral condyles, trochlea, and patella. After this cartilage diagnostic, the surgeons performed the PMM surgery and removed the injured tissue (all injuries occurred in the posterior horn). All surgeries were performed by a group of 4 physicians at the University of Pittsburgh Medical Center, and all surgeons were experienced with the ICRS grading system.

All PM subjects included in the study exhibited either grade 0 or grade 1 articular cartilage on the medial tibial plateau, and all subjects had grade 0 articular cartilage on the lateral tibial plateau. Exclusion criteria for the study included previous injury/surgery to the affected limb (with the exception of anterior cruciate ligament injury/reconstruction), age outside of the 25-55 year range and/or BMI > 35. Subjects with anterior cruciate ligament (ACL) injuries who had undergone surgical ACL reconstruction were not excluded, since ACL and meniscal injuries are often concomitant and these individuals are known to be at high risk for OA. Subjects participated between 2-12 months post-surgery if they underwent isolated PM, or between 6-12 months post-surgery if they underwent ACL reconstruction with concomitant PM. Table 2 shows demographics of the 3 participating groups. None of the distributions of the 3 groups were not deemed to be statistically different (Kruskal-Wallis ANOVA, $p > 0.05$).

Table 2. Age, sex, concomitant ACL injury, and BMI distributions of the 3 groups in this study. Kruskal-Wallis ANOVAs performed on the BMI and age distributions yielded no significant differences between groups.

Subject Demographics			
	PM softened	**PM healthy**	**Uninjured control**
Number of subjects	5	4	10
Age	44.0 ± 8.5 years	32.5 ± 5.9 years	35.8 ± 12.2 years
Sex	1F, 4M	2F, 2M	4F, 6M
Concomitant ACLr	3	1	N/A
BMI	28.0 ± 4.3	23.5 ± 4.0	24.0 ± 3.7

2.2.2 Kinematic Testing

Subjects performed two tasks: a step-loading activity and running on a level treadmill. The inclusion of both of these tasks allowed examination of joint space changes during both sustained

creep testing and repetitive, cyclical loading. The step-loading activity utilized a modified leg press machine, with an axial load equivalent to half of the subject's body weight applied distally to the affected leg, as shown in Figure 12. The leg press was equipped with an electromagnet, which held the weight just above the foot until externally triggered by the automated testing system to release the weight onto the subject. This test approximates loading conditions to the knee experienced during two-legged standing, but enables rapid application of a fixed load at a specified knee flexion angle.

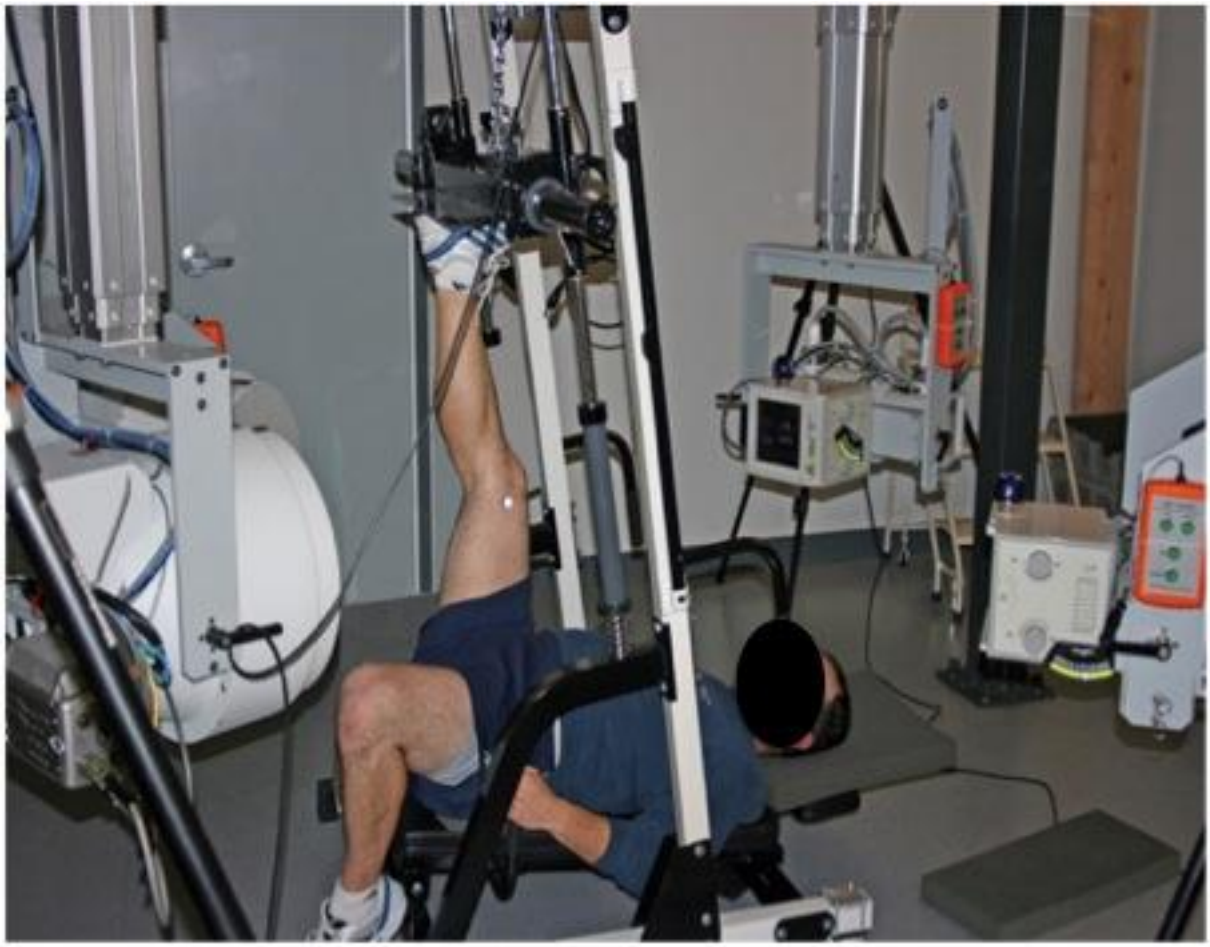

Figure 12. Modified leg press used in kinematic testing

The step loading activity was performed twice – once with the knee at full extension and again with the knee at 15° of flexion. Subjects were placed at the prescribed flexion angle at the beginning of each test using a goniometer, and a visual feedback system helped them to maintain the initial angle within 5 degrees. Before each test, subjects rested supine for thirty minutes to allow for the articular cartilage to return to its unloaded state. Thirty minutes has been used as pre-test cartilage relaxation time by others assessing cartilage strain[123,124], and post-processing calculations showed that the joint space returned to a constant value at the beginning of each test. Following the leg press activities, the subject rested for another 30 minutes and then ran on a level, instrumented treadmill at 2.5 m/s (Bertec Corp.). Subsequent analysis of the tibiofemoral joint space indicated that 30 minutes was enough time for the cartilage to fully relax, resulting in consistent joint space values at the beginning of each activity. To further minimize the risk of diurnal effects on articular cartilage[125], we attempted to schedule testing for the morning.

Testing was performed within the dynamic stereo X-ray (DSX) system, which uses biplane radiography during dynamic trials to characterize joint motion. Dynamic, stereo X-rays were generated with 1 ms pulsed exposures at 90 kV/160 mA (or less, depending on subject size), with a source-to-detector distance of 1.8 m and an inter-beam angle of approximately 60 degrees. Each 40 cm image intensifier (Thales, Inc.) was coupled with a 4 megapixel, 14 bit digital video camera (Phantom 10, Vision Research, Inc.). Image acquisition occurred simultaneously for both cameras, synchronized with x-ray pulse generation. For the step-loading trials, DSX images were captured at varying frame rates to characterize the different areas of the load-deformation curve. X-rays were first captured at 50 frames/s from 0.4 seconds before the weight was released until 0.8 second after the weight was released, and then at 4 frames/s for the next 19 seconds. 10-frame bursts (at 150 frames/s) were then acquired once per minute until the

subject had either held the weight for 5 minutes or was too fatigued to continue. During the running trial, images were collected during stance phase (0.7 s per acquisition) at 150 frames/s. X-ray collection began as soon as the treadmill reached 2.5 m/s, and collection repeated at one-minute increments until 5 minutes or subject fatigue. The estimated effective radiation dose for this study (estimated using direct entrance exposure measurements and PCXMC dose estimate software, STUK - Radiation and Nuclear Safety Authority, Helsinki, Finland; http://www.stuk.fi/pcxmc) was approximately 0.32 mSv. This is a fraction of the 3 mSv average background exposure received by most Americans from natural sources such as radon gas and cosmic rays [126].

2.2.3 Data Processing

In addition to kinematic testing, all subjects underwent a unilateral CT scan of the affected joint (0.6 mm slices including 10 cm above and below the joint line). The scans were segmented with Mimics (Materialise Inc., Ann Arbor, MI, USA) to create subject-specific bone models of the femur and tibia using a previously-described method [127,128]. The segmented bone models were then matched to the X-ray images gathered during kinematic testing using a computerized, model-based tracking technique [129,130]. Briefly, custom software created a virtual reconstruction of the testing environment, in which the segmented bone models were manually positioned via ray-traced projections of digitally reconstructed radiographs (DRRs). These manually-placed DRRs were then used as an initial guess for an algorithm that automatically manipulated the bone to a position that maximized the correlations between the DRRs and actual radiographs. The results from two adjacent frames were then used to project an initial guess for the subsequent frame, and the optimization process was repeated for all frames in a trial. The

location and orientation of the femur and tibia were then projected into 3D space, and their motions and positions relative to one another were calculated. The performance of this system has been extensively validated, with precision in the order of 0.1 mm for *in vitro* testing[129] and averaging 0.6 degrees/0.5 mm for *in vivo* tibiofemoral kinematics during running [131].

The tibiofemoral joint space was extracted for each frame from the central subregion of the medial tibial plateau, shown in Figure 13. This location was chosen because it corresponds with the location the assessed cartilage grade. For the leg-press trials, joint space values of this subregion for the entire loading phase were plotted against time. These distances were normalized to the unloaded joint space value at the beginning of the trial. For the running trials, joint space values from the central subregion of the medial tibial plateau were extracted at each foot strike and normalized to the joint space value of the first running trial. These normalized distances were then plotted against time.

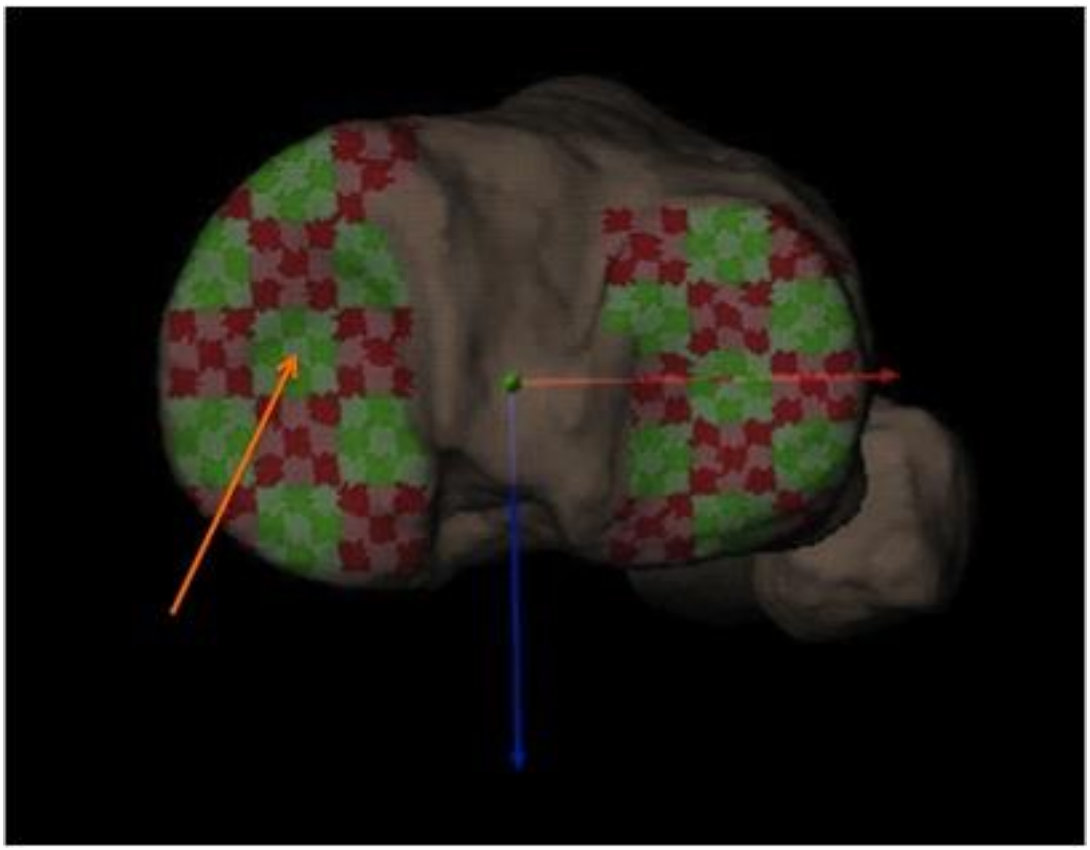

Figure 13. Tibia with anatomical axes and defined subregions. The orange arrow is pointing to the subregion on the medial plateau where all joint space measurements were taken for each subject and trial.

Running kinematics were calculated as motion of the tibia relative to the femur. Translations were defined as the 3-dimensional distance between the centers of the tibial and femoral coordinate systems, and were separated into anterior-posterior, medial-lateral, and superior-inferior directions. The superior-inferior translation measurements were excluded from kinematic analysis. Rotations were similarly calculated of the tibia relative to the femur, and included flexion-extension, ab/adduction, and external-internal rotation. Running kinematics were analyzed from 0.1 second before to 0.1 second after foot strike.

2.2.4 Statistics

The effect of softened articular cartilage on the change in tibiofemoral joint space during the leg press activity was assessed using a Kruskal-Wallis ANOVA comparing PM softened, PM healthy, and uninjured control groups at 0.5, 1, 5, 10, 15, and 18 seconds after weight application. Between-group differences in joint space during running, assessed at 1, 2, 3, 4, and 5 minutes after the start of the running trial, were evaluated with a separate Kruskal-Wallis ANOVA. Time scales were separated because the literature has that shown much of the joint space deformation occurs in the first 20 seconds of loading[113], and we wanted to examine several timepoints in this initial range. Differences in the tibiofemoral running kinematics data between the PM softened, PM healthy, and uninjured control groups were assessed at 0.1 and 0.05 seconds before foot strike, at foot strike, and at 0.05 and 0.1 seconds after foot strike using a Kruskal-Wallis ANOVA. If the Kruskal-Wallis tests reported a significant difference by group ($p<0.1$), post-hoc Mann-Whitney t-tests were performed to clarify areas of significance. All statistical analyses were performed using SPSS software (version 19.0).

2.3 RESULTS

Figure 14 shows the change in joint space during the step-loading activity at full extension during the initial loading phase (first 20 seconds of weight application), and Figure 15 shows the change in joint space during running for 5 minutes.

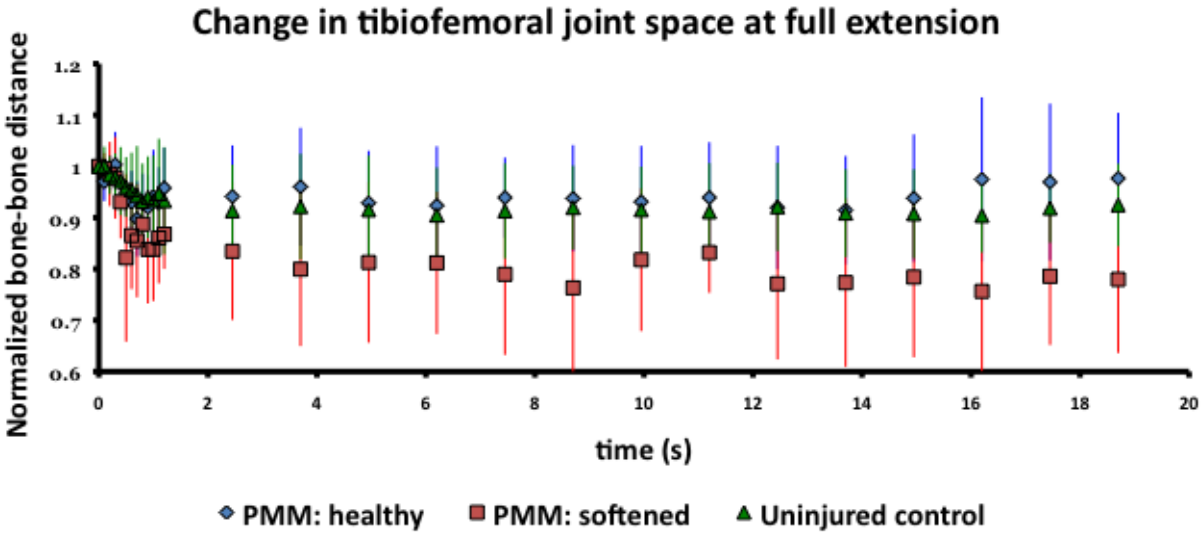

Figure 14. Normalized change in joint space during full extension leg press activity. In this chart, the red line represents normalized tibiofemoral joint space of the PM softened group, the blue line represents joint space of the PM healthy group, and the green line represents joint space data of the uninjured control group. * represents significant differences between the PM group with softened articular cartilage and the uninjured controls, and + represents significant differences between both PM groups.

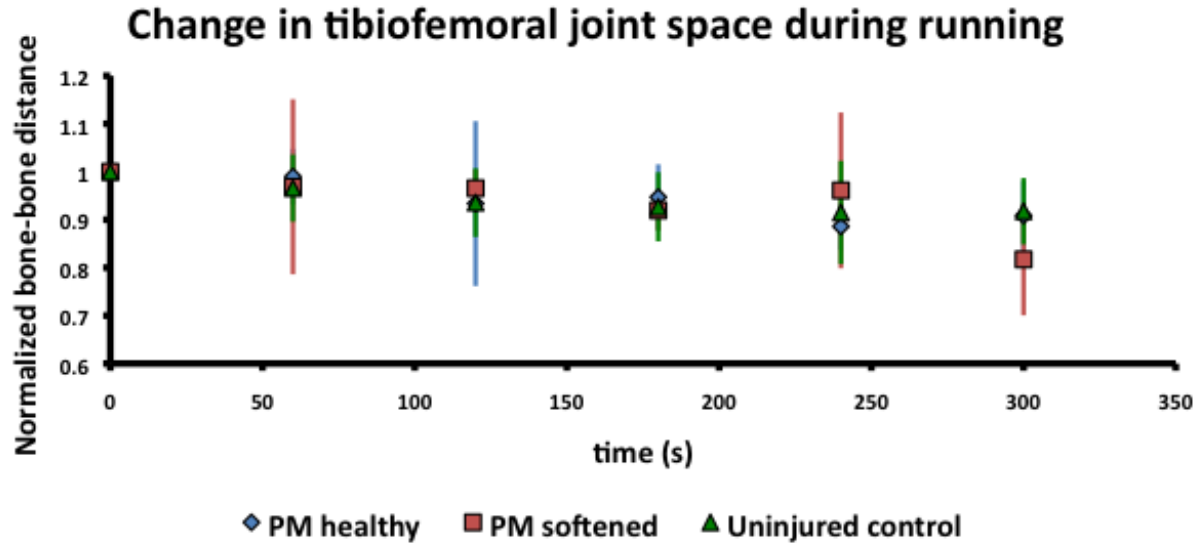

Figure 15. Normalized change in joint space during level running. Again, in this plot the red data represent normalized tibiofemoral joint space of the PM softened group, the blue data represent joint space of the PM healthy group, and the green data represent joint space data of the uninjured control group. No significant differences were observed between groups.

In terms of the leg press activity, significant differences between groups were seen at 0.5 seconds ($p=0.04$) and differences trending on significance were seen at 18 seconds ($p=0.068$) after weight bearing. Post-hoc testing revealed significant differences between the load-response curves of the PM softened and uninjured control groups at 0.5 and 18 seconds after weight bearing ($p=.020$ and $p=.039$, respectively), and differences between both PM groups at 18 seconds after weight bearing ($p=.086$). No differences were found between the PM group with healthy articular cartilage and the uninjured controls. There were no significant differences between the tibiofemoral joint space of any of the groups during running. It should be noted that the leg press data from the 15° flexion trials are not included in this analysis. Subjects had trouble maintaining the flexion angle for the duration of the weight application, resulting in joint flexion/extension motion that introduced considerable variability in the location of tibiofemoral contact and confounded data analysis.

To analyze the long-term creep response of the different groups, time points were categorized into 90, 120, 180, 240, and 300sec, +/- 15 seconds. No significant differences were found between groups at any of the time points. The largest difference was seen at 180 sec between the PM groups, but did not reach statistical significance.

There were no statistically significant differences in tibiofemoral kinematics during running between the partial meniscectomy groups. Both surgical groups exhibited more anterior tibial translation than the uninjured controls from 0.1 before to 0.1 seconds after foot strike (Figure 16). Specifically, the softened group displayed significantly more anterior translation for the entire data range ($p<0.05$) while the healthy group exhibited more anterior tibial translation at 0.05 seconds after foot strike ($p=0.1$). It is unclear if these differences between the uninjured group and PM groups are due to partial medial meniscectomy or concomitant ACL injury.

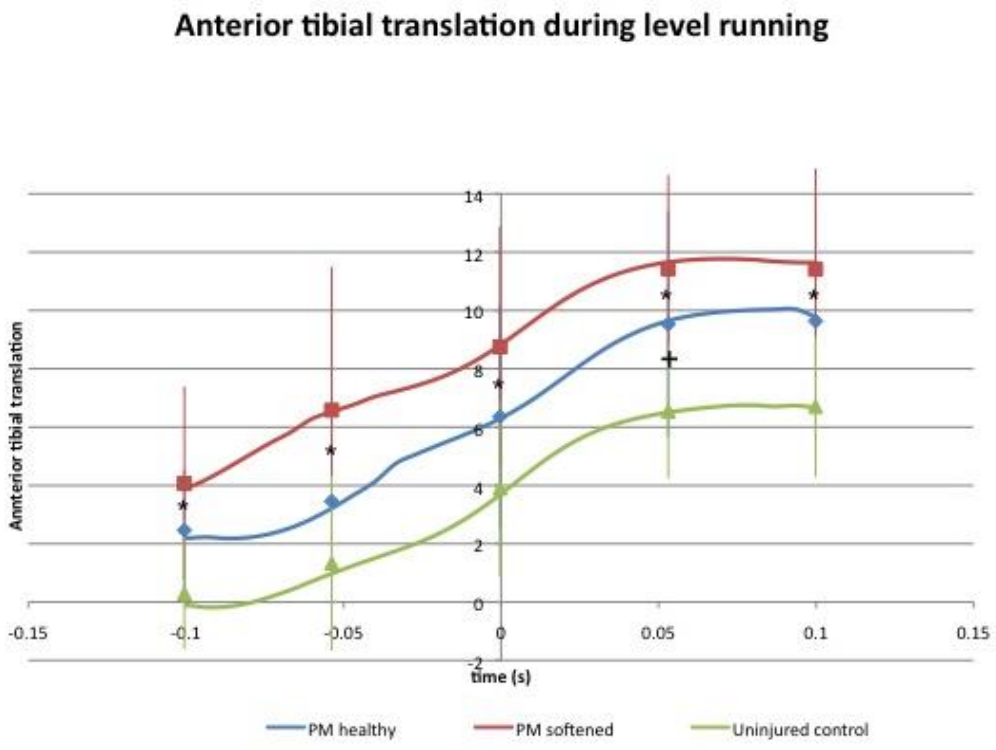

Figure 16. Anterior tibial translation during level running. Once again, the red lines represent running kinematics of the PM softened group, blue lines represent kinematics of the PM healthy group, and green lines represent kinematics of the uninjured control group. The PM softened group exhibited significantly more anterior tibial translation than the uninjured controls for the entire range of motion (signified by *), while the PM healthy group exhibited more anterior translation than the uninjured controls less consistently (signified by +).

2.4 DISCUSSION

The results of this study indicate that dynamic stereo radiography can be used during a creep test to detect different cartilage grades in vivo. Subjects with grade 1 articular cartilage exhibited a different load-response curve than individuals with grade 0 articular cartilage. Subjects with softer articular cartilage underwent a larger change in joint space during the axial compression introduced by the leg press, and their joint space compressed at least 10% more than subjects with healthy cartilage. Contrary to our hypothesis, there were no differences between PMM

grade 0 and uninjured control subjects. In order to assess the area of cartilage softening, we measured changes in joint space at the center of the medial tibial plateau. This region is uncovered by the meniscus, which may be why we did not see the effect of PMM in the healthy cartilage subjects. Therefore cartilage status rather than meniscal injury was responsible for the differences in joint space deformation between groups. It is possible that cartilage softening is indicative of early mechanical damage in the cartilage's collagen matrix, and that softened cartilage is more porous and allows water to escape more easily from its microstructure. These microscopic changes in the cartilage's architecture manifest themselves as larger and faster changes in joint space over time during compressive loading.

Differences between the subject groups were only visible in the leg press activity and not in the repetitive loading of the running trials. We speculate that this behavior reflects the viscoelastic nature of articular cartilage. During a sustained force application, the interstitial water has time to escape from the collagen matrix. Deficits in the grade 1 superficial zone collagen matrix lead to the grade 1 subjects to undergo more joint space compression than the grade 0 subjects. Under fast repetitive loads, however, the tibiofemoral forces are absorbed by the collagen matrix and the interstitial water is incompressible, resulting in little change in joint space over time. Thus differences between grade 0 and grade 1 are indistinguishable. These results mimic *in vitro* testing with cartilage specimens. Ronken, et al, performed confined creep and indentation tests on samples of bovine articular cartilage and measured the change in specimen thickness over time[132]. Similar to the current study, it was found that creep testing yielded differences in cartilage thickness while repetitive indentation testing did little to impact the thickness of the cartilage specimen over time. These similarities indicate that not only are

there significant parallels between *in vitro* and *in vivo* work in this area, but also that softened and healthy articular cartilage are functionally similar in many activities.

Interestingly, significant differences in joint space between groups are only seen in the initial loading phase. Subsequent analysis showed that an average of 60% of the total joint space deformation occurs in the first second of loading, and about 75% of the total deformation occurs within the first 20 seconds. Thus, we are able to see significant differences between groups when the joint is actively compressing and has not yet reached a static equilibrium. All groups exhibit consistent percentages of joint space deformation in the initial second and 20 seconds of loading, so while subjects with softened articular cartilage exhibit greater total joint space deformation, all groups deform at comparable relative rates. These rates of joint space deformation are similar to other work examining the strain of articular cartilage *in vivo*, where 60% of the total deformation occurred in the initial second of loading and between 75-80% of the total deformation occurred in the first 20 seconds[112,113]. This supports the assertion that there are many functional similarities between healthy and softened articular cartilage. The ability of softened articular cartilage to behave like healthy tissue may be why none of the subjects complained of the physical symptoms of OA.

The lack of significant differences in kinematics between the partial meniscectomy groups indicates that subjects with softened articular cartilage have not yet developed gait patterns characteristic of OA. Research has shown that patients with OA exhibit altered kinematics during gait, specifically larger external knee adduction moments[100,120]. It is unknown, however, at what point these alterations appear during the progression of the disease. Patterns of adduction during gait have not yet emerged in the grade 1 population, however, because softened articular cartilage is able to function similarly to healthy tissue. Therefore,

analysis of knee kinematics during gait cannot be used as an indicator for softened articular cartilage and early cartilage damage.

It is worth noting that although not statistically significant, the PMM softened group is a bit heavier and older than the other groups. Therefore it is possible that the cartilage of these older and heavier subjects behaves differently than in younger, healthier individuals. This being said, however, all subjects regardless of age or BMI were asymptomatic for OA. The present technique is able to delineate differences in joint compression behavior between subjects before any complaints of knee pain. Additionally, articular cartilage was scored as grade 1 if it met the ICRS guidelines. Subject weight and age were not considered during scoring. Future studies will attempt to expand on this work and minimize any possible differences in group demographics.

There are several limitations to this study. In an effort to minimize the effect of confounding variables in our analysis, strict inclusion criteria were employed, resulting in a relatively low sample sizes. Because of difficulty recruiting subjects with isolated PMM, we included subjects who had undergone a concomitant ACL reconstruction. A primary assumption of this inclusion is that ACLr will not affect the compressibility of the knee joint during static or dynamic activities. We believe this assumption to be valid because the same region of the meniscus was injured and removed in all subjects. Another limitation is that we assumed the cartilage grade would remain unchanged from surgery to testing. Although we tried to test subjects quickly after they were cleared for running, we acknowledge that months elapsed between surgery and assessment and it is possible that there may have been additional cartilage degeneration. All subjects, however, were asymptomatic for OA at the time of testing. Thus even if there was additional cartilage deterioration, this technique provides a novel method to

detect differences in knee creep behavior between subjects based on their baseline cartilage scores before they present with symptoms of OA. A final limitation of our study is the objective nature of cartilage grading. As previously stated, all surgeons were experienced using the ICRS scoring system. There was quite a bit of variability in the PMM grade 0 group, and some of the subjects in this group underwent much more joint compression than others during the creep test. It is unclear if this variability is from the low sample size or inconsistencies in cartilage scoring between surgeons. We did not assess the inter-surgeon reliability of the ICRS grading in the present study, and the literature is mixed regarding classification of ICRS grade 0 and grade 1 cartilage[133,134]. Regardless, the purpose of this study was to develop a quantitative method to detect differences in function due to cartilage softening, which will definitively categorize subjects into groups based on cartilage behavior rather than qualitative scoring that can vary between surgeons.

This work has served as a pilot study to exploit mechanical differences between healthy and softened cartilage groups using the DSX system. In the future, we plan to model the change in joint space at full extension to better qualify the microscale biomechanics of softened articular cartilage. We will employ a viscoelastic model to understand how the elastic and viscous components of cartilage change with superficial cartilage damage. Our long-term goal is to use this data to develop a clinical diagnostic for detecting softened articular cartilage without the need for surgery. By characterizing the most sensitive measures and time points for imaging, it may be possible to acquire clinically useful data on cartilage function using readily-available clinical imaging equipment. Such a diagnostic could functionally assess the presence and behavior of softened cartilage and at-risk joints.

2.5 CONCLUSION

Although softened articular cartilage is difficult to detect using traditional methods, it represents the early stages of cartilage damage before OA. Softened articular cartilage behaves differently than healthy tissue during an *in vivo* creep test, and exhibits significantly more joint space deformation during the initial phase of loading. Differences between groups are not seen in kinematics or joint space measurements during running. While softened cartilage appears to have many functional similarities with healthy cartilage, the ability to detect the damaged tissue before it progresses to OA may aid in earlier intervention and treatment of the disease.

To validate the testing design, we performed a similar testing protocol on a cadaver knee and examined the change in joint space at the central subregion of the medial tibial plateau. The methodology and results are expanded upon in Appendix A. Briefly, we found that the creep response of the cadaver specimen was very similar to the averaged response from all subjects *in vivo,* and fairly similar to the creep response of the uninjured control subjects alone. Similarities between *in vivo* and cadaver results indicate that we are measuring the passive properties of the joint, and do not need to account for active muscle forces.

The next step in developing a clinical diagnostic to detect softened cartilage is to model the change in joint space using a qualitative model. We will employ a viscoelastic model to understand how the elastic and viscous components of cartilage change with superficial cartilage damage. This will help to better qualify the microscale biomechanics of softened articular cartilage and understand the material properties that may delineate softened from healthy tissue.

A major question left unanswered from this chapter is when kinematic patterns of OA, such as increased tibial adduction, occur in the progression of the disease. Partial medial meniscectomy and meniscal injury are associated with an increased risk of OA, and a theory for

this increased prevalence of OA is kinematic alterations that change the loading of articular cartilage after injury. This being said, however, it is unknown how the kinematics of the knee are changed after meniscal injury, but before the development of OA. Therefore it may be useful to understand how different medial meniscal injuries affect knee kinematics.

3.0 EFFECT OF POSTERIOR HORN MEDIAL MENISCUS ROOT TEAR ON IN VIVO KNEE KINEMATICS

Chapter 2 examined the kinematics resulting from softened articular cartilage. Although there were no differences resulting from early cartilage damage, an interesting trend appeared when comparing subjects with partial medial meniscectomy and uninjured controls. Subjects who underwent meniscal treatment had slightly more lateral tibial translation throughout the running task than uninjured controls, though it did not reach statistical significance.

Partial medial meniscectomy is a relatively common treatment for minor meniscal tears. A more severe medial meniscal injury, however, is medial meniscal root tear. This injury severs one of the connections between the tibial plateau and the medial meniscus, thus compromising the tissue's ability to distribute load and guide medial femoral motion.

Although lateral tibial translation did not reach statistical significance in partial medial meniscectomy subjects, it is unknown how more severe meniscal injuries affect the joint in vivo. An *in vivo* study examining the tibiofemoral kinematics resulting from medial meniscal root tear could provide a baseline for other more common meniscal injuries, and show the extent to which medial meniscal injury can alter human movement.

3.1 INTRODUCTION

Arthroscopic meniscal surgery (CPT 29881, 29880) is the most common procedure reported in the orthopaedic literature [50-52]. While an injury to the meniscus most commonly occurs in the main body of the tissue, tears to the posterior root are becoming increasingly recognized in orthopaedic practice [45,46]. These injuries have the potential to trigger a debilitating course of osteoarthritis, and patients presenting with this injury have been found to exhibit a rapid progression of osteoarthritis in the injured knee [47-49]. Additionally, posterior medial meniscal root tears are frequently misdiagnosed and left untreated [46].

Of the literature, most work examining medial meniscal root tears (MMRT) focuses on treatment options and less on those left untreated. Few studies have examined the biomechanical implications of MMRT. *In vitro* work has found cadaver knees to exhibit decreased contact area and increased pressure after a tear to the posterior root of the medial meniscus [135,136]. Additionally, cadaver knees demonstrate increased lateral tibial translation and varus alignment with MMRT [137]. Surgical repair has been shown to restore normal loading conditions in an *in vitro* setting [135-137]. There are no *in vivo* studies examining the kinematics resulting from an untreated medial meniscal root tear.

The purpose of this study was to examine the *in vivo* knee kinematics and arthrokinematics (kinematics of the articulating joint surfaces) resulting from an untreated tear to the posterior root of the medial meniscus during three different activities. We hypothesize that the injured knee will demonstrate significantly more lateral tibial translation and adduction than the uninjured knee during all three activities. Additionally, we hypothesize that the medial compartment will exhibit significantly different arthrokinematics than the lateral compartment in the affected limb.

3.2 METHODS

3.2.1 Subjects

9 subjects with recent but not acutely symptomatic, MRI-identified MMRT participated in this IRB-approved study. Subjects were recruited for the study if they showed the presence of an isolated posterior horn MMRT seen on MRI and exhibited minimal joint space changes in the medial compartment and normal joint space in lateral compartment on plain radiographs compared to the uninjured, contralateral limb (flexion weight-bearing, lateral merchant, and long standing cassette X-rays were obtained in all patients). All participants were free from any other lower body injury and exhibited normal joint alignment (within 3° varus) that was symmetrical to the uninjured, contralateral limb. Data from two subjects were discarded because of limping during testing and excessive dynamic joint space narrowing (seen in dynamic testing but not on plain films), leaving 7 subjects for analysis (6 F, 1 M, age 57.4±9.3 years).

3.2.2 Kinematic Testing

Kinematic testing comprised of 3 activities: level walking, decline walking, and squatting. Each task was repeated for three trials, and both the injured and contralateral limbs were tested. Gait trials were performed with an instrumented treadmill (Bertec Corp.) that was set to a velocity of 1.0 m/s for both level and decline walking. For squatting trials, subjects were instructed to bend their knees as far as possible without significant pain. One of the subjects was unable to bend their knee for all of 25°-70° of flexion, so n=6 for the squatting trials in order to capture a large range of flexion.

Testing was performed within the dynamic stereo X-ray (DSX) system, which uses biplane radiography during dynamic trials to characterize joint motion. The lab setup for each activity can be seen in Figure 17.

Figure 17. Laboratory setup – dynamic stereo X-ray (DSX) system, including dual-belt, instrumented treadmill, and customizable safety railings. Top left: Oblique configuration for level walking; Top Right: Oblique configuration with treadmill inclined and treads running in reverse for decline walking; Bottom Left: Horizontal configuration for squatting.

Dynamic, stereo X-rays were generated using a protocol of 90 kV, 160 mA (or less, depending on subject size), with 1 ms pulsed exposures. Images were acquired for either 1 s at 100 Hz (gait) or 2 s at 50 Hz (squat), using 40 cm image intensifiers (Thales, Inc.), coupled to 4 megapixel, 14 bit digital video cameras (Phantom 10, Vision Research, Inc.), with a source-to-detector distance of 180 cm. The effective radiation exposure for all dynamic imaging trials (estimated using direct entrance exposure measurements and PCXMC dose estimate software, STUK - Radiation and Nuclear Safety Authority, Helsinki, Finland; http://www.stuk.fi/pcxmc)

was less than 0.2 mSv. Bilateral CT scans added approximately 1 mSv (estimated from CT scanner DLP reports), for a total of 1.2 mSv. This is considerably less than the average exposure of approximately 3 mSv per year from natural sources such as cosmic rays and radon gas [126].

3.2.3 Data Processing

In addition to kinematic testing, all subjects underwent a bilateral computed tomography (CT) scan using a GE LightSpeed CT Scanner (GE Medical Systems, LightSpeed Pro 16) with a slice spacing of 1.25 mm and a field of view that extended from 15 cm below to 15 cm above the joint line. Single slices through the hip and ankle centers were also acquired to enable definition of anatomic coordinate systems for the tibia and femur. The scans were then segmented with Mimics (Materialise Inc., Ann Arbor, MI, USA) to create patient-specific bone models of the femur and tibia using a previously-described method [127,128]. To enable region-specific analyses, sub-regions of the articulating surfaces were defined from the 3D surface models, as shown for the femoral condyles in Figure 18 and tibial plateau in Figure 19.

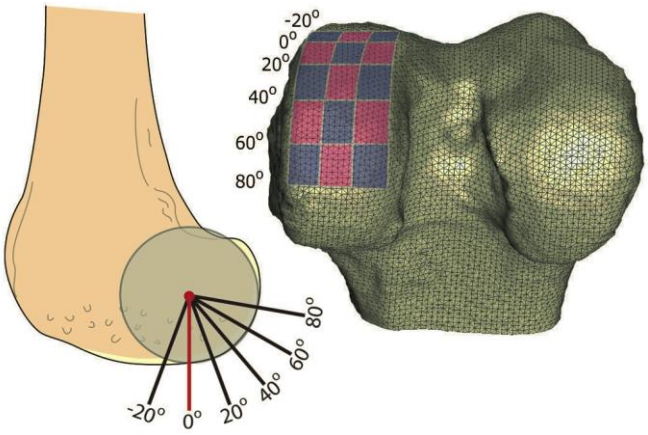

Figure 18. Regions for the medial femoral condyle divide the articular surface into 3 medial-lateral zones and 5 longitudinal zones, defined by planes at 20° increments relative to a sphere fitted to the condyle.

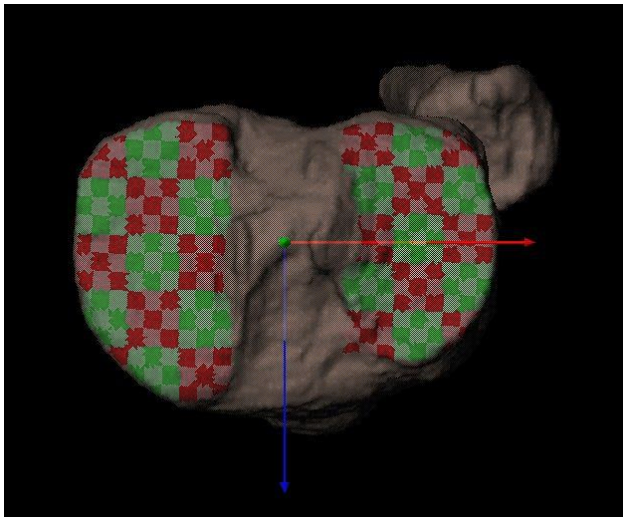

Figure 19. The medial and lateral tibial plateaus are both divided into 3 medial-lateral regions and 5 anterior-posterior regions. These regions are then subdivided into 9 subregions. The figure also shows the defined anatomical axes.

The segmented bone models were then matched to the X-ray images gathered during kinematic testing using a computerized, model-based tracking technique [129,130]. Briefly, custom software created a virtual reconstruction of the testing environment, in which the segmented bone models were manually positioned via ray-traced projections of digitally reconstructed radiographs (DRRs). These manually-placed DRRs were then used as an initial guess for the

computer to automatically manipulate the bone to a position that maximized the correlations between the DRRs and actual radiographs from kinematic testing. This process was repeated for all frames in a trial. The location and orientation of the femur and tibia were then projected into 3D space, and their motions and positions relative to one another were calculated. Figure 20 shows the final product, with a representative joint contact analysis from a single level walking trial. The performance of this system has been extensively validated, with precision in the order of 0.1 mm for *in vitro* testing[129] and averaging 0.6 degrees/0.5 mm for *in vivo* tibio-femoral kinematics during running [131].

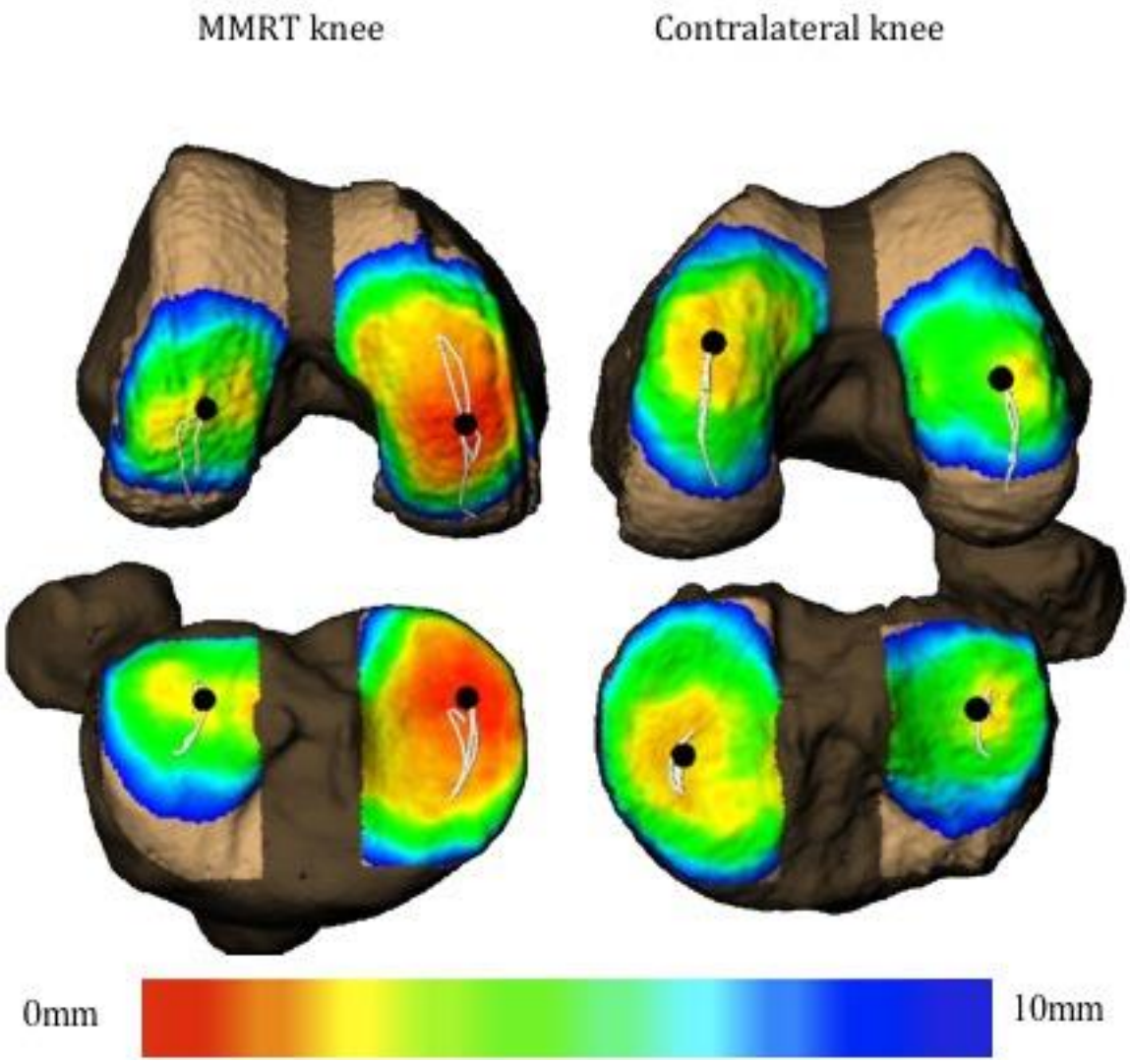

Figure 20. Representative joint contact analysis from a single trial. The image shows affected and unaffected knees opened to compare joint contact patterns. Color maps demonstrate instantaneous joint space (bone-to-bone distances), while black dots demonstrate instantaneous location of joint contact (location of closest bone-to-bone distance) and white lines show the contact path throughout the chosen range of movement.

Kinematic measures were calculated as motion of the tibia relative to the femur, as previously described [138]. Translations were defined as the 3-dimensional distance between the centers of the tibial and femoral coordinate systems, and were separated into anterior-posterior, medial-lateral, and superior-inferior directions. Rotations were similarly calculated of the tibia

relative to the femur, and included flexion-extension, ab/adduction, and external-internal rotation.

Arthrokinematic parameters were determined for the medial and lateral compartments of both knees, as previously described[128]. The instantaneous point of closest contact was calculated for both compartments as the distance-weighted centroid of the region of closest proximity between the femoral and tibial subchondral bone surfaces. Anteroposterior (AP) excursion was defined for both medial and lateral knee compartments as the distance along the AP-axis between the most anterior and posterior tibial contact points. Similarly, mediolateral (ML) excursion was defined as the distance along the ML-axis between the most medial and lateral tibial contact points over the same time interval. Contact path length was calculated as the sum of frame-to-frame differences in contact point location.

3.2.4 Statistics

Limb-to-limb kinematic differences and changes over time or flexion angle were assessed with SPSS software using a two-way repeated-measures ANOVA. Both gait trials were assessed over time, using the interval from 0 to 0.2 seconds following heel strike (corresponding to the loading response phase of gait). While data was collected at 100 frames/s, comparisons were made at 0, 0.06, 0.1, 0.16, and 0.2 seconds after heel strike. Squatting trials were assessed as a function of flexion angle, from 25 to 70 degrees (the maximum range of data that was available across all subjects), and comparisons between limbs were made at 25, 35, 45, 55, and 65 degrees. If the ANOVA reported a significant limb-to-limb difference ($p<0.05$) or a significant limb-by-time/flexion angle interaction ($p<0.10$), post-hoc paired t-tests were performed at all time points/flexion angles (with Holm corrections for multiple pairwise comparisons[139]) to clarify

areas of significance. Arthrokinematic differences were assessed using paired t-tests between the medial and lateral compartments of the affected limb ($p<.05$).

3.3 RESULTS

3.3.1 Tibiofemoral Kinematics

During level walking, lateral tibial translation was greater in the meniscus-injured limb relative to the contralateral, uninjured limb, as shown in Figure 21 (repeated-measures ANOVA; $p=.035$). Specifically, there were greater amounts of lateral tibial translation in the affected limb at 0.15 and 0.20 seconds after heel strike (post-hoc t-tests; $p=0.017$ and $p=0.018$, respectively).

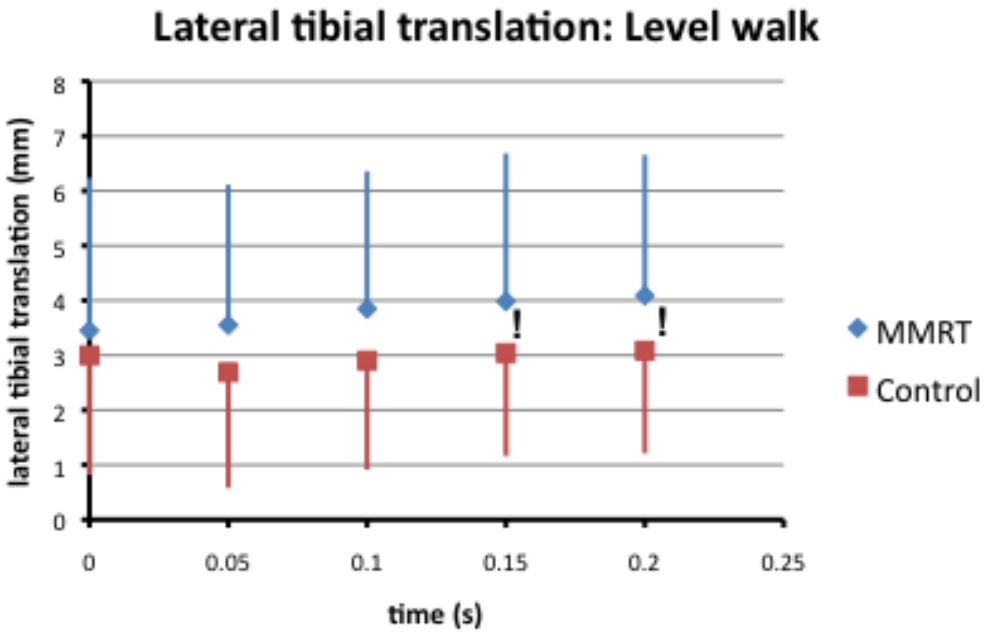

Figure 21. Lateral translation of the tibia with respect to the femur during level walking, where error bars represent standard deviation. ! represents trending differences ($p < 0.02$). The MMRT knee is consistently more laterally translated throughout the range of motion than the contralateral limb.

Results for decline walking were similar to those for level walking, with significantly more lateral translation in the affected limb (repeated-measures ANOVA; p=.015), as seen in Figure 22. Post-hoc testing revealed that the affected limb demonstrated more lateral tibial translation at heel strike, 0.05 and 0.1 seconds after heel strike (post-hoc t-tests, p=0.008, p=0.035 and p=0.019, respectively).

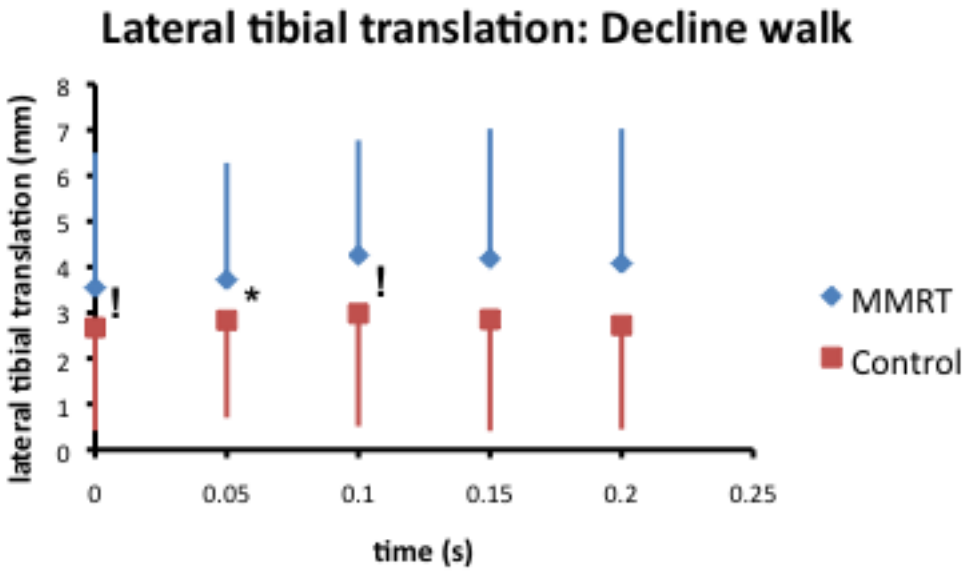

Figure 22. Lateral translation of the tibia with respect to the femur during decline walking, where error bars represent standard deviation. * represents significant differences between limbs (p<0.01), and ! represents trending differences (p<0.05). Again, the MMRT knee is consistently more laterally translated than the contralateral limb throughout the range of motion, and the differences are significant shortly after heel strike.

Squatting also induced significantly more lateral tibial translation in the MMRT limb (repeated measures ANOVA; p=.039), as seen in Figure 23. Significant differences between limbs are seen at 65 degrees of flexion (post-hoc t-tests; p=0.01). Additionally, the MMRT limb is more adducted than the contralateral limb throughout the range of motion (Figure 24), though these differences did not reach statistical significance (repeated measures ANOVA; p=0.155). No other kinematic parameter reached statistical significance in any of the other activities.

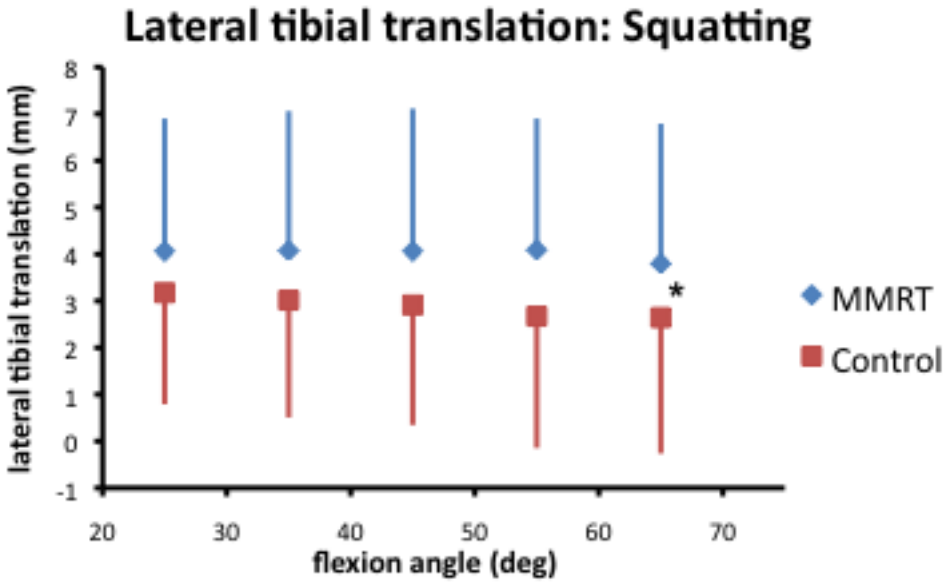

Figure 23. Lateral translation of the tibia with respect to the femur during squatting, where error bars represent standard deviation. * represents significant differences between limbs. Once again, the affected limb exhibits significantly more lateral tibial translation than the contralateral limb.

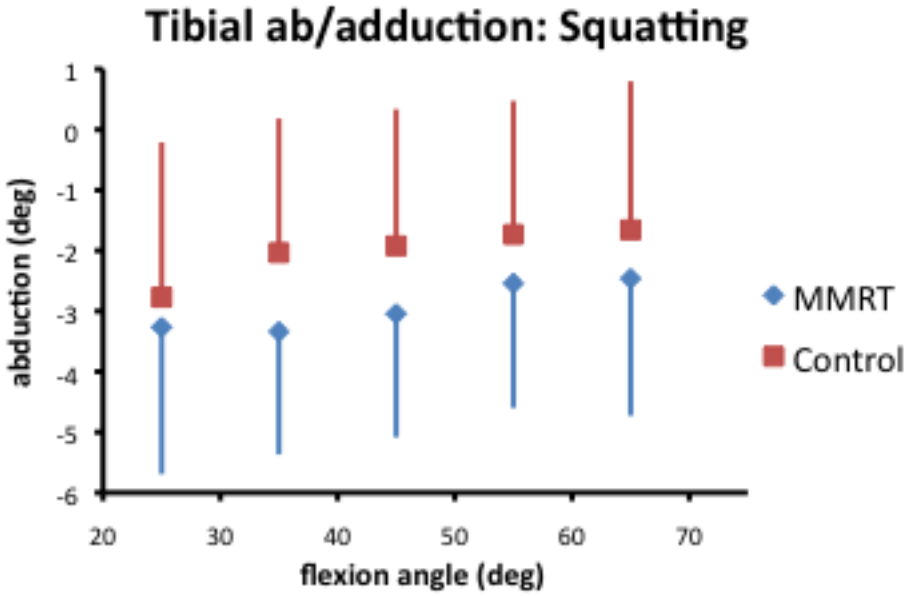

Figure 24. Ab/adduction of the tibia with respect to the femur during squatting, where error bars represent standard deviation. Differences between limbs were not statistically significant, but the MMRT limb is consistently more adducted than the contralateral limb.

3.3.2 Arthrokinematics

There were no arthrokinematic differences between the affected and contralateral limb in any of the tested activities. In the affected limb, however, the medial compartment was found to display more mobility than the lateral compartment. These differences are illustrated in Table 3.

Table 3. Compartmental differences in arthrokinematics (AP excursion, ML excursion, and total path length) in the MMRT limb in the three activities. The medial compartment consistently experiences more excursion and total joint contact path than the lateral compartment. These differences are more pronounced in decline walking when compared to level walking.

Level Walk				**Decline Walk**				**Squatting**			
	med	lat	p-value		med	lat	p-value		med	lat	p-value
AP	3.10	2.21	0.253	AP	1.32	0.671	**0.008**	AP	1.90	1.40	0.450
ML	0.79	0.53	0.134	ML	5.98	4.26	**0.056**	ML	0.59	0.51	0.465
Path	4.47	2.81	**0.021**	Path	7.05	4.81	**0.03**	Path	3.24	1.89	0.115

Specifically, during level walking, the medial compartment exhibited significantly greater total contact path length when compared to the lateral compartment (p=0.021). During decline walking, the medial compartment exhibited significantly more AP excursion (p=0.008) and contact path length (p=0.03) than the lateral compartment.

3.4 DISCUSSION

The most notable result of this study is that all activities elicit lateral tibial translation in the affected limb. This was also found in the *in vitro* cadaver studies. Allaire, at al attribute this lateral tibial translation to the lack of a meniscal buttress against the medial femoral condyle, which allows for the tibia to translate laterally relative to the femur. This explanation appears to hold true *in vivo*. Although it was not found to be significant, the magnitude of lateral tibial translation and arthrokinematic differences were greater in decline walking when compared to level walking. This may suggest that joint instability as a result of MMRT is task-dependent.

Allaire, et al, also found increased adduction resulting from MMRT, specifically at 30° of flexion. This adduction is attributed to the combination of lateral tibial translation with the loss of the medial meniscal spacer between the femur and tibia. This was mirrored *in vivo*, with the affected limb demonstrating increased adduction throughout the range of flexion during the squatting activity. MMRT results in the loss of hoop stresses, causing the observed varus angulation and a previously undescribed lack of dynamic restraint to adduction during loading. These changes may produce a decrease in dynamic medial compartment joint space and allow the knee to rotate into adduction during loading. This varus alignment resulting from MMRT could indicate the presence of early degenerative changes in the articular cartilage that are not yet visible on weight-bearing radiographs.

There are notable differences between the present study and previous *in vitro* findings. Allaire found increased external tibial rotation, which does not appear *in vivo*. This may be attributed to static vs. dynamic loading conditions. *In vitro* studies looking at MMRT apply static loads to cadaver knees at various flexion angles, and thus examine the passive properties of the MMRT knee. These testing conditions are unable to account for the changes in muscle activation and joint motion seen in dynamic activity. Muscle contraction during dynamic activities may stabilize the MMRT joint and restrict tibial rotation.

The increased external rotation seen *in vitro* may dynamically manifest itself as increased joint contact in the medial compartment compared to the lateral compartment in the MMRT knees. These differences in arthrokinematics between compartments may suggest that the medial meniscus plays a large role in constraining femoral condyle motion on the tibial plateau rather than solely dissipating forces. Additionally, the lack of a significant difference between the overall anteroposterior translation of the tibia in the MMRT versus contralateral knees

illustrates that some traditional measures of kinematics may be insufficient to describe the changes that occur with MMRT. The lack of meniscal restraint in the medial compartment seen with MMRT may produce a more complex motion in which the tibia rotates about the intact lateral compartment.

Lateral tibial translation and alterations in arthrokinematics appear to be emphasized in more difficult tasks, which again indicates that joint instability resulting from MMRT may be task-dependent. Research has shown that the medial meniscus plays a significant role in restricting anterior tibial translation and tibial rotation [42]. Decline walking results in more shear forces than level walking, which necessitates greater knee stability. The injured medial meniscus will have an impaired ability to guide knee motion, which leads to greater amounts of lateral tibial translation and medial compartment excursion during more demanding tasks.

There are a few limitations to our study. An a priori power analysis yielded an n of 10 for statistical significance, though for reasons previously discussed, the sample size was cut to 7 for analysis. Additionally, there was large between-subject variability, which may be characteristic of MMRT injuries and impossible to minimize. This being said, it is possible that a larger sample size will lower the data's variability and yield more statistically significant differences resulting from MMRT injury. As previously mentioned, the average age of the subjects was 57.4 years. Although the intended subject population was younger, all younger MMRT patients sustained concomitant injuries and were deemed ineligible for study participation. Future work will examine the *in vivo* kinematics of MMRT repair. *In vitro* studies have found that MMRT repair adequately restores the contact mechanics and kinematics of the injured knee, and it is unknown if these results will also be seen *in vivo*.

3.5 CONCLUSION

This study is the first one of our knowledge to investigate the *in vivo* kinematics of an unrepaired medial meniscal root tear. MMRT is severe in the spectrum of meniscal injuries in that it is often misdiagnosed and leads to a rapid progression of osteoarthritis. This injury results in the complete loss of circumferential fiber function, hindering the ability of the meniscus to distribute load and/or guide femoral motion. Knowledge of the kinematics and arthrokinematics resulting from this injury may shed light on the mechanism of osteoarthritis progression in this population, and assist in the development of effective repair techniques. Additionally, this study may serve as a baseline for more common meniscal injuries and treatments, such as partial meniscectomy, where some of the circumferential fiber function is retained. Therefore it is possible that the small, statistically insignificant lateral tibial translation seen in the PM subjects of Chapter 2 may have an effect over time on the development of OA.

The results of this study are useful to relate the kinematics resulting from medial meniscal injury to altered loading patterns and possibly the mechanical development of OA after injury. Since we do not know the cartilage grades of these subjects, however, we can not link the altered kinematics resulting from MMRT to early cartilage damage. In order to further the development of our clinical diagnostic to detect softened cartilage, we need to continue examining the results of Chapter 2 where the subjects have known cartilage grades.

4.0 EVALUATION OF QUALITATIVE IN VIVO VISCOELASTIC MODELING OF TIBIOFEMORAL JOINT SPACE AS AN INDICATOR OF EARLY CARTILAGE DAMAGE

In Chapter 2 it was established that functional differences exist *in vivo* between joints with grade 0 and grade 1 articular cartilage. These differences are only apparent, however, during creep tests where a sustained force is applied for a certain amount of time. Creep testing is often performed *in vitro* to assess the mechanical properties and behavior of articular cartilage plugs, and researchers are able to model the experimental data with viscoelastic or mixed models. These models allow for the quantification of mechanical behavior, and comparisons can then be made between different types of tissues.

The results of Chapter 2 suggested that the joint is behaving viscoelastically during the leg press activity. That being said, we will attempt to model the creep behavior of the joints with different grades of articular cartilage using a simple spring-dashpot model. This represents the first time that *in vivo* joint behavior has been modeled viscoelastically. Modeling will be deemed a success if it is able to adequately fit the experimental data and give material properties that are clinically and physiologically meaningful.

4.1 INTRODUCTION

Osteoarthritis (OA) is characterized by the deterioration of articular cartilage[140]. Though typically reported in older patients, studies have shown that meniscal injury and partial meniscectomy may trigger the early onset of OA[43,44]. Partial meniscectomy patients have a 50% risk for the development of OA[54], and typically do not recognize the symptoms until the disease has progressed to an irreversible state. Often during partial meniscectomy or other arthroscopic procedures, surgeons identify areas of "softened" articular cartilage. These areas are undetectable using traditional radiographs and have few visible signs of damage, but are softer than healthy tissue when arthroscopically probed during surgery. Cartilage softening has been related to changes in the tissue's collagen matrix[109]. These alterations could represent early structural damage that can lead to irreversible cartilage damage and OA.

Several researchers have viscoelastically modeled the *in vitro* mechanical behavior of articular cartilage to characterize arthritic changes in the tissue. These models attempt to characterize the elastic and viscous components of articular cartilage in order to obtain material properties that make physiological sense regarding the known biology of cartilage. Biphasic[20,141], triphasic[17], and poroelastic theory[29,142], among many others[143,144], have been used to characterize varying states of articular cartilage under various loading conditions. All of this work had led to an abundance of knowledge regarding the material properties of this tissue. While this research is critical for the development of tissue-engineered therapies for OA, it cannot be directly applied *in vivo*.

Previous work in Chapter 2 has found differences between the *in vivo* load-response curves of subjects with healthy and softened articular cartilage. Subjects with softened articular cartilage experience significantly larger amounts of joint space compression as a result of

sustained force application when compared to individuals with healthy articular cartilage. Upon further inspection, the load-response curves closely resemble those seen during *in vitro* creep testing of viscoelastic materials. Therefore, viscoelastic modeling of *in vivo* creep testing may elucidate on material properties that distinguish subjects with early cartilage damage.

Because of the complexity of the knee joint *in vivo*, we will model previously observed displacements with spring-dashpot models of viscoelasticity. Specifically, we will pursue the Voigt model and standard linear solid (SLS) model to simulate creep testing *in vivo* (Figure 25). These two models were formulated to model the displacement of a viscoelastic material in response to a sustained force, and have been used to model articular cartilage *in vitro*[145,146]. The difference between the two models is the extra spring term in the SLS model, which allows for the accurate modeling of materials with large amounts of deformation immediately after force application. The spring and dashpot elements that comprise these models are able to capture the elastic and viscous nature of a viscoelastic material, respectively. Biologically, the spring element may model the solid collagen matrix, while the dashpot can model the interstitial water of articular cartilage.

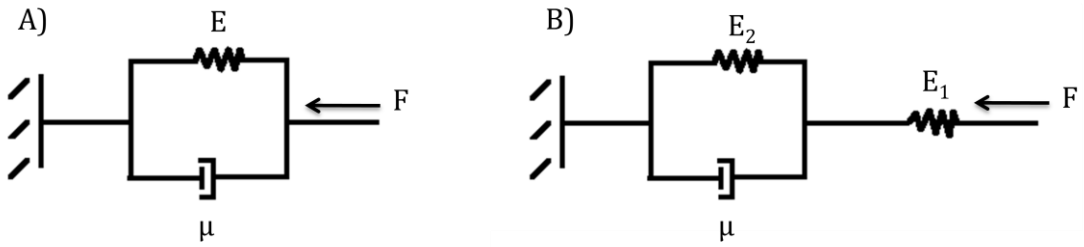

Figure 25. Visual representations of the Voigt model (A) and SLS model (B) during creep testing

The purpose of this study is to use a viscoelastic model to accurately depict the *in vivo* response of the knee to a creep load, and to determine material properties that are able to distinguish between subjects with healthy and softened articular cartilage. We hypothesize that

the simplicity of the spring-dashpot models will adequately characterize *in vivo* creep behavior. Additionally, we hypothesize that subjects with softened articular cartilage will have smaller elastic moduli than subjects with healthy cartilage.

4.2 METHODS

4.2.1 Subjects

19 subjects participated in this University of Pittsburgh IRB-approved study and were separated into 3 groups – partial medial meniscectomy (PM) subjects with softened articular cartilage (n=5, 4M, 1F), PM subjects with healthy articular cartilage (n=4, 2M, 2F), and age/sex matched healthy controls (n=10, 6M, 4F). Table 4 details subject demographics.

Table 4. Demographics of participating subjects

	PM softened	PM healthy	Uninjured control
Number of subjects	5	4	10
Age	44.0 ± 8.5 years	32.5 ± 5.9 years	35.8 ± 12.2 years
Sex breakdown	1F, 4M	2F, 2M	4F, 6M
Concomitant ACLr	3	1	N/A
BMI	28.0 ± 4.3	23.5 ± 4.0	24.0 ± 3.7

Articular cartilage status was graded during arthroscopy using the International Cartilage Repair Society (ICRS) scale, where grade 0 represents healthy cartilage and grade 1 represents softened cartilage[73]. Patients from a group of four surgeons at the University of Pittsburgh Medical Center participated in the study, and all surgeons had experience grading with the ICRS scale. Exclusion criteria for the study included previous injury/surgery to the affected limb,

lateral compartment injury, age outside of the 25-55 year range, BMI >35, and concomitant injury to other structures in the knee not including the anterior cruciate ligament (ACL). Subjects participated between 2-12 months post-surgery if they underwent an isolated PM, or between 6-12 months post-surgery if they underwent ACL reconstruction with concomitant PM.

4.2.2 Kinematic Testing

Subjects performed a step-loading activity that utilized a modified leg press machine, where weight equivalent to half of the subject's body weight was applied to the affected leg at full extension, as shown in Figure 26. Before testing, subjects rested supine for thirty minutes to allow for the articular cartilage to return to its unloaded state.

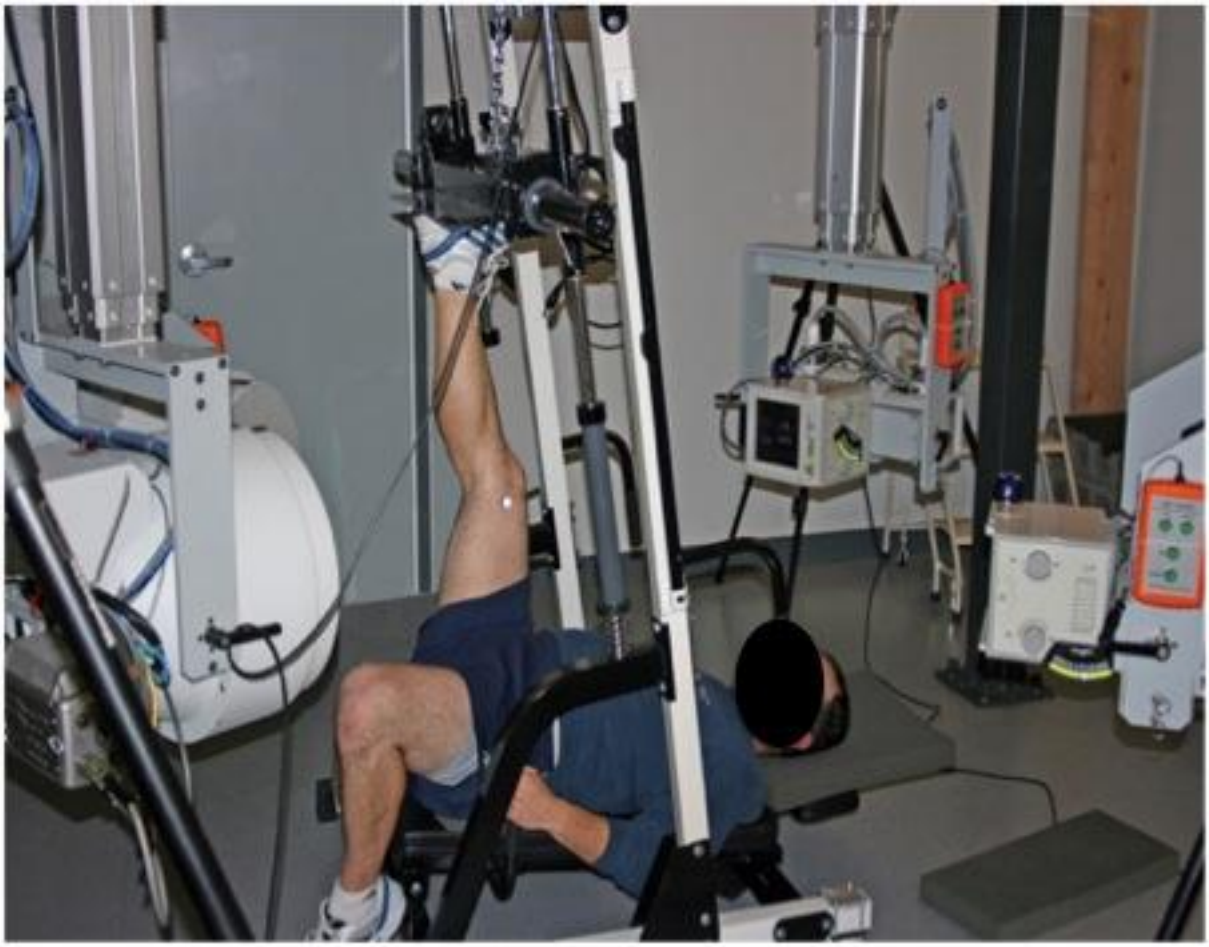

Figure 26. Modified leg press used in kinematic testing. Same legpress used in Chapter 2.

Testing was performed within the dynamic stereo X-ray (DSX) system, which uses biplane radiography during dynamic trials to characterize joint motion. X-rays were generated with 1ms pulse widths at 90 kV/200 mA, and were collected using 40 cm image intensifiers (Thales, Inc.). Both image intensifiers were placed 180 cm from their respective X-ray source, and were coupled with a 4 megapixel, 14 bit digital video camera (Phantom 10, Vision Research, Inc.). Stereo-radiographic images were captured at varying frame rates to characterize the different areas of the load-deformation curve. X-rays were first captured at 50 frames/s from 0.4 seconds before the weight was released until 0.8 second after the weight was released, and then at 4 frames/s for the next 19 seconds. We then collected 10-frame bursts at 150 frames/s in one-

minute increments until the subject had held the weight for 5 minutes, or was too fatigued to continue.

4.2.3 Data Processing

In addition to kinematic testing, all subjects underwent a unilateral CT scan. The scans were segmented with Mimics (Materialise Inc., Ann Arbor, MI, USA) to create subject-specific bone models of the femur and tibia using a previously described method [127,128]. The segmented bone models were then matched to the X-ray images gathered during kinematic testing using a computerized, model-based tracking technique [129,130]. Briefly, custom software created a virtual reconstruction of the testing environment, in which the segmented bone models were manually positioned via ray-traced projections of digitally reconstructed radiographs (DRRs). These manually-placed DRRs were then used as an initial guess for the computer to automatically manipulate the bone to a position that maximized the correlations between the DRRs and actual radiographs from kinematic testing. This process was repeated for all frames in a trial. The location and orientation of the femur and tibia were then projected into 3D space, and their motions and positions relative to one another were calculated.

4.2.4 Tibial Plateau Profiles

In order to identify the area of the tibial plateau where softened cartilage can be distinguished from healthy cartilage, tibiofemoral joint space was extracted for each frame from the anterior, central, ridge, and posterior areas of both the medial and lateral tibial plateaus, shown in Figure 27. These joint space values were normalized to the unloaded joint space value at the beginning

of the trial by dividing each joint space value by the unloaded joint space. Normalized change in joint space was then transformed to creep displacement by subtracting each subsequent normalized joint space value from the normalized unloaded joint space value. Normalized displacement values were then averaged together by group at each time point. Normalized joint space was only calculated for the initial phase of loading, or the first 20 seconds.

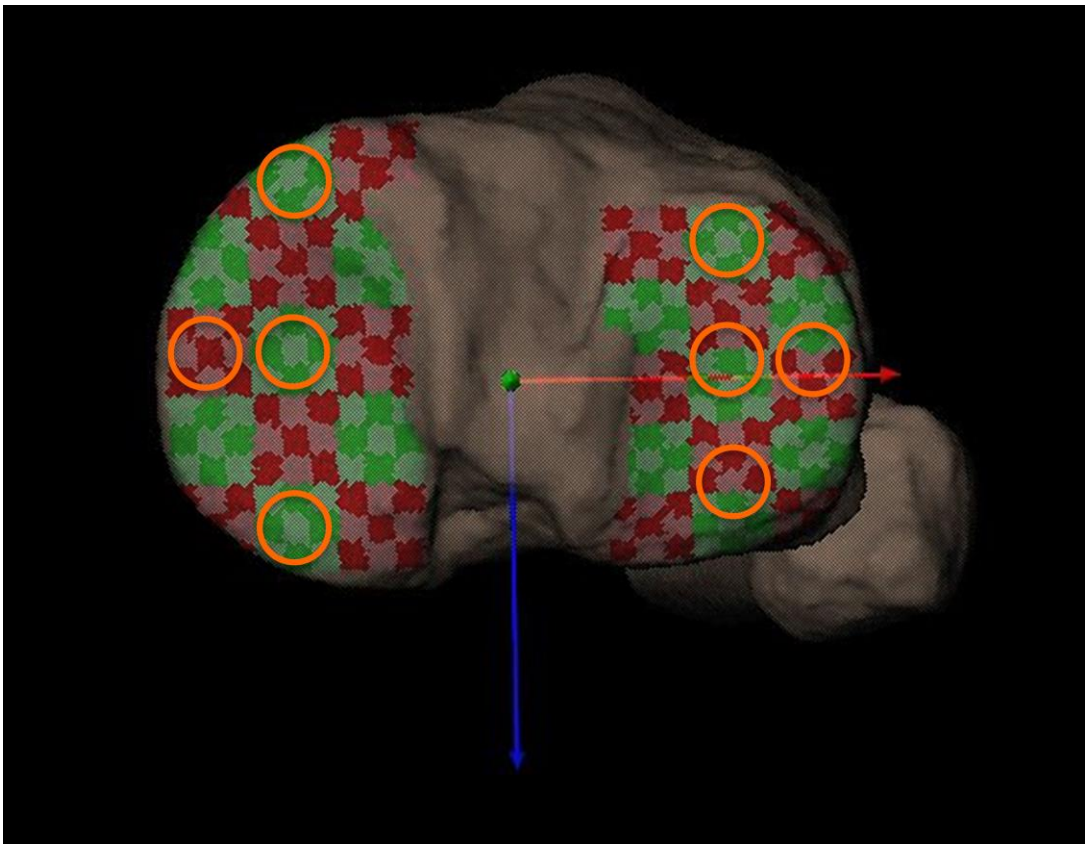

Figure 27. Tibia with anatomical axes and defined subregions. The orange circles correspond with the subregions on the medial and lateral plateaus where joint space measurements were taken for each subject and trial.

4.2.5 Viscoelastic Modeling

The creep response of both the Voigt model (Equation 9) and standard linear solid model (Equation 10) were fitted by group in all regions of both compartments using Matlab

(Mathworks, Natick, MA). Material properties were determined for each model using a nonlinear optimization function that minimizes the squared differences between the experimentally-observed and the model-predicted normalized displacements. Since all material properties represent stiffness or viscosity values, the parameters were constrained to be positive numbers. SLS modeling yielded E_1, E_2, and μ values for each prediction, while Voigt modeling gave E and μ material properties. Coefficient of determination (R^2) was used to determine the closeness of fit, as defined in Equation 11.

$$J(t) = \frac{1}{E}(1 - e^{\frac{E}{\mu}t})$$

Equation 9. Creep response of the Voigt model

$$J(t) = \frac{1}{E_1} + \frac{1}{E_2}(1 - e^{\frac{E_2}{\mu}t})$$

Equation 10. Creep response of the standard linear solid (SLS) model

$$R^2 = 1 - \frac{\Sigma(y_{pred_i} - y_{obs_i})^2}{\Sigma(y_{obs_i} - \overline{y_{obs}})^2}$$

Equation 11. Coefficient of determination (R^2) to determine closeness of fit

4.2.6 Modeling with Fewer Timepoints

Once the optimal model was determined, we attempted to replicate the viscoelastic modeling of the initial loading phase with fewer timepoints. Using fewer timepoints will assist in the

translation of this method into a clinical diagnostic for the detection of softened cartilage. 60% of the joint space compression was previously found to occur in the initial second of loading, regardless of cartilage grade, while 75-80% of the total deformation was found to occur in the first 20 seconds of loading. This being said, we chose non-weight bearing, 0.5, 1.0, and 20.0 seconds after loading as our timepoints to fully characterize the creep response with as few timepoints as possible. Model fit and material properties were again optimized for each subject group using Matlab, and R^2 was used to determine the closeness of fit. Comparisons were made between the fit using the total initial loading phase and the fewer timepoints to assess the ability of the fewer timepoints to characterize the creep response during initial loading.

4.3 RESULTS

4.3.1 Tibial Plateau Profiles

Construction of the medial and lateral tibial plateau profiles indicated that meniscal status and cartilage grade influence the joint's creep response, and Figure 28 shows the medial plateau profile. No differences were observed between any of the groups in any subregions of the lateral tibial plateau. Similarly, no differences were observed between groups in the anterior portion or medial edge of the medial tibial plateau. In the posterior region of the medial plateau, however, both groups who underwent partial meniscectomy exhibited significantly more compression than the uninjured control groups ($p=0.036$, repeated measures ANOVA, SPSS version 19). Previous work found that significant differences exist between PM subjects with varying cartilage grades in the central portion of the medial tibial plateau.

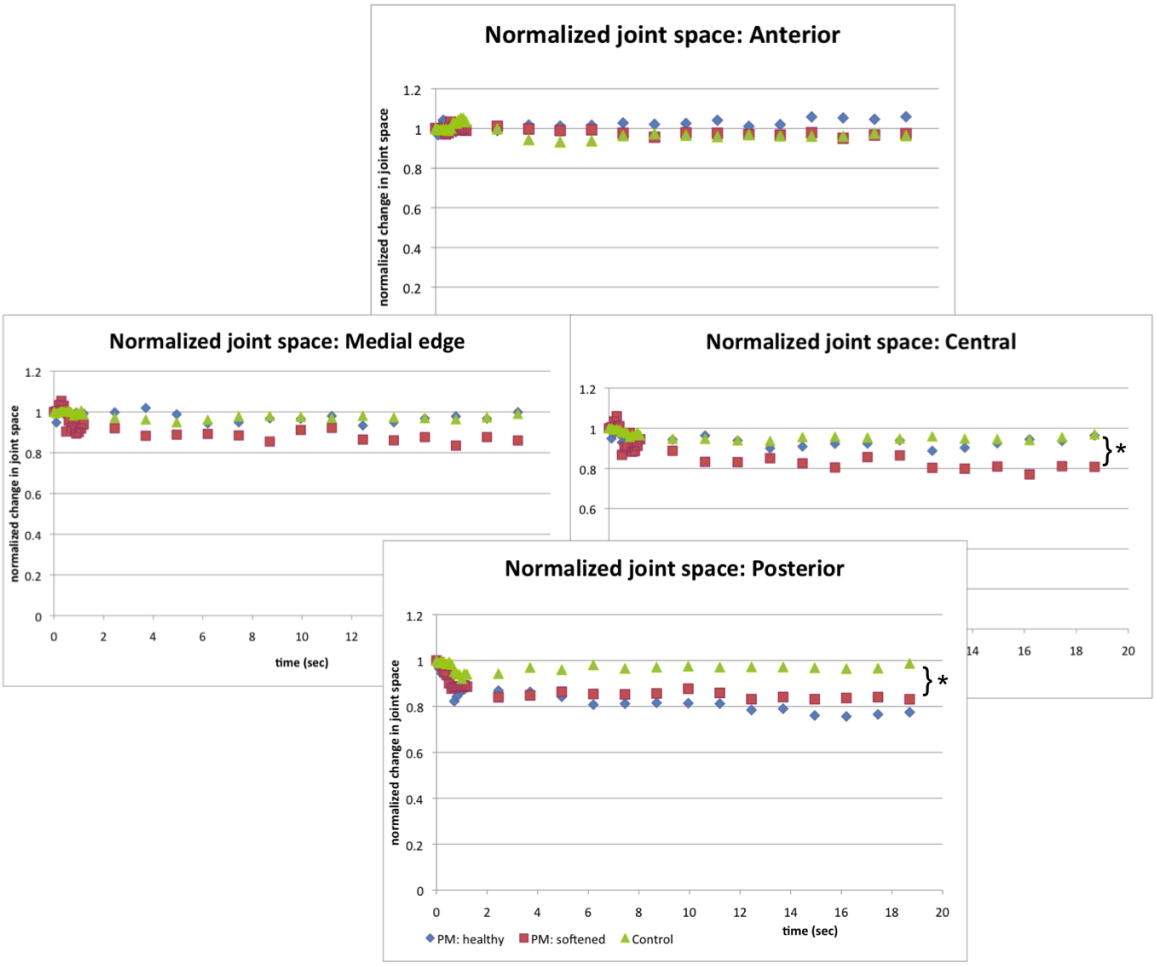

Figure 28. Joint space profile during creep testing of different regions of the medial tibial plateau. The placement of the plots relative to each other represents a top-down view of the medial meniscus. * represents significant differences between groups, seen in the posterior region and the central region.

4.3.2 Viscoelastic Modeling

Both models fit the data similarly. The central subregion of the medial tibial plateau was the only area where the PM softened group exhibited a different load response than the other groups, likely because this region was scored as grade 1 during surgery. The model fits in this central subregion of the medial tibial plateau were used to determine the optimal viscoelastic model for the *in vivo* data. The observed and model-predicted displacements are shown in Figure 29 and

30 for each group after Voigt and SLS modeling, respectively. The data from one of the PM healthy subjects was discarded after significant movement was observed while the subject held the weight at full extension, resulting in a larger flexion angle and inconsistent measurements of joint space.

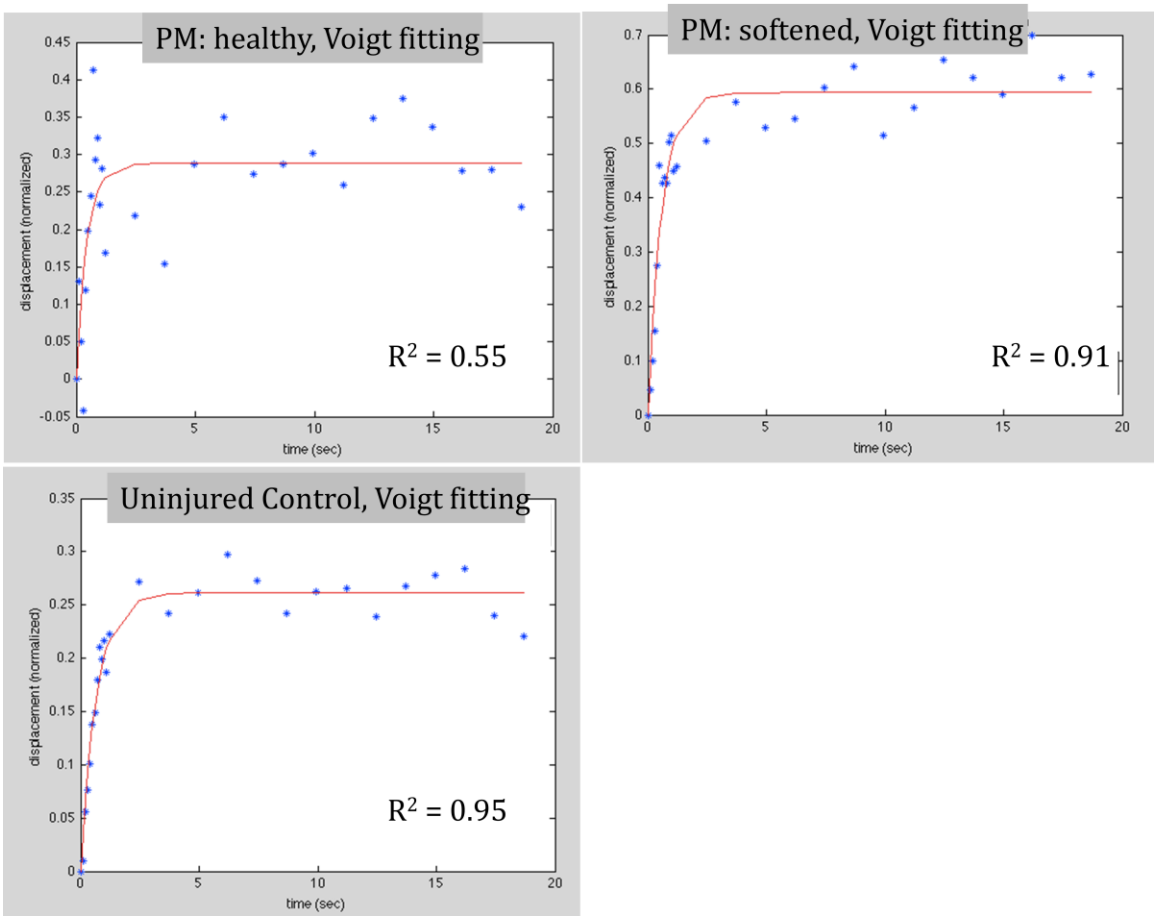

Figure 29. Voigt modeling of the total initial phase of the affected knee during creep testing at full extension. The blue data points represent experimentally-observed displacement, and the red lined it the Voigt model fitted to each data set.

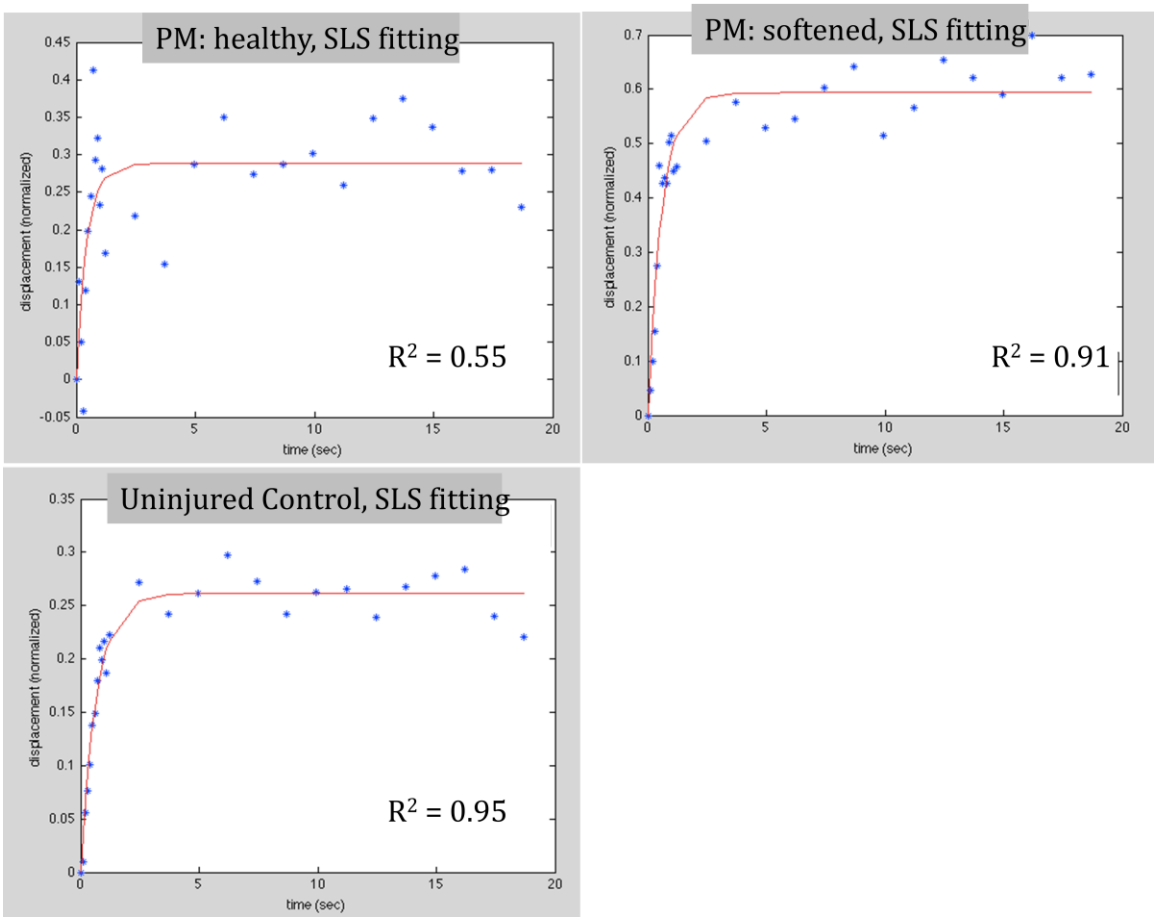

Figure 30. SLS modeling of the total initial phase of the affected knee during creep testing at full extension. The blue data points represent experimentally-observed displacement, and the red lined it the SLS model fitted to each data set.

Tables 5 and 6 show the stiffness and viscosity values for the central subregion of the medial plateau resulting from Voigt and SLS modeling, respectively. The elastic modulus is smaller for the PM softened group than for the PM healthy or uninjured control groups. Additionally, both PM groups exhibit a lowered viscosity value when compared to the uninjured control group. The E_1 term in SLS modeling, however, is less consistent or meaningful between groups. The added complexity of the SLS model does not help the fit of the prediction, so the Voigt model is deemed the best fit for this *in vivo* data.

Table 5. Material properties and coefficient of determination from Voigt modeling of the entire initial phase of loading

	Elastic Modulus (E)	Viscosity (μ)	R^2
PM: healthy	3.47	1.54	0.55
PM: softened	1.68	0.99	0.91
Uninjured Control	3.82	2.59	0.95

Table 6. Material properties and coefficient of determination from SLS modeling of the entire initial phase of loading

	E_1	E_2	μ	R^2
PM: healthy	$1.38x10^8$	3.47	1.54	0.55
PM: softened	$3.20x10^7$	1.68	0.99	0.91
Uninjured Control	$6.65x10^6$	3.83	2.59	0.95

4.3.3 Modeling with fewer timepoints

Voigt modeling with fewer timepoints adequately characterized the initial phase of loading. The material properties and R^2 values were similar to those seen when modeling the entire initial phase of loading (Table 7). Notably, the modeling fit the PM healthy group much better using fewer timepoints, though the material properties are still fairly similar between models.

Table 7. Material properties and coefficient of determination from Voigt modeling using non-weightbearing, and 0.5, 1,0 and 20 seconds after loading.

	E	μ	R^2
PM: healthy	4.28	1.13	0.999
PM: softened	1.65	0.65	0.99
Uninjured Control	4.40	2.07	0.99

4.4 DISCUSSION

Viscoelastic behavior is observed during *in vivo* creep loading of the knee, specifically, in the central subregion of the medial tibial plateau. The complexity of the knee, including the meniscus, articular cartilage, and synovium, left questions as to whether or not the known viscoelastic nature of articular cartilage would be visible *in vivo.* The central subregion, however, is uncovered by the medial meniscus. The lack of fibrocartilage leaves the articular cartilage to be the sole determinant of the joint displacement in this area of the tibial plateau.

Because of the lack of meniscal distraction in the central region of the medial plateau, differences between cartilage grades are apparent. Group differences in joint compression are also visible in the posterior region of the medial tibial plateau, though it is because of meniscal status and not cartilage grade. All of the PM subjects sustained injuries in the posterior horn of the medial meniscus, and this region of the tissue has been partly removed in all surgical subjects. These differences are not visible in the anterior region or anywhere in lateral compartment, where meniscal tissue is intact in all subjects regardless of cartilage grade.

Additionally, the articular cartilage of the lateral compartment was graded as healthy (grade 0) in all subjects, which explains the similarities between groups in the central region of the lateral plateau.

The Voigt model is able to sufficiently characterize the viscoelastic behavior of the central region in the medial tibial plateau during the initial phase of loading. Because of the complexity of the in vivo conditions, this modeling is more qualitative than quantitative in nature. The elastic modulus and viscosity values from this modeling do not reflect the material properties of the articular cartilage or other specific knee structures, they are qualitative measures of the stiffness and viscosity of the knee joint *in vivo*. Importantly, however, the material properties from modeling each group make physiological sense. A major conclusion of both the Voigt and SLS modeling was that the elastic modulus is lowered in the softened articular cartilage group when compared to the groups with healthy articular cartilage, which supports our initial hypothesis. If the spring term of the spring-dashpot models is analogous to the solid collagen matrix of articular cartilage, the lowered elastic modulus of the grade 1 subjects implies deficiencies in this solid matrix. This assertion is supported by *in vitro* studies that have shown that grade 1 cartilage plugs exhibit lower stiffness values when compared to grade 0 samples[77]. This observation is also seen clinically during surgery, where grade 1 cartilage is identified by the tissue's softness in response to being probed. OA is known to being at the articulating surface of articular cartilage[18], and the lowered elastic modulus of softened articular cartilage reflects mechanical damage to the superficial zone.

Additionally, modeling indicates that the PM groups have lowered viscosity values when compared to the uninjured control groups. The viscosity term implies the joint's ability to disperse load throughout the joint. Therefore the subjects with an impaired medial meniscus

have joints that are less able to disperse load evenly around the joint. Circumferential hoop stresses allow the meniscus to function during compression to disperse load evenly across the tibial plateau[39]. Partial meniscectomy disrupts this function of the medial meniscus, which is apparent in Voigt modeling.

The results of this study also suggest that the initial loading phase can be accurately modeled by 4 specific timepoints. Using fewer timepoints will necessitate fewer X-rays to detect early cartilage damage. This will decrease the radiation for both the patient and health professional, and will further simplify the technique to allow for enhanced ease of use and repeatability. The material properties are similar to what was seen during modeling of the full initial load, and the parameters continue to make sense physiologically. Interestingly, the viscosity term did not converge as easily as when modeling with more points. This is because the viscosity term is more dependent on the long-term creep response. To remedy this, we tried including an additional data point at 1 minute of loading. The inclusion of this data point sacrificed the integrity of the initial phase and stiffness values, however, and did little to help the viscosity values converge. This being said, modeling with four timepoints gives R^2 values that are still adequate and elastic moduli that are consistent.

There are a few limitations to this study. It was difficult to recruit subjects who were eligible for participation given the strict enrollment criteria, which led to small sample sizes of the PM groups. This being said, the modeling is based off of previous work that found statistical significance between groups using this subject set. Additionally, 4 surgeons participated in this study, which may have left the PM subjects with inconsistently-graded cartilage. This inconsistency may be the reason why the PM group with grade 0 cartilage had consistently lowered R^2 values – all subjects of the group may not have actually had grade 0 cartilage if

graded by a single surgeon. The purpose of this work, however, is to develop a more quantitative method to classify cartilage integrity, which could supplement surgical findings and reduce future variability. Finally, the complexity of the in vivo loading may not yield stiffness and viscosity values that are similar to what has previously been found using cartilage plugs and a more controlled system. This work should be considered a qualitative model as opposed to quantitatively defining the material parameters of softened and healthy articular cartilage.

4.5 CONCLUSION

The results of this chapter indicate that the Voigt model is able to fit experimental data from softened and healthy joints, representing the first time viscoelastic modeling has been used to model *in vivo* joints. More importantly, however, the material properties are different and meaningful between groups, providing additional insight on the differing mechanical behavior and physiology of subjects with healthy and softened cartilage. The determination of the fewer timepoints that can adequately characterize the creep response of the joints, indicates that we will be able to capture fewer X-rays during a clinical diagnostic, thus making the method more feasible for the orthopaedic clinic.

The next step in developing a clinical diagnostic for the detection of early cartilage damage is to translate the legpress setup into something that is simple, repeatable, and executable given the constraints and resources in orthopaedic clinics. These results will then be modeled with the Voigt model to compare material properties between groups and develop simple parameters that delineate the groups from each other.

5.0 DEVELOPMENT OF A CLINICAL DIAGNOSTIC TO FUNCTIONALLY DETECT EARLY CARTILAGE DAMAGE IN VIVO

As discussed in Chapters 2 and 4, we are able to detect and model differences in ICRS cartilage grade using an *in vivo* creep test. We would now like to translate the methodology and findings into something that is feasible for the orthopaedic clinic. Such a diagnostic will need to be simple for health professionals to easily and reliably perform on subjects at risk for the development of OA. This tool could quickly inform a subject of their risk of having early cartilage damage and later developing OA. Therefore subjects may choose to modify his or her lifestyle or pursue OA-modifying treatments before the cartilage damage has spread to an irreversible state.

Since most clinics do not have access to biplane X-ray systems and the cost of such analyses is prohibitively expensive, we will attempt to replicate the results from the legpress study using both the traditional biplane radiography and single-plane analyses. Additionally, the difficulty of the leg press task deems it inadequate for clinical use. Therefore we will pursue another way to elicit a creep response in the knee joints.

5.1 INTRODUCTION

Osteoarthritis, or OA, is characterized by the degeneration and deterioration of articular cartilage[140]. OA is most commonly reported in the knee[7], and results in diminishing joint function and the loss of patient mobility[147,148]. While the disease most commonly affects older patients[31], musculoskeletal injury has been implicated as a risk factor for the early-onset of knee OA[149]. Anterior cruciate ligament reconstruction (ACLr) and medial meniscal injury have been linked to the development of OA[43,44], though not all patients who sustain these injuries and procedures will go on to develop the disease. In fact, it's been reported that 40% of ACL reconstructions result in OA[150], while 50% of patients who undergo partial medial meniscectomy develop OA[54]. It is unknown why certain patients will later present with OA while others maintain healthy cartilage.

Studies have found that cartilage damage begins at the superficial zone and spreads through the tissue until it reaches subchondral bone[18]. Superficial zone damage is apparent to surgeons during arthroscopic surgery, and is identified by its slight softening during probing compared to healthy tissue. This type of damage is quantified by the International Cartilage Repair Society (ICRS)[73], and corresponds with grade 1 on the ICRS cartilage scoring system. Superficial zone cartilage damage is correlated with increased matrix disorganization[109], which lead to compromised mechanical properties under load[77] and cartilage softening.

Several imaging and biological biomarkers have been developed to detect OA in vivo[92,151-154]. These methods attempt to detect the elevated water content that is associated with OA. Certain MRI and ultrasound modalities have been shown to distinguish grade 1 articular cartilage from healthy tissue[94,95,155]. Though these methods are promising, they are largely dependent on the facility's hardware and software, and have varying degrees of accuracy[96].

Additionally, they only identify damaged tissue by water content, which may not always correlate with mechanical softening and do not address the functionality of early cartilage damage. There is no diagnostic method that assesses the presence of softened tissue via the functionality of the affected joint.

Previous work in Chapter 2 detected the presence of softened cartilage using an *in vivo* creep test. Subjects were situated in a modified leg press, and held half body weight with their affected limb for 5 minutes while biplane X-ray images were periodically captured of the joint. Results showed that joints with softened cartilage (grade 1) compressed significantly more than joints with healthy (grade 0) cartilage. Additionally, viscoelastic modeling of these creep curves in Chapter 4 showed that joints with softened cartilage were characterized by a smaller elastic modulus than healthy joints. The complexity of the testing setup, however, did not lend to a simple clinical diagnostic that can be used by health professionals.

The purpose of the present study is to translate previous results into a diagnostic method that can be performed in the orthopaedic clinic to detect softened articular cartilage. We hypothesize that joints with softened cartilage will exhibit significantly more medial compartment joint compression than joints with healthy cartilage using both biplane and single plane analyses. Additionally, we hypothesize that Voigt modeling of the results will again show that that the joints with softened cartilage exhibit a lowered elastic modulus than joints with healthy cartilage.

5.2 METHODS

5.2.1 Subjects

13 subjects participated in this University of Pittsburgh IRB-approved study. Subjects had all undergone ACLr two years before testing, and were classified intraoperatively as having grade 0 (n=7) or grade 1 (n=6) articular cartilage in accordance with the ICRS grading scale. ACLr was performed by a surgeon from a group of 3 surgeons at the University of Pittsburgh Medical Center, and surgeons randomly performed either single or double-bundle ACLr with a quadriceps tendon autograft. Subjects were included in the present study if they exhibited either grade 0 or diffuse grade 1 articular cartilage on their medial tibial plateau, had a healthy, uninjured contralateral limb, were between the ages of 16 and 45 years old, and had a BMI under 30. Subjects were ineligible to participate if they had more than 1/3 of the medial meniscus removed, had sustained a concomitant ligamentous or lateral meniscus injury in the affected limb, or had reinjured the affected limb between surgery and testing. Because medial meniscal injury occurs so commonly with ACL injury, and previous work showed that we are able to separate meniscal injury from cartilage status, we did not exclude subjects with a concomitant medial meniscal injury. Table 8 shows the demographics of both groups.

Table 8. Demographic information of subjects in the grade 0 and grade 1 groups. No significant differences were seen in age at testing, sex, BMI, concomitant injury, type of quadriceps allograft, or time to surgery.

	Grade 1	**Grade 0**
Age	22.17 ± 6.56 years	24.43 ± 9.91 years
Sex	4 male 2 female	5 male 2 female
BMI	24.07 ± 3.51 kg/m^2	26.23 ± 2.66 kg/m^2
Concomitant Injury	1 no meniscal injury 1 stable meniscal tear 2 meniscal repairs 2 partial meniscectomy	1 no meniscal injury 4 stable meniscal tears 2 meniscal repairs
Type of quadriceps autograft	1 double bundle 5 single bundles	1 double bundle 6 single bundles
Time to Surgery	120.00 ± 124.92 days	155.86 ± 124.70 days

5.2.2 Kinematic Testing

Subjects were first positioned within the dynamic stereo X-ray (DSX) system to ensure the X-ray imaging of both the affected and contralateral limb simultaneously during testing. Feet positions were recorded on the floor so that subjects would be able to place themselves in the correct location when transitioning from sit to stand. Subjects were then instructed to rest and remain non-weightbearing for 30 minutes on a clinical examination table that was also situated within the DSX system. After the 30-minute rest period, subjects were instructed to transition from sitting on the exam table to standing on the pre-defined locations, while maintaining their legs in extension. The clinical exam table was set at a subject-specific height so that the subject was able to slide off the table and transition from non-weight bearing to weight bearing with minimal change in flexion angle. The subject then stood for 3 minutes, and was instructed to remain still and not shift his/her weight. The testing setup is shown in Figure 31.

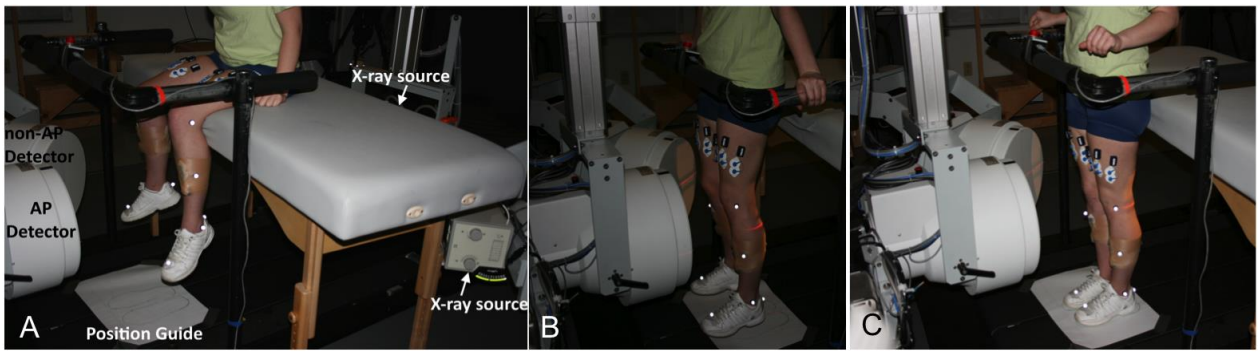

Figure 31. Subject positioning within the DSX system during the 30 minute rest period (A) immediately before weight-bearing, when the initial X-ray capture is triggered (B) and while standing (C)

Biplane X-rays were generated with 1 ms pulsed exposures at 80 kV/200 mA (or less, depending on subject size), with a source-to-detector distance of 1.8 m and an inter-beam angle of approximately 60 degrees. Each 40 cm image intensifier (Thales, Inc.) was coupled with a 4 megapixel, 14 bit digital video camera (Phantom 10, Vision Research, Inc.). Image acquisition occurred simultaneously for both cameras, synchronized with X-ray pulse generation. Stereo X-rays were captured at 4 frames/second for the first 2.5 seconds of testing. This initial X-ray capture was triggered while the subjects were transitioning from sit to stand but were still non-weightbearing, in order to capture images of the resting joint space and immediately after standing. Another X-ray was captured at 20 seconds after standing, and a final burst of 10 frames was captured at 150 frames/second at 3 minutes after standing. This testing was performed on forceplates so that we could determine when the subjects transitioned from non-weightbearing to weightbearing.

5.2.3 Biplane Data Processing

All subjects underwent a bilateral CT scan (0.6 mm slices including 10 cm above and below the joint line). Scans were then segmented with Mimics (Materialise Inc., Ann Arbor, MI, USA) to create subject-specific bone models of both femurs and tibias using a previously-described method [127,128]. The segmented bone models were then matched to the X-ray images gathered during kinematic testing using a computerized, model-based tracking technique [129,130]. Briefly, custom software created a virtual reconstruction of the testing environment, in which the segmented bone models were manually positioned via ray-traced projections of digitally reconstructed radiographs (DRRs). These manually-placed DRRs were then used as an initial guess for an algorithm that automatically manipulated the bone to a position that maximized the correlations between the DRRs and actual radiographs. The results from two adjacent frames were then used to project an initial guess for the subsequent frame, and the optimization process was repeated for all frames in a trial. The location and orientation of the femur and tibia were then projected into 3D space (Figure 32A-C), and their motions and positions relative to one another were calculated. The performance of this system has been extensively validated, with precision in the order of 0.1 mm for *in vitro* testing[129] and averaging 0.6 degrees/0.5 mm for *in vivo* tibiofemoral kinematics during running [131].

The tibiofemoral joint space was extracted for each frame at the dominant subregion, and the ten joint space values were averaged together for the 3 minute burst. The dominant subregion was defined as the subregion of the medial tibial plateau that was the location of the closest point of contact during the majority of the 3-minute testing (Figure 32D). These joint space values were then normalized to the non-weightbearing joint space value at the beginning of the trial by dividing each joint space value by the non-weightbearing joint space. Normalized

change in joint space was then transformed to creep displacement by subtracting each normalized joint space values from the non-weightbearing normalized joint space value.

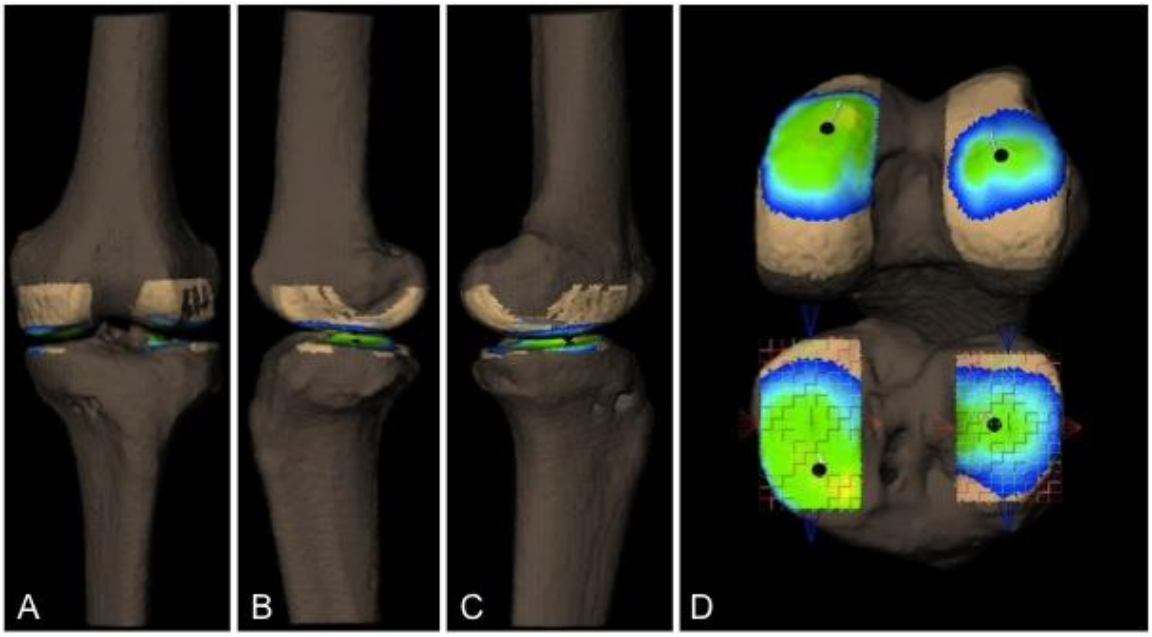

Figure 32. Subject-specific 3D bone models of the affected knee from front (A), lateral (B), medial (C), and disarticulated (D) views. The colors in the tibiofemoral joint space represent distance between the femur and tibia with blue being greater distances and yellow being closer distances. The black dots represent areas of closest contact, and the subregions of the tibial plateau are visible in D.

Previous work in the lab showed that we are able to model the creep response of the knee joint *in vivo* using 5 timepoints – non-weightbearing and 0.5, 1, 20, and 180 seconds after loading. Because of this previous data, we extracted the non-weightbearing, 0.5 and 1-second X-ray images from the initial 2.5 second X-ray capture. We identified when the subject transitioned from non-weightbearing to weightbearing by examining the forceplate data, and were then able to determine which frames represented 0.5 and 1-second after standing. This left us with 5 normalized displacement values for each subject. These values were then averaged between subjects by timepoint for both cartilage grades.

5.2.4 Single Plane Data Processing

For the single plane radiographic images, joint space width (JSW) was measured using the ImageJ software for Windows provided by the National Institutes of Health. Measurements were initially made on distortion corrected images with a resolution of 1.2658 pixels per mm and 16 bits per pixel (Figure 33A). To provide better visualization of the joint space, measurements were ultimately made on raw images with an applied 5x5 Horz Edge filter. For optimal joint space measurements, we adjusted the brightness and contrast adjustments to 4.545 pixels per mm and 8 bits per pixel (Figure 33B-C). Joint space was measured from the middle of the most inferior and flattest portion of the femoral condyle to the most superior region of the anterior tibia plateau (Figure 33C). If the lines of anterior and posterior tibia plateaus could not be differentiated, the measurement was made in a way to minimize JSW. This method will be referred to as the PMM (perceived midpoint minimum) method.

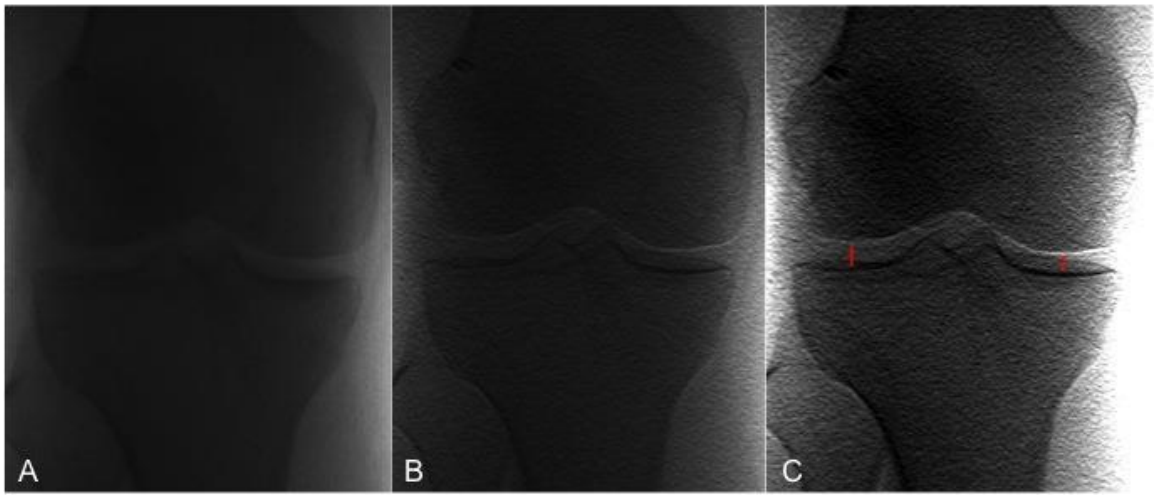

Figure 33. Single plane radiographs with optimization process shown. A) Raw radiograph. B) Radiograph with the Horz Edge filter applied. C) Radiograph with the Horz Edge filter and brightness/contrast adjustments. JSW as determined by the PMM method is represented by the red bars.

To assess the reliability of the PMM method, we performed reliability testing on the single plane radiographs of a single subject. Intra- and inter- reliability statistics were calculated using Intraclass Correlation Coefficient (ICC, two-way mixed effect analysis of variance, single measure); consistency and absolute agreements were calculated. A single observer made 3 measurement trials with 1-week intervals. For the PMM method, both the AP and non-AP views were analyzed. Inter-reliability was based on the measurements by 2 orthopaedic surgeons, 1 engineering graduate student, 1 medical student, and 1 undergraduate student. All were instructed to measure joint space using the PMM method.

5.2.5 Viscoelastic Modeling

Previous work found that the Voigt model was a better fit when the 3-minute timepoint is discarded, so the modeling was performed with the non-weightbearing, 0.5, 1, and 20-second data. The creep response of the Voigt model (Equation 12) was fitted to the experimental data points by cartilage grade using Matlab (Mathworks, Natick, MA). Material properties were constrained to be positive numbers, and were determined for each group using a nonlinear optimization function that minimizes the squared differences between the experimentally-observed and the model-predicted normalized displacements. Modeling gave stiffness (E) and viscosity (μ) material properties. Coefficient of determination (R^2) was used to determine the closeness of fit, as defined in Equation 13. Modeling was performed for each subject individually, as well as by cartilage grade.

$$J(t) = \frac{1}{E}\left(1 - e^{\frac{E}{\mu}t}\right)$$

Equation 12. Creep response of the Voigt model

$$R^2 = 1 - \frac{\Sigma(y_{pred_i} - y_{obs_i})^2}{\Sigma(y_{obs_i} - \bar{y}_{obs})^2}$$

Equation 13. Coefficient of determination (R^2) to determine closeness of fit

5.2.6 Statistics

The effect of softened cartilage on the change of normalized displacement using the biplane method was assessed by cartilage group and by limb (affected vs. contralateral) using a repeated-measures (RM) ANOVA comparing the groups at 0.5, 1, 20, and 180 seconds after loading. A separate RM ANOVA was performed for the PMM method results, and effect of cartilage grade was assessed for the AP and non-AP views. Significance for all analyses was set a priori at α=0.05. To correlate the results of biplane and PMM analyses, we used Pearson's correlation coefficient. To assess the reliability of the PMM method, we performed intra- and inter-reliability statistics using Intraclass Correlation Coefficient (ICC, two-way mixed effect analysis of variance, single measure); consistency and absolute agreements were calculated. For intra-reliability, a single observer made 3 measurement trials on a single subject with 1-week intervals. For inter-reliability, measurements of the same single subject were compared between 2 orthopaedic surgeons, 1 graduate student, 1 medical student, and 1 undergraduate student. Both the AP and non-AP views were analyzed with intra- and inter-reliability. All statistical tests were performed using SPSS (version 19.0).

5.3 RESULTS

5.3.1 Biplane Measurements

Significant differences were found between the creep response of the grade 0 and grade 1 groups, as shown in Figure 34. The group with softened articular cartilage underwent significantly more joint compression than the group with healthy articular cartilage (p=.028). Post-hoc independent t-tests revealed significant differences at 1 second after standing (p=.037) and differences trending on significance at 3 minutes (p=.054). There were no significant differences by limb, or grade-dependent differences in the contralateral limb.

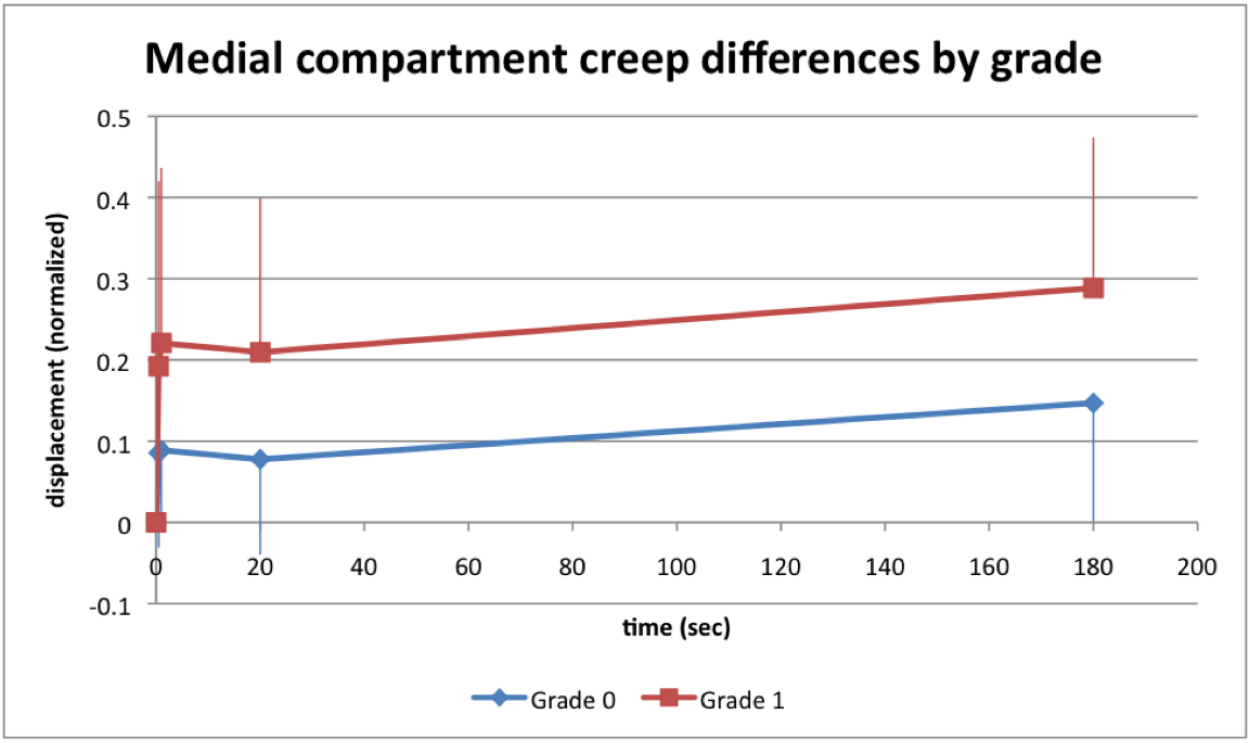

Figure 34. Differences in creep response by grade using biplane measurements. Blue points represent the grade 0 group, and red represents the grade 1 group. * signifies significant differences by group, and ! signifies differences trending on significance.

5.3.2 Single Plane Measurements

Significant differences were not found between cartilage grades using the PMM method with the AP or non-AP view (p=.927 and p=492, respectively). Figures 35 and 36 shows the change in joint space at the 5 timepoints using both the AP and non-AP views.

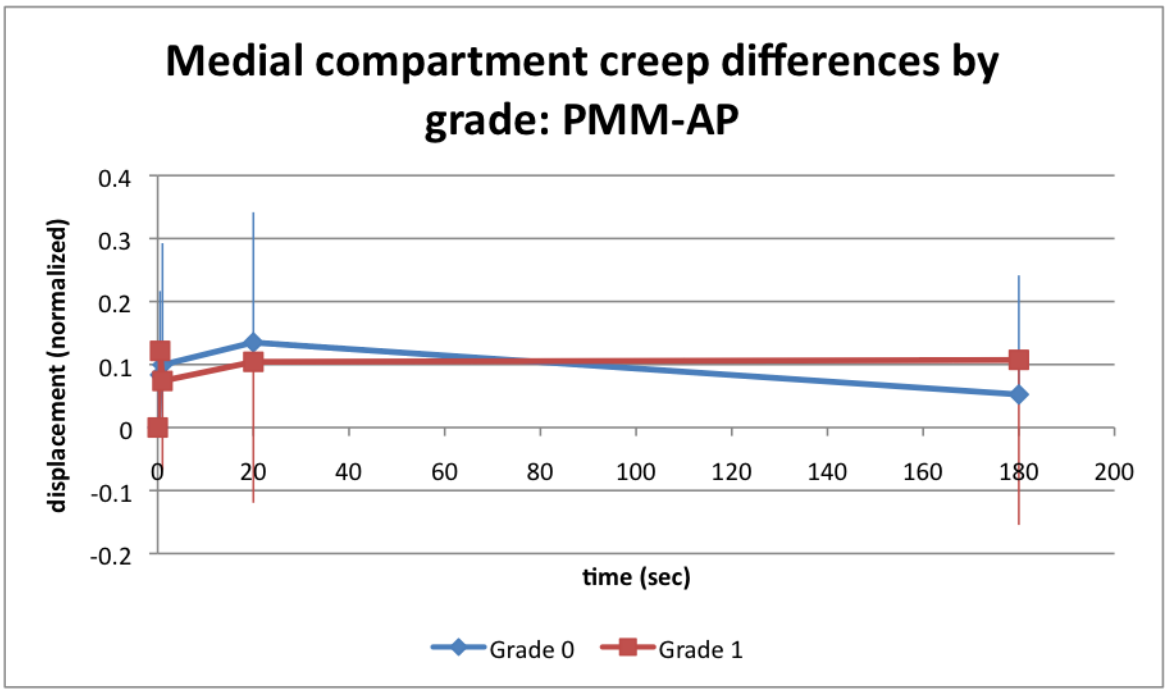

Figure 35. Differences in creep response by grade using the PMM method from the AP radiographs. Blue points represent the grade 0 group, and red represents the grade 1 group. No significant differences were found between groups.

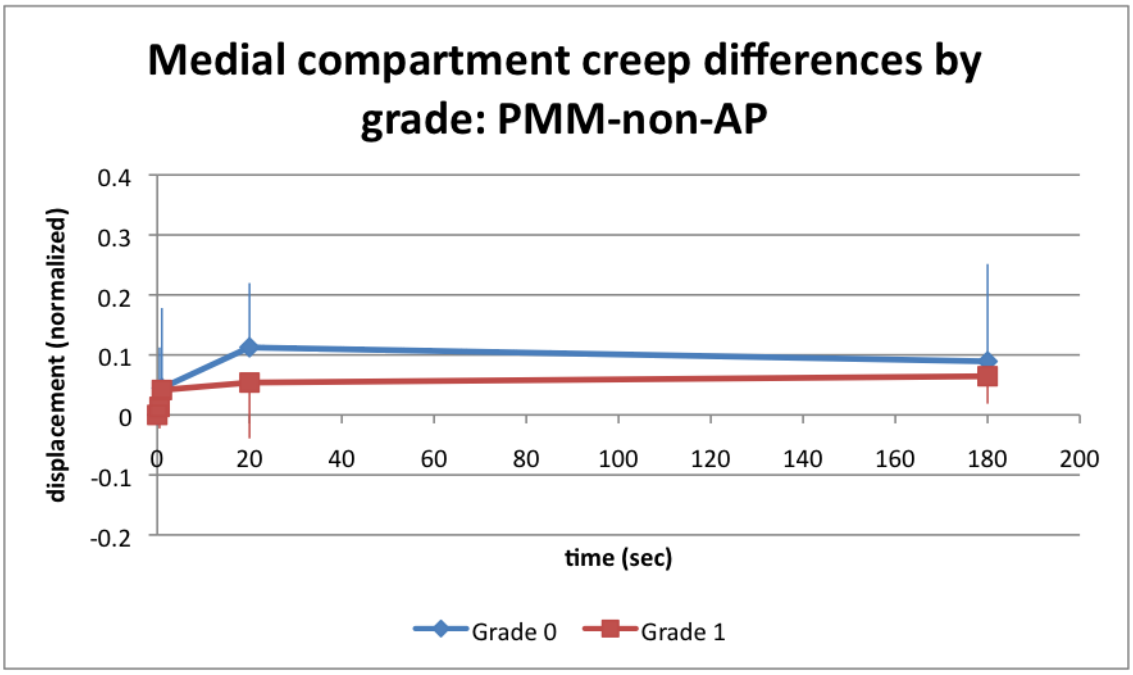

Figure 36. Differences in creep response by grade using the PMM method from the non-AP radiographs. Blue points represent the grade 0 group, and red represents the grade 1 group. No significant differences were found between groups.

Although the PMM measurements were unable to delineate between the grades, there were significant correlations between the single plane measurements and the biplane measurements of joint space. **Table 9** details the Pearson's correlation coefficients between each PMM view and the biplane measurements.

Table 9. Pearson's correlations for normalized displacement by grade comparing calculations from the biplane and PMM measurements. * represents statistical significance (p < .05).

	Biplane vs AP view	Biplane vs non-AP view
Grade 0	0.054, p > 0.05	0.433, p = 0.021*
Grade 1	0.584, p = 0.003*	0.623, p = 0.001*

The PMM method was found to be fairly reliable, and the results are summarized in **Table 10.** ICCs for both intra-reliability and inter-reliability were statistically significant at p < 0.001.

Table 10. Summary of reliability statistics with ICCs for AP and non-AP single plane radiographs. All reliability calculations were found to be significant.

	PMM-AP	PMM non-AP
Intra-reliability		
Consistency agreement	0.884, $p < 0.001$	0.917, $p < 0.001$
Absolute agreement	0.819, $p < 0.001$	0.888, $p < 0.001$
Inter-reliability		
Consistency agreement	0.829, $p < 0.001$	0.748, $p < 0.001$
Absolute agreement	0.641, $p < 0.001$	0.631, $p < 0.001$

5.3.3 Voigt Modeling

Voigt modeling was only performed for the biplane measurements, since this technique yielded significant differences between groups. The model fit both groups similarly, shown in Figures 37 and 38.

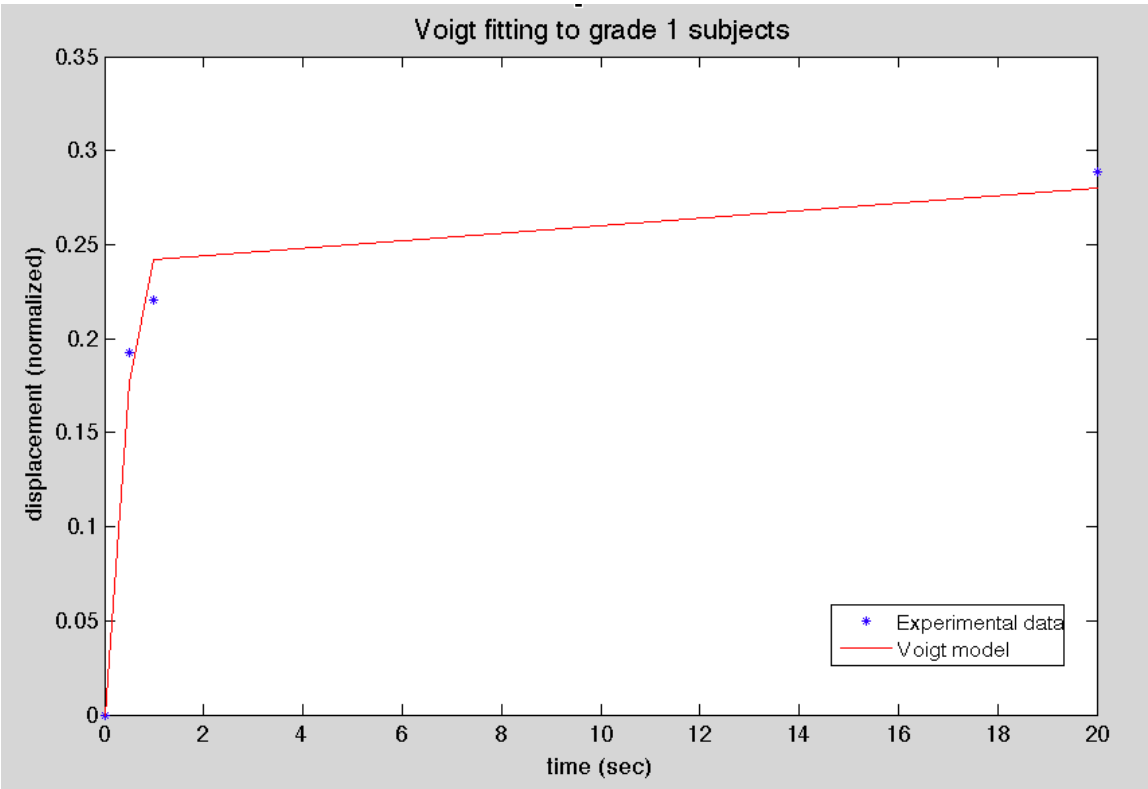

Figure 37. Voigt modeling of the initial creep phase (first 20 seconds) of the grade 1 subjects. The blue data points represent the experimental data averaged by group, and the red line is the Voigt fit.

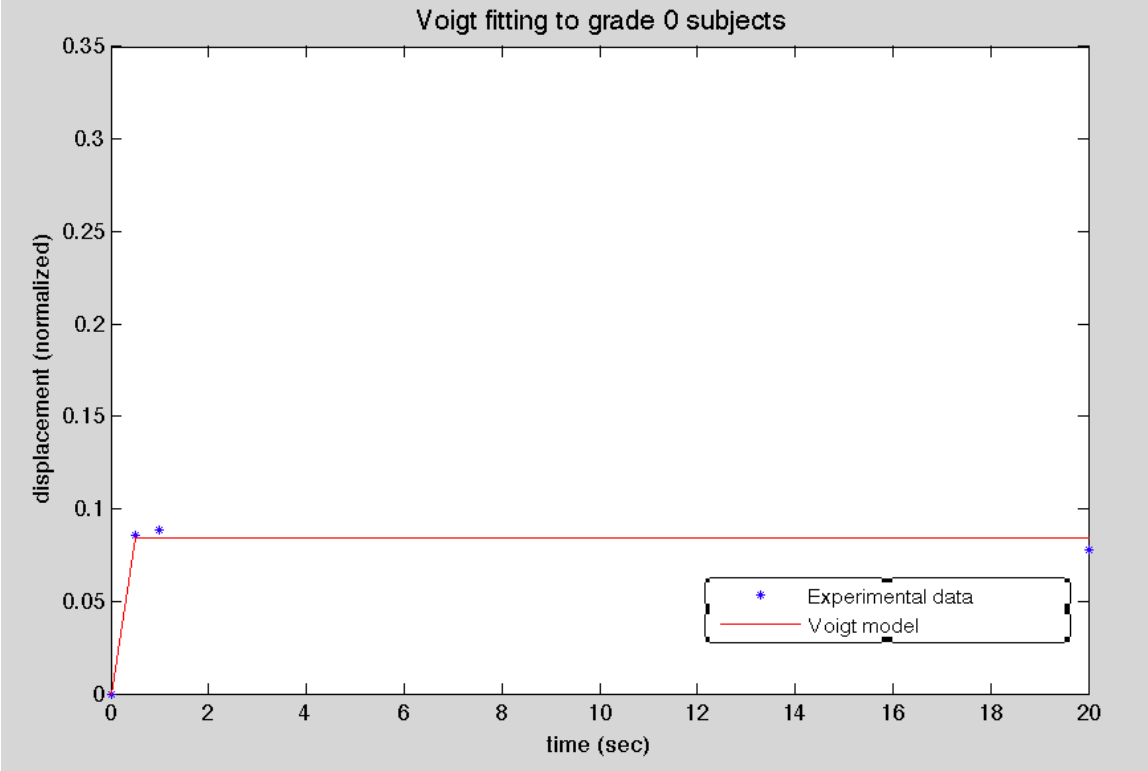

Figure 38. Voigt modeling of the initial creep phase (first 20 seconds) of the grade 0 subjects. The blue data points represent the experimental data averaged by group, and the red line is the Voigt fit.

Once again, the elastic modulus from Voigt fitting was lower for the softened group than the healthy group. The material properties from Voigt modeling of the displacements by group are detailed in Table 11. The viscosity values are comparable to those obtained in Chapter 4. We performed Voigt modeling for each subject individually, and these modulus and viscosity values, as well as R^2, are available in Appendix C.

Table 11. Material properties from Voigt modeling of grade 0 and grade 1 subjects. The similar R^2 values indicate the comparable fit of the model to both groups. More importantly, the softened group has a lower elastic modulus than the healthy, grade 0 subjects.

	Elastic modulus	Viscosity	R^2
Grade 0	11.89	0.167	0.988
Grade 1	3.57	1.79	0.983

5.4 DISCUSSION

This diagnostic represents a novel method of detecting early cartilage damage based on the mechanical behavior of the joint *in vivo*. We found that the subjects with grade 1 articular cartilage undergo significantly more joint compression than subjects with uninjured cartilage, thus supporting our first hypothesis. We believe that this is a direct result of the softening that is correlated with early cartilage damage. Softening stems from deficiencies in the superficial zone of the cartilage's solid collagen matrix, leading to altered mechanical behavior. This standing diagnostic is able to exploit these differences in collagen matrix integrity to classify subjects based on cartilage grade.

Differences between grades are further supported using Voigt modeling of the creep response. Specifically, the grade 1 group was found to have a lower elastic modulus than the group with healthy cartilage. Lowered elastic modulus corresponds with lowered stiffness of the tissue, which is clinically observed during arthroscopy. These results match trends that were seen in previous work *in vivo*, and other *in vitro* studies examining the mechanics of different

grades of cartilage damage[77]. The lowered elastic modulus in the grade 1 group helps to actually quantify the mechanical differences between the two groups.

Preliminary analysis of the differences in elastic modulus between groups indicates that there may be a cutoff value that discerns between healthy and damaged cartilage. To calculate this cutoff value, we modeled each subject individually and determined the average elastic modulus for the grade 0 and grade 1 subjects by group. We then calculated the root of sum of squares (RSS) value, which combines the error from both groups. This RSS value was then added to the average elastic modulus for the grade 1 group, and yielded a cutoff of 6.5. Inspection of the individual elastic modulus values indicate that 83% (5/6) of the softened cartilage subjects are modeled with an elastic modulus below 6.5 while all of the subjects with healthy cartilage are modeled with an elastic modulus above 6.5. The material parameters from modeling each subjects individually are detailed in Appendix C. These differences in modeling material properties allow for the rapid classification of subjects into those who are and are not at risk for the development of OA. Health professionals may be able to determine a subject's risk for the presence of early cartilage damage by measuring 4 joint space values. Further implementation of this technique as a clinical diagnostic would automate the Voigt fitting of the measured joint space values and alert clinicians of the risk of softened cartilage based on the joint's elastic modulus value.

Grade-dependent differences, however, are only detectable using biplane radiography. We were unable to see grade-dependent differences using single-plane analysis. This being said, there were significant correlations between the biplane and PMM results. The largest correlations were seen when examining the grade 1 data. Grade 1 subjects undergo larger amounts of joint space deformation during the standing trial, which is likely easier to detect

using the PMM method. There were also some significant correlations comparing the non-AP single-plane analysis with the biplane results of the grade 0 subjects. These correlations indicate that while the PMM results were not statistically significant by cartilage grade, there may be measures we can take to optimize the process for single-plane analysis of change in joint space.

Overall, excellent intra- and inter- reliability was seen with the PMM method, with "excellent" defined as an ICC > 0.75[156]. Using a consistency agreement produced higher ICC values than an absolute agreement because the trend of joint space measurements at the time points of interest were analyzed as opposed to exact reproducibility in those measurements. However, it should be noted that there was a larger decrease in ICC between consistency and absolute agreements when comparing intra-reliabilty to inter-reliability. These results support the conclusion that the PMM is a reliable method of measuring joint space particularly if the person has previous experience in using the method.

Many of the AP views were deemed to be malrotated during the AP PMM analyses, which may have contributed to the lack of significance in single-plane analyses. Malrotation was defined by Dupuis et al. as instances where the apex of the tibial spine crossed the midline of the femoral notch, or where the projection of the tibial spine overlapped on the femoral condyle[157]. Malrotation likely resulted from two major factors. First, although subjects were instructed to maintain their knees in full extension as they transitioned from sit-to-stand, many of them felt more comfortable bending their knees as they stood. This also introduced some variability in flexion angle between subjects. Secondly, we optimized subject placement and X-ray configuration for biplane radiography as opposed to single-plane analyses in order to assess the ability to replicate pervious work with a standing trial. For the AP views of the affected leg, 65% of the images were malrotated. To better understand the effect of this malrotation, we

performed the MDPT (midpoint) JSW technique[157] on the same subject that we had previously done the PMM intra-reliability statistics on. The MDPT method had excellent reliability, with ICCs at 0.924 and 0.914 for consistency and absolute agreements respectively. Coincidentally this subject had minimal malrotation, suggesting that the reliability of joint space measurements can be maximized with images that are not malrotated. This underscores the importance of subject positioning when measuring joint space.

Something to note for the use of this tool as a diagnostic is that it is very important that the subject not move or shift his/her weight during the standing trial. Although we instructed all subjects to remain still, one of the subjects with softened cartilage shifted weight between the 1 second and 20 second acquisition. This lead to a 5° change in tibial rotation and a dramatic change in location of closest point of contact, as well as an alteration of tibiofemoral orientation. As previously mentioned, the Voigt model was then unable to fit to the data properly and had to be modified for the subject's inclusion in the study. With DSX processing we are able to calculate tibiofemoral orientation as well as bone-bone distance, which helps to assess any extraneous subject movement. Small changes in tibiofemoral orientation may be more difficult to detect using single-plane measurements.

A critique of the previous work in Chapter 2 was the diverse subject population. Although not statistically significant, the grade 1 subject group was a bit older and heavier than the grade 0 group, which may have introduced confounding variables. It was difficult to recruit subjects who had undergone PM and were young, healthy, and had no previous injuries. A major reason for the difficulty was the simultaneous recruitment for the present study, which primarily aims to detect differences between single and double-bundle ACLr techniques and has similar inclusion/exclusion criteria. The subject population in the present study is younger and

has a lower BMI, and is very similar between cartilage grades. The similarities between groups eliminate possible confounding factors such as obesity and age from our results.

It is interesting to note that there were no differences between the ACLr and contralateral limbs. This finding was expected. Although many may be inclined to assume that the contralateral limb has intact, grade 0 cartilage, we do not actually know the cartilage status since it was not operated on. Additionally, the contralateral limb is known to go through changes after ACLr. Appendix B details the changes in muscle activation patterns after surgery, and previous work in our lab has shown that jump-landing kinematics are altered in the contralateral limb. Bilateral MRIs may help to determine the contralateral limb's cartilage status.

There are a few limitations to this study. All subjects were 2 years post-op from ACLr, and we used intraoperative notes to classify subjects by cartilage grade. It is possible that the cartilage grade at testing may have changed since the date of surgery. All subjects were asymptomatic for OA, however, and we believe it is valid to assume that the 2 groups have different grades of cartilage damage, even if the damage has progressed from grade 1. An additional limitation is that we recruited from a pool of 3 orthopaedic surgeons at the University of Pittsburgh Medical Center. The objective nature of cartilage scoring may introduce surgeon-specific differences in the recorded cartilage integrity. It worked out that all grade 1 subjects were from the same surgeon, however, which minimizes variability in the grade 1 group. All surgeons were familiar and experienced with the ICRS scoring scale. Another limitation is our relatively small sample sizes. Previous work, however, was able to find significant grade-dependent differences using comparable sample sizes. The homogenous subject populations between groups leaves us confident that the results we are able to find is purely from differences in cartilage integrity. A final limitation is that we did not use an ideal subject configuration for

single-plane joint space analyses. The goal of this study was the recreate a previous study using a clinically-feasible setup, and the biplane results proved that this was achieved. In the future, we hope to further optimize this diagnostic for single-plane JSW measurements and detect grade-dependent differences.

5.5 CONCLUSION

This clinical diagnostic represents a novel method to functionally detect knee joints with early cartilage damage. We are able to see differences in creep behavior between subjects with softened and healthy cartilage using biplane X-rays. Additionally, Voigt modeling indicates that the subjects with softened cartilage exhibit a lowered elastic modulus in the affected joint. Although we are unable to see significant differences in creep behavior using single-plane analyses, we hope to optimize the procedure to avoid confounding variables such as malrotation. The simplicity of this diagnostic allows for the implementation in most orthopaedic clinics, and has the potential to help many patients. Early detection of cartilage damage in asymptomatic individuals will allow for earlier intervention and better treatment of the disease.

6.0 CONCLUSION

6.1 SUMMARY OF FINDINGS

The purpose of this thesis was to develop a non-invasive method to detect early cartilage damage that will likely lead to osteoarthritis. By exploiting the mechanical differences between softened and healthy cartilage, we were able to detect functional differences between the two cartilage grades during an *in vivo* creep test. Specifically, the joints with softened cartilage underwent significantly more compression than the joints with healthy cartilage. These differences between grades are undetectable looking at tibiofemoral joint space or kinematics during running. Additionally, we were able to set a baseline of *in vivo* kinematic patterns for meniscal injury.

We then sought to model these results and derive material properties that reflected the clinical and physiological differences between the cartilage grades. The Voigt model provided to be a simplistic and accurate representation of the knee joint during an *in vivo* creep test. The model is able to fit the data using multiple and few data points. Additionally, the lowered elastic modulus in the grade 1 group reflects the deficits in the collagen matrix that lead to the tissue's softening.

Finally, we translated our creep and modeling findings into a clinical diagnostic that can be used by health professionals to detect grade 1 cartilage in the orthopaedic clinic. This diagnostic uses joint space measurements from timed X-rays that assess the change in joint space

over a 3-minute span. The diagnostic then models the change in joint space and is able to categorize the risk of softened cartilage based on the elastic modulus value of the affected joint.

6.2 FUTURE WORK

This project has several possible future directions. We have T1 and T2 MRIs of both the legpress and diagnostic subjects, and an interesting project could be to correlate MRI findings with the functional results of grade 0 and grade 1 cartilage. Currently MRI is the gold standard of *in vivo* cartilage research, and the addition of MRI results to these studies would be a great piece to the puzzle of OA development.

The diagnostic needs to be further optimized for use in the orthopaedic clinic. This includes tweaking subject positioning for single-plane analysis and optimizing the X-ray dosage for accurate visualization and measurement of JSW. Additionally, we need to further pursue the development of the necessary hardware and software for this clinical diagnostic. Hardware is necessary for timed X-ray capture, specifically a timer box that will obtain images at 0, 0,5, 1, 20, and 180 seconds. We could also use a seating/loading device that will accurately and reliably place subjects in the correct location for optimal JSW with single-plane measurements. Software is also needed to process and model of the change in joint space, and automatically output the patient's risk for cartilage damage.

6.3 ACKNOWLEDGEMENTS

I would like to acknowledge and thank my advisor, Dr. Scott Tashman, for giving me the flexibility and support to design and pursue my own project. When I came to the lab I was given the legpress project of Chapter 2, though Dr. Tashman allowed me to formulate my own ideas as to how the project should proceed. I would also like to thank everyone who has worked in the Biodynamics Laboratory and the Orthopaedic Research Laboratory for their endless help, feedback, and inspiration over the past four years, and my thesis committee for their support.

Figure 39. Students and staff of the Biodynamics Laboratory

My primary hope in doing this work was to develop something that can directly help individuals suffering from OA. This diagnostic has the potential to alert patients and clinicians before damage has spread through the articular cartilage. In doing so, the diagnostic may allow patients to seek treatments that will slow or stop the progression of the disease, thus improving the patient's quality of life.

APPENDIX A

CADAVER VALIDATION OF IN VIVO LEG PRESS DESIGN

Because of the novelty of the leg press design in Chapter 2, we wanted to compare our *in vivo* results to more traditional, *in situ* cadaver studies. Studies using cadaveric and cartilage plug specimens are the gold standard of cartilage deformation research, and we were concerned that the complexity of the *in vivo* knee joint may lend some unexpected differences that we had not considered. Comparisons between *in vivo* and *in situ* methods will indicate the effect of active muscle forces, and assess if we are actually measuring the passive properties of the knee joint.

A.1 INTRODUCTION

A principal goal of scientific research is to mimic a specific human condition or system in order to maximize clinical relevance. Cadaveric joints are often used in orthopaedic biomechanics to assess the behavior of the joint in response to a certain injury or situation. While cadaveric studies are unable to mimic human muscle activation, these studies do limit the number of confounding variables and are able to make assumptions based on the relative simplicity of the testing system.

Previously in Chapter 2 we examined how softened articular cartilage affects joint compression during a creep test. Subjects were classified as having undergone partial medial meniscectomy (PM) with softened cartilage, PM with healthy cartilage, or being an uninjured, healthy control. Differences were found between the groups with healthy and softened articular cartilage, though it is unknown if we are truly measuring the passive properties of the joint and cartilage. Therefore comparisons with a cadaveric study will allow us to assess the complexity of the *in vivo* system and understand if there are other variables such as active muscle forces that we may need to consider.

The purpose of this experiment was to compare the *in vivo* leg press setup of Chapter 2 to a similar creep setup using a cadaver limb. We hypothesize that the cadaver and *in vivo* joints will compress similarly during a 5-minute creep test.

A.2 METHODS

A.2.1 Kinematic Testing

A single cadaver knee was used for this testing. This specimen was from a 60 year old male, had no knee injuries, and was free from visible cartilage defects. The knee was oriented in full extension, and half-body weight was applied axially to the femur (setup shown in Figure 40). Unlike the setup in Chapter 2, the cadaver specimen was oriented in a standing configuration, with the femur on top of the tibia.

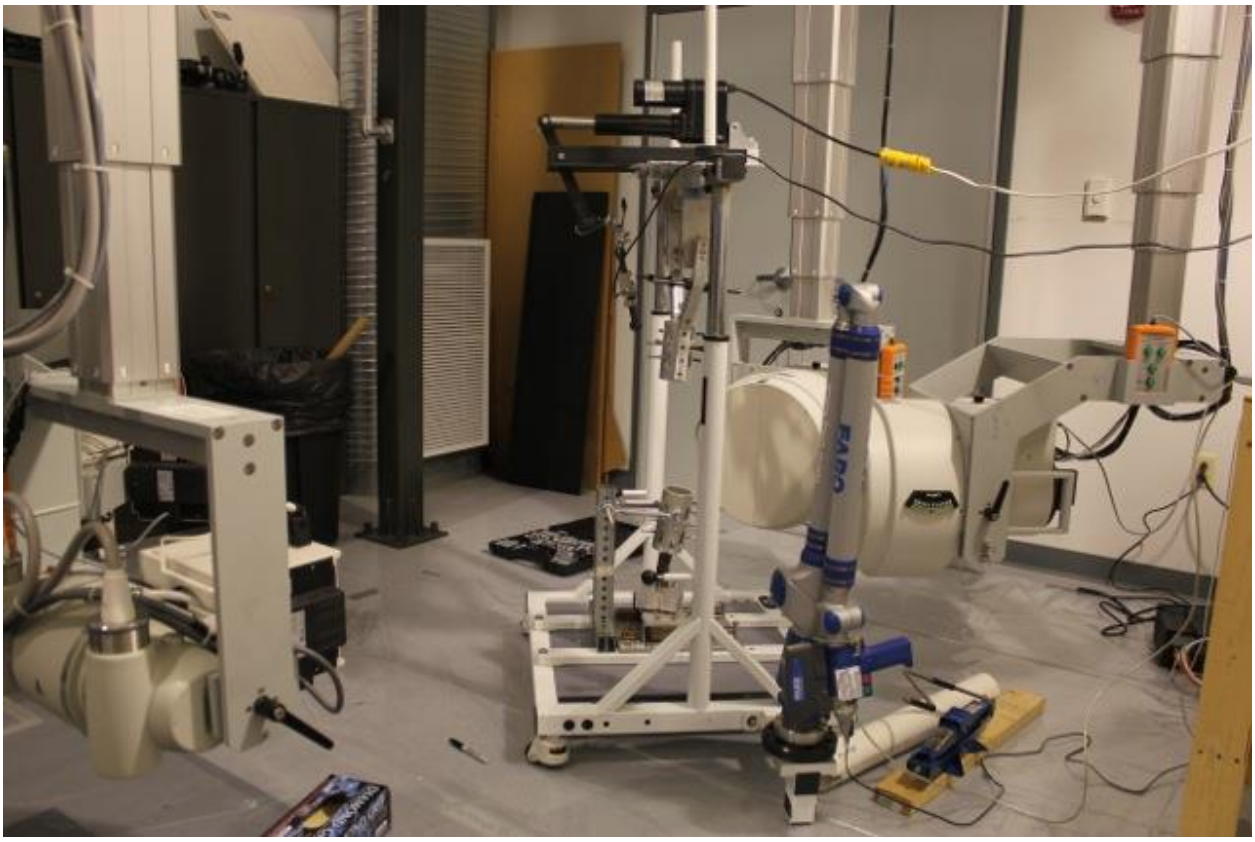

Figure 40. Setup for cadaver testing. In the middle of the image is the modified legpress that was used to apply half-body weight axially to the specimen.

Biplane X-rays were generated with 1 ms pulsed exposures at 80 kV/63 mA. Each 40 cm image intensifier (Thales, Inc.) was coupled with a 4 megapixel, 14 bit digital video camera (Phantom 10, Vision Research, Inc.). Image acquisition occurred simultaneously for both cameras, synchronized with X-ray pulse generation. Stereo X-rays were captured at bursts of 100 frames/second. Specifically, images were captured at non-weightbearing, 98, 290, 470, and 1010 seconds of loading.

A.2.2 Data Processing

The specimen underwent a CT scan (1.25 mm slice thickness), which was segmented with Mimics (Materialise Inc., Ann Arbor, MI, USA) to create subject-specific bone models of both the femur and tibia using a previously-described method [127,128]. We then performed similar data processing as in Chapter 2 to obtain the orientation of the femur and tibia relative to each other in all frames.

Joint space was calculated from the central subregion of the medial tibial plateau, shown in Figure 41. These joint space measurements were normalized to the non-weightbearing measurement, and were then transformed into a displacement similarly to Chapter 3. Displacement measurements were plotted against time and compared to *in vivo* displacement data.

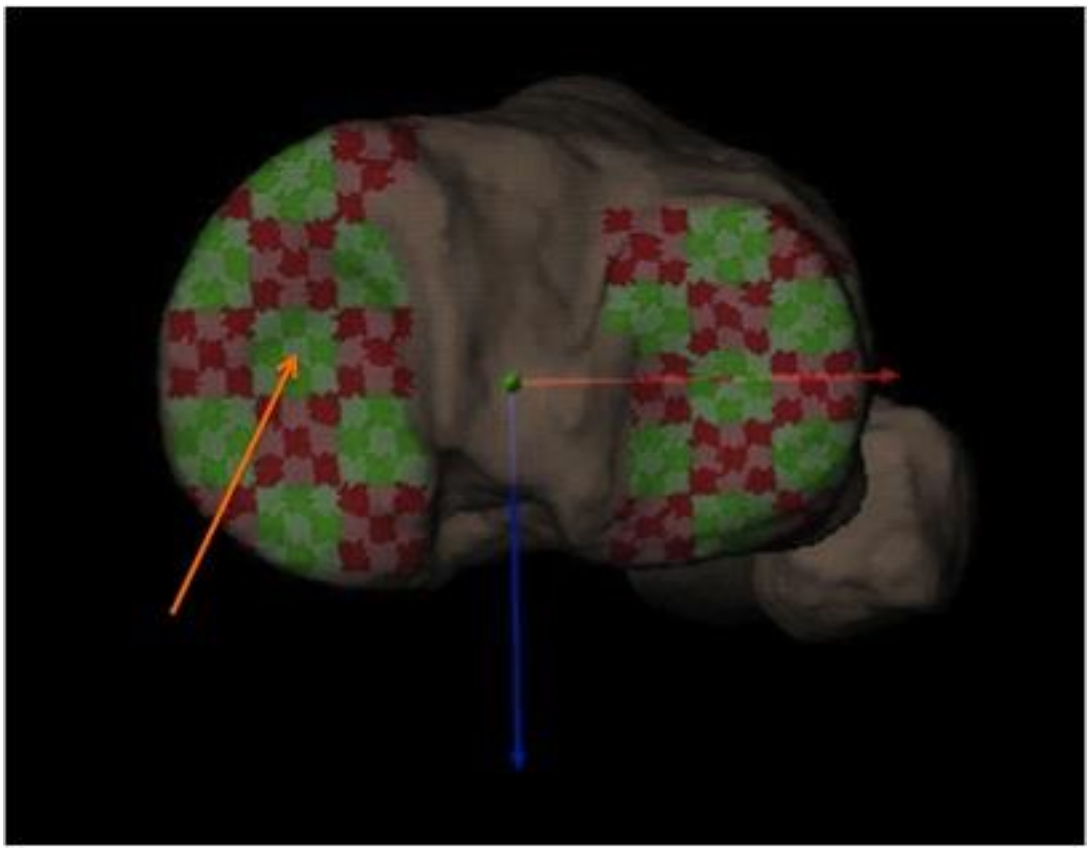

Figure 41. Location on medial tibial plateau where joint space measurements were taken. This location is the same as in Chapter 2.

The *in vivo* and cadaver X-rays were captured at different timepoints, so we chose to analyze those that overlap between the two studies. From the *in vivo* data we used points from non-weightbearing, 90, and 300 seconds after loading. These points were compared to the non-weightbearing, 98, and 290 seconds after loading from the cadaver testing. Since the *in vivo* protocol did not extend past 5 minutes, we are only to compare these 3 data points between the methods. We then fit separate polynomial curves to the data from the different methods.

A.3 RESULTS

Both the cadaver and *in vivo* results were found to be very similar. Figure 42 shows all of the *in vivo* results averaged together, regardless of subject group, compared with the cadaveric results.

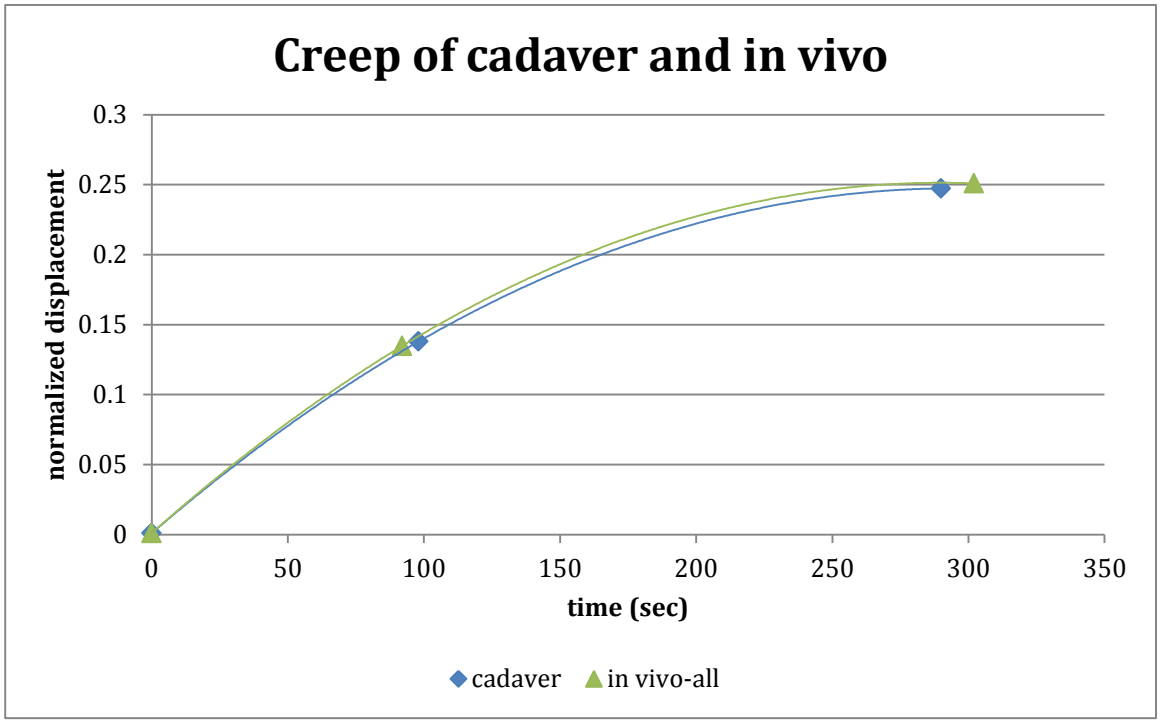

Figure 42. Creep curves of cadaver (blue) and *in vivo* (green) knees. The *in vivo* data has been averaged between all subjects who participated in Chapter 2.

We separated the *in vivo* data into subject groups (uninjured control, PM softened, PM healthy) to make further comparisons between *in vivo* assessments and cadaveric results, shown in Figure 43. The *in vivo* control appears to be the closest match to the cadaveric results when separated by subject groups.

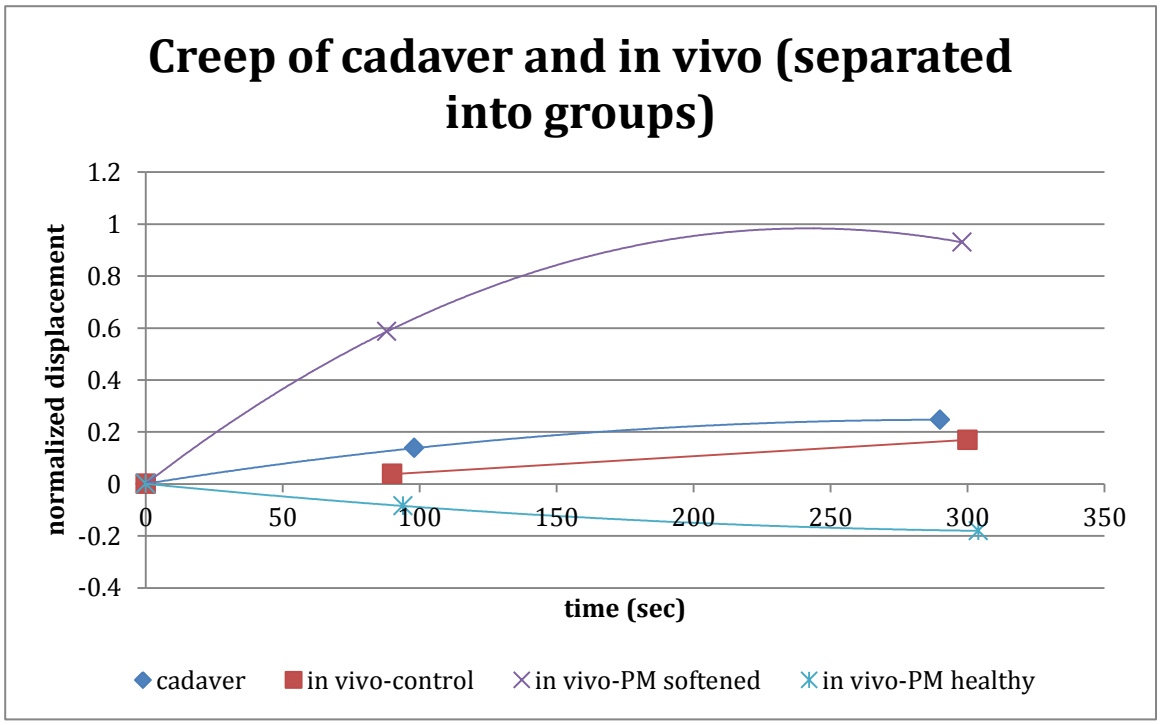

Figure 43. Creep curves of cadaver (blue) and *in vivo* knees. In this plot, the *in vivo* knees have been separated by grade and meniscal status. The red points represent uninjured control subjects, the purple crosses are subjects who have undergone partial medial meniscectomy and had softened cartilage, and the light blue asterisks are subjects who have undergone partial medial meniscectomy and had healthy articular cartilage (grade 0).

Upon further inspection, however, averaging all of the *in vivo* subjects together is better matched to the cadaver data, as shown in Figure 44.

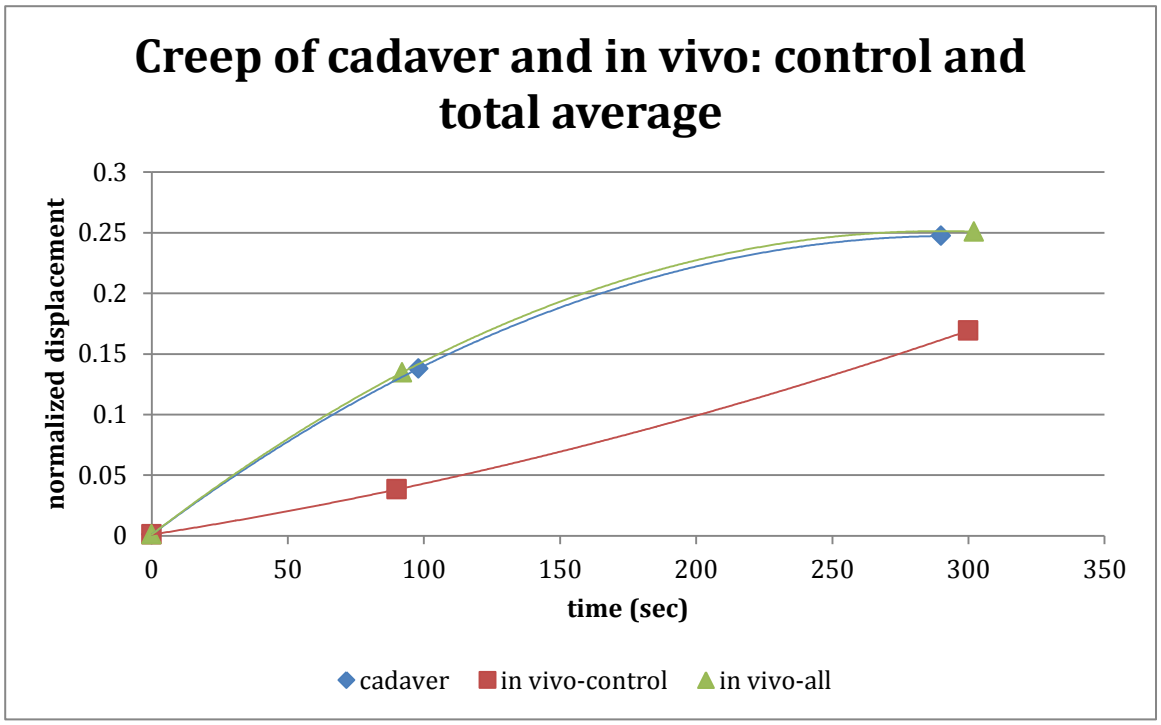

Figure 44. Creep curves of cadaver (blue) and *in vivo* knees. In this plot, the *in vivo* knees have been separated into the uninjured control subjects (red) and the total average of all subjects (green).

A.4 DISCUSSION

Similarities between the *in vivo* and cadaveric results indicate that active muscle function does not need to be considered with the *in vivo* analyses of Chapter 2. Therefore although the *in vivo* knee joint may be complex, we are able to model the viscoelasticity of the joint similarly to what is done *in vitro* and *in situ*. Another concern we had was that the difficulty of the task in Chapter 2 may have forced the subjects to involuntarily shake during testing. This shaking may have introduced confounding flexion angles and muscle forces that would need to be considered in later analyses. The similarities to cadaveric results indicate that if these confounding factors exist, they are not significant enough to need to be accounted for.

We were able to model the viscoelasticity of the joints *in vivo* using a Voigt model, and we attempted similar modeling of the cadaveric results to be able to compare the material parameters. We previously found when modeling our *in vivo* results that it was important to include data points from immediately after load application, in order to characterize the elastic response of the joint. Unfortunately, it was difficult to capture these images seconds after load application in the cadaver study. These long-term data points represent the viscosity term of the model, and the lack of short-term points make the model unable to converge on an elastic modulus value. This being said, we are confident that if we perform testing again and capture images closer to the instant of load application, we will be able to use Voigt modeling to derive the material properties of the cadaveric joint.

There are several limitations to this small study. Due to lack of time and funds we only used 1 cadaver specimen. The purpose of the study, however, was to qualitatively evaluate similarities between *in vivo* and cadaveric studies, which we are able to do with these results. Another limitation is the lack of timepoints captured closer to instant load application. Due to technical difficulties we captured images when we could, and had to wait between image acquisitions. In Chapters 3 and 4, however, we only capture 5 images and are able to make comparisons between different states of cartilage.

A.5 CONCLUSION

Because of the similarities between cadaveric and *in vivo* results, we are confident that we are able to measure and model the passive properties of joints with different states of articular cartilage. These results add onto the many similarities between *in vivo* and cadaveric results in

orthopaedic biomechanics research. The cadaver testing was performed by Eric Thorhauer, and I would like to thank him for his assistance.

As discussed in the motivation of this study, muscle activation is a central component of human subject research. In terms of knee osteoarthritis, strength deficits and prolonged muscle contraction have been reported in the leg muscles of affected limbs[158,159]. Similar work on muscle function and activation has been done on the limbs of subjects after they have sustained a musculoskeletal injury that will increase the risk of OA development. Appendix B will further explore alterations in muscle activation patterns after ACL reconstruction.

APPENDIX B

CHANGES IN CONTRALATERAL LIMB MUSCLE ACTIVATION TIMING AFTER ANTERIOR CRUCIATE LIGAMENT RECONSTRUCTION

Although the purpose of this thesis is to examine the mechanical factors that lead to early cartilage damage and OA, it is important to also consider muscle function. This is especially a concern after musculoskeletal injury. Injuries such as ACL reconstruction have been associated with muscle strength impairment and neuromuscular adaptations after surgery. Other work has found significant differences in muscle strength between the contralateral limb of ACL-reconstructed individuals and uninjured control subjects. Therefore after injury, the reconstructed limb may not be the only one that is altered.

Lack of muscle function allows the affected limb to weaken, and is therefore more susceptible to further injury and OA. This being said, the purpose of this study is to compare the muscle activation timing patterns of contralateral limbs in ACL-reconstructed patients to those of healthy, non-injured patients at 5 months and 1 year after surgery.

B.1 INTRODUCTION

While anterior cruciate ligament (ACL) reconstruction can restore knee function and mobility after ACL injury [160,161], it may fail to restore normal muscle function [162-164]. In addition to altered magnitude of electromyographic (EMG) recordings, deficits in flexor [163,165] and extensor [163,166,167] muscle strength have been found in the reconstructed limb when compared to the uninjured contralateral limb after surgery. Strength deficits in the reconstructed limbs are even greater relative to limbs of uninjured individuals [168], suggesting that the reconstructed leg may not be the only limb affected by the injury and surgery.

The goal of rehabilitation after ACL surgery is to return the reconstructed limb to the activity level of the contralateral limb, and it is assumed that the contralateral limb has remained healthy and strong. Hiemstra, et al addressed this assumption using dynamometry in ACL-reconstructed and in healthy, uninjured subjects and found that the flexor and extensor muscles of the contralateral limb are significantly weaker than those of healthy, uninjured controls [169]. It is unknown if these differences are the result of contralateral limb deconditioning after injury, rehabilitation protocols, or a neuromuscular adaptation after injury.

Electromyographic (EMG) studies of ACL-deficient subjects have shown that certain tasks elicit earlier muscle activation in deficient subjects when compared to uninjured healthy controls [170]. Similar changes have been found when comparing reconstructed limbs to uninjured controls [171]. In addition to earlier activation, muscles in the reconstructed limbs remained active for a greater percentage of the gait cycle than in the control subjects. The present study seeks to establish a similar relationship between the contralateral limbs and uninjured controls.

The purpose of this study is to compare the muscle activation patterns of contralateral limbs in ACL-reconstructed patients to those of healthy, non-injured patients at 5 months and 1

year after surgery. Specifically, the goal is to analyze differences in muscle activation timing and the duration of muscle contraction throughout the gait cycle. We hypothesize that contralateral limbs will exhibit prolonged muscle contraction when compared to uninjured control subjects, and that these differences will be maintained for at least 1 year after surgery. Changes in contralateral limb neuromuscular control would suggest that rehabilitation protocols after ACL injury/reconstruction may need to account for changes in muscle function that occur in both limbs.

B.2 METHODS

B.2.1 Subjects

Subjects between the ages of 16 and 50 years undergoing unilateral, primary arthroscopic ACL reconstruction were prospectively recruited for the study. Exclusion criteria included any substantial previous injury to either the reconstructed or contralateral limb, including damage to any other structures in the knee of the reconstructed limb besides the ACL. Subjects with minor concomitant meniscal tears were eligible if the tear affected less than 1/3 the radial width of the meniscus. Screening was based on injury history, preoperative MRI, and findings during arthroscopic reconstruction. The study was approved by the Henry Ford Health System Institutional Review Board for human subject research, and informed consent was obtained prior to subject enrollment.

25 ACL-reconstructed (ACLr) patients (18 male mean age 29.3 (SD 6.9) years, 7 female mean age 35.5 (SD 9.4) years) and 33 healthy control subjects (19 male mean age 33.6 (SD 10.2)

years, 14 female, mean age 38.3 (SD 6.7) years) participated in this study. Subjects had to have a minimum of one month between injury and surgery (mean, 12 months; range 1-121 months). One of these subjects had waited ten years to undergo ACL reconstruction; excluding this subject decreases the average time from injury to surgery to 8 months. All ACLr patients received autografts, including ten with hamstring tendon (2F, 8M, mean age 34.1 (SD 2.69), six with ipsilateral patellar tendon, (2F, 4M, mean age 31.50 (SD 3.84), and seven with contralateral patellar tendon (3F, 4M, mean age 34.00 (SD 2.76) autografts. Surgeries were performed by one of three participating surgeons at Henry Ford Health System, using a transtibial drilling approach for femoral tunnels and interference screw fixation. All patients went through a uniform, prescribed rehabilitation regimen. ACLr subjects were assessed once they were cleared to engage in light sports activities, which was typically 4-6 months after surgery.

15 ACLr patients returned for additional kinematic testing at 1 year after surgery (mean age 34.1 (SD 8.1), 5F, 10M). Of these subjects, seven received hamstring tendon autografts (1F, 6M), three had ipsilateral patellar tendon grafts (1F, 2M), and five had contralateral patellar tendon grafts (3F, 2M).

B.2.2 Muscle Activation Patterns

Active EMG surface electrodes (Motion Control, Inc.) were placed over the vastus medialis and lateralis, medial and lateral hamstrings, rectus femoris, and the gastrocnemius of both limbs. Surface electrodes were oriented longitudinally over the muscle belly in order to ensure optimal muscle selectivity. EMG data was collected while subjects ran on a 10° decline treadmill (Model L8, 46x152 cm belt, Landice Corp. Randolph, NJ, USA) at 2.5 m/s (Figure 45).

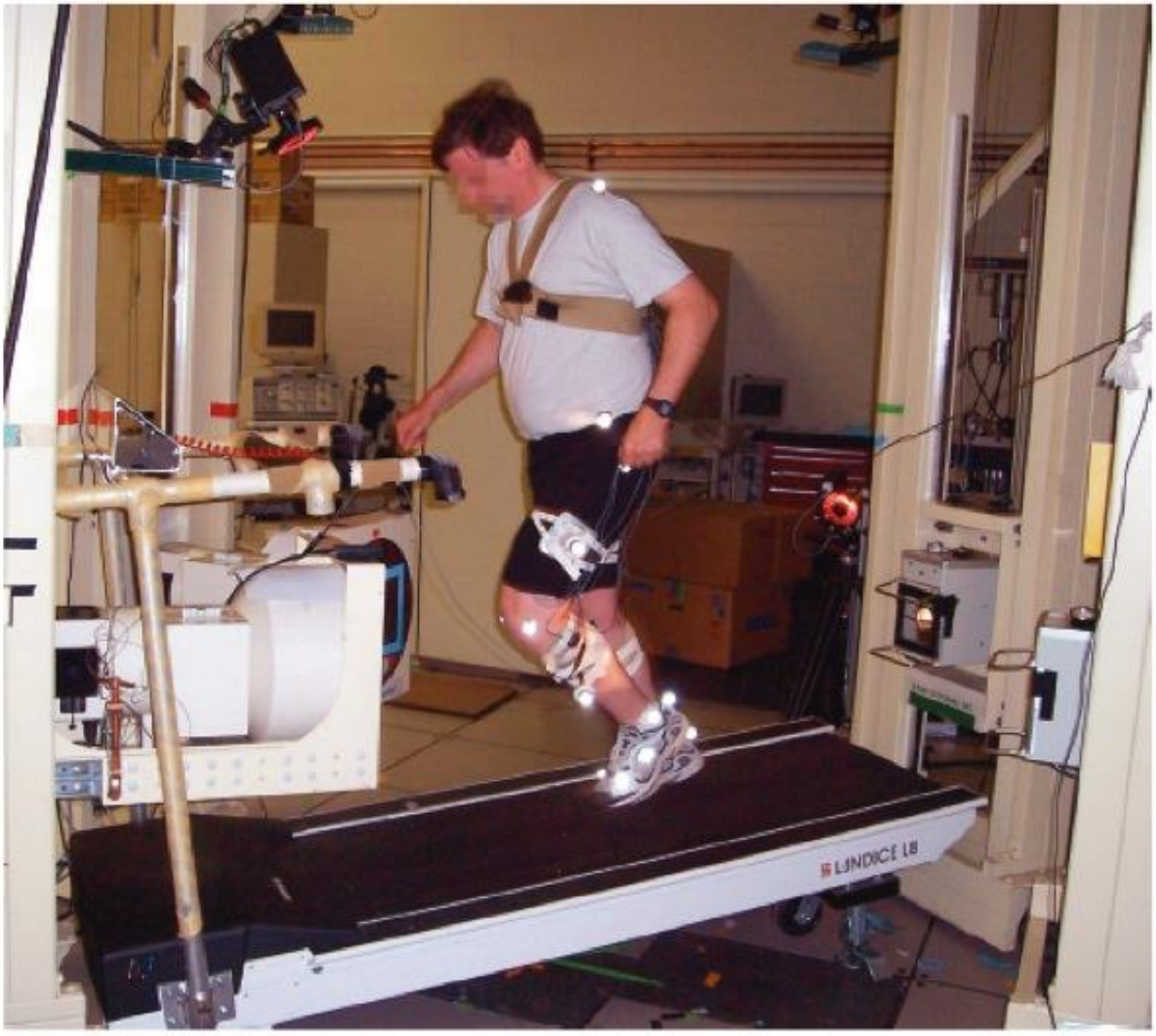

Figure 45. Subject running on decline treadmill with EMG electrodes and accelerometer.

Decline running was chosen over level running because of the stress it puts on the ACL, and 2.5 m/s has been found to be a speed at which participants feel comfortable running. Subjects wore an accelerometer strapped to the tibia to allow for the extraction of foot strike times and ensemble averaging during data processing. Data was collected for 3-6 gait cycles from each of 3 trials, for a minimum of 9 full cycles per subject.

B.2.3 Data Processing

EMG data was processed with Matlab (Mathworks, Inc.) using in-house code. Data from each muscle was full-wave rectified and low-pass filtered (20 Hz bidirectional 4^{th}-order Butterworth), and heel strikes were extracted from the accelerometer data and applied to the EMG data for ensemble-averaging across all collected gait cycles within a trial. Mean and standard deviation of the EMG data's quietest 10% interval of the resulting averaged gait cycle were determined for each muscle, and the baseline for muscle activity was determined to be two standard deviations above the quietest 10% value. Onset of muscle contraction (activation time) and total duration of muscle contraction were extracted as the primary parameters for comparison across groups. Activation time was defined as the point in the gait cycle when muscle activity surpassed the predefined baseline value, and duration of muscle contraction was the continuous period of time in the gait cycle where muscle activity surpassed the baseline. These parameters were averaged across trials for each muscle in the contralateral limb of ACLr subjects, and in a randomly chosen limb of control subjects.

B.2.4 Statistics

All statistical analyses were performed with SPSS software, version 19.0 (SPSS, Chicago, IL, USA). A two-way repeated measures ANOVA was used to look at the effect of limb (healthy control subjects versus contralateral ACLr) on both factors (activation time and duration of muscle contraction) at 5 months post-op in all 6 muscles. Significance was set a priori at α=0.05. If the repeated measures ANOVA showed a significant effect of limb, the analysis was followed up by separate one-way ANOVAs by factor to further clarify areas of significance.

Friedman's ANOVA was used assess the effect of limb at 12 months post-op, and once again, significance was set at α=0.05. If this test showed a significant effect of limb, post-hoc testing included separate Kruskal Wallis tests by factor. Statistical significance was defined as a $p<0.05$, while statistical trends were defined as $p<0.06$. Nonparametric statistical analyses were performed at the later timepoint because of the unequal sample sizes between subject populations at 1 year after surgery.

B.3 RESULTS

B.3.1 5 Months Post-Op

Significant differences were found for both muscle activation time and duration of muscle contraction at 5 months after ACLr. Figure 46 visually depicts muscle activation patterns during an ensemble-averaged gait cycle of both ACLr contralateral limbs and uninjured control subjects in all examined leg muscles. The starting point of each line represents muscle activation time, and the total length of each line is the duration of muscle contraction.

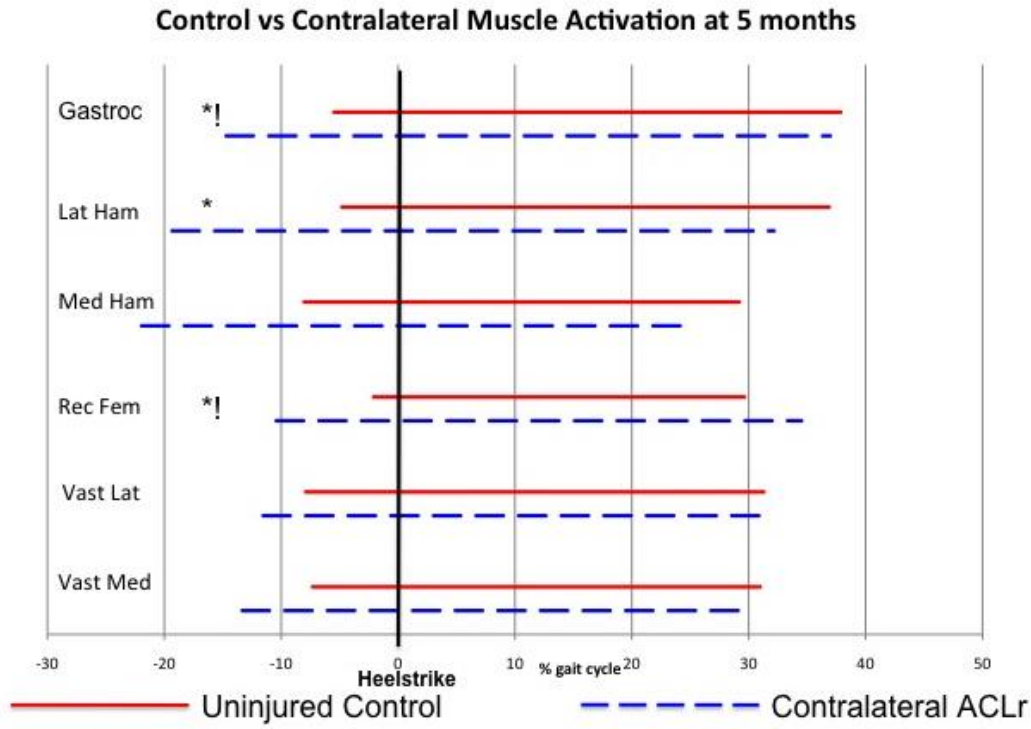

Figure 46. This figure shows the muscle activation timing patterns as percentage of gait cycle in healthy, uninjured subjects and ACLr contralateral limbs at 5 months after surgery. Red lines depict the muscle activation patterns of uninjured control subjects, and the blue dashed lines show activation patterns of the contralateral limb in ACL-reconstructed patients. * represents significant differences in muscle activation time, and ! represents significant differences in duration of muscle contraction.

Activation of the rectus femoris (p=.003), medial hamstrings (p=.039), lateral hamstrings (p=.028), and gastrocnemius (p= .030) of uninjured individuals occurred significantly later in the gait cycle than in the contralateral limb of ACL-reconstructed individuals (Table 12). Similarly, the rectus femoris (p<.001) and gastrocnemius (p=.005) muscles contracted for a significantly shorter time in healthy individuals than in the contralateral limb of ACL-reconstructed patients.

Table 12. Muscles at 5 months post-op with significant and trending differences between ACLr-contralateral and uninjured subjects, and their corresponding p-values.

Muscle activation timing at 5 months after surgery	
Activation Time	Duration of Contraction
Rectus Femoris: 8.29% (p=.003)	Rectus Femoris: 12.54% (p<.001)
Gastrocnemius: 7.11% (p=.030)	Gastrocnemius: 8.22% (p=.005)
Lateral Hamstrings: 13.84% (p=.028)	
Medial Hamstrings: 12.89% (p=.039)	

B.3.2 1 Year Post-Op

Similar trends are seen at 1 year post-ACLr. Figure 47 visually depicts muscle activation patterns during an ensemble-averaged gait cycle of both ACLr contralateral limbs and uninjured control subjects. The starting point of each line represents muscle activation time, and the total length of each line is the duration of muscle contraction at 1 year after ACLr.

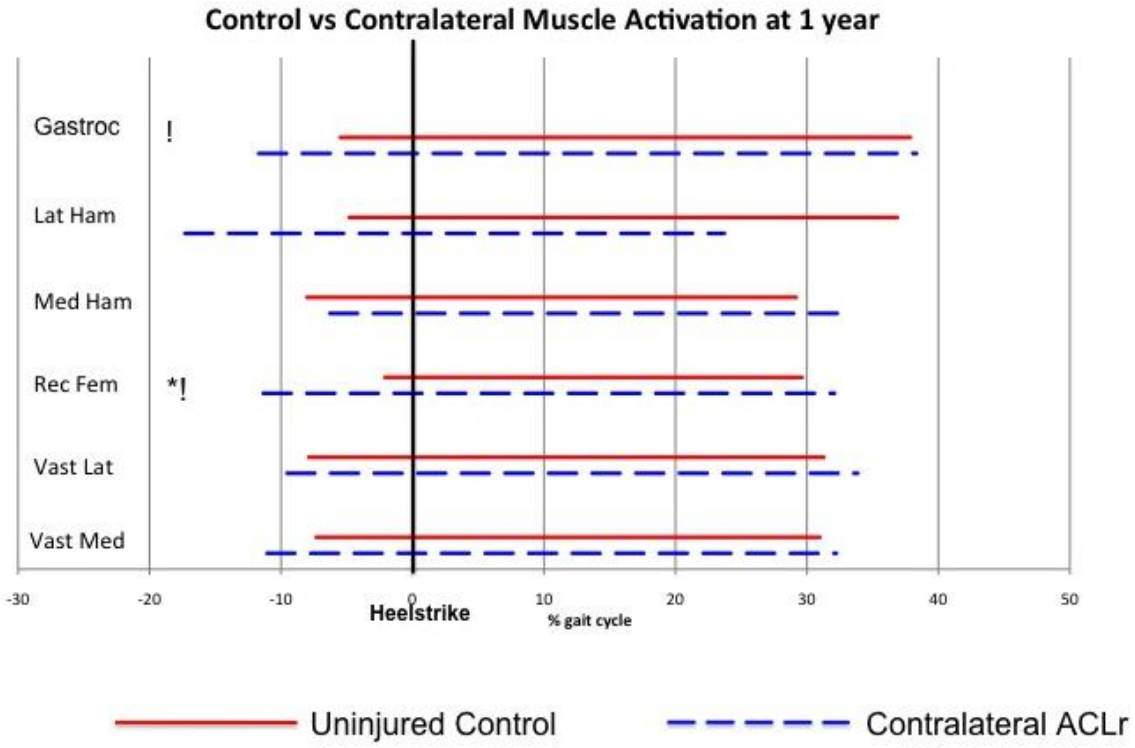

Figure 47. This figure shows the muscle activation timing patterns as percentage of gait cycle in healthy, uninjured subjects and ACLr contralateral limbs at 1 year after surgery. Red lines depict the muscle activation patterns of uninjured control subjects, and the blue dashed lines show activation patterns of the contralateral limb in ACL-reconstructed patients. * represents significant differences in muscle activation time, and ! represents significant differences in duration of muscle contraction.

Results at 1 year after surgery were generally similar to the 5-month findings. As shown in Table 13, significant differences in muscle activation were found for the rectus femoris (p=.007) and differences trending on significance were found with the lateral hamstring (p=.058). Differences in duration of muscle contraction between the contralateral and healthy limbs were significant for the rectus femoris (p=.002) and the gastrocnemius (p=.037). There were no statistically significant changes in muscle activity patterns of the contralateral limb between 5 and 12 months after ACLr.

Table 13. Muscles at 5 months post-op with significant and trending differences between ACLr-contralateral and uninjured subjects, and their corresponding p-values.

Muscle activation timing at 1 year after surgery			
Activation Time		Duration of Contraction	
Rectus Femoris: 9.48%	(p=.007)	Rectus Femoris: 10.49%	(p=.002)
Lateral Hamstrings: 13.41%	(p=.058)	Gastrocnemius: 6.18%	(p=.037)

B.4 DISCUSSION

These results support the hypothesis that ACL reconstruction affects neuromuscular function of the contralateral limb. Specifically, ACLr appears to have the most affect on the muscle contraction patterns of the lateral hamstrings, gastrocnemius, and rectus femoris. Alterations in muscle contraction patterns are maintained at 1 year after surgery.

Interestingly, these results are strikingly similar to those seen when comparing muscle activation patterns of ACL reconstructed limbs to healthy, uninjured control subjects during decline running at 5 months after surgery[171] (Figure 48). Statistical comparisons between the muscle activation patterns of the reconstructed and contralateral limbs at 5 months post-op yield no significant differences.

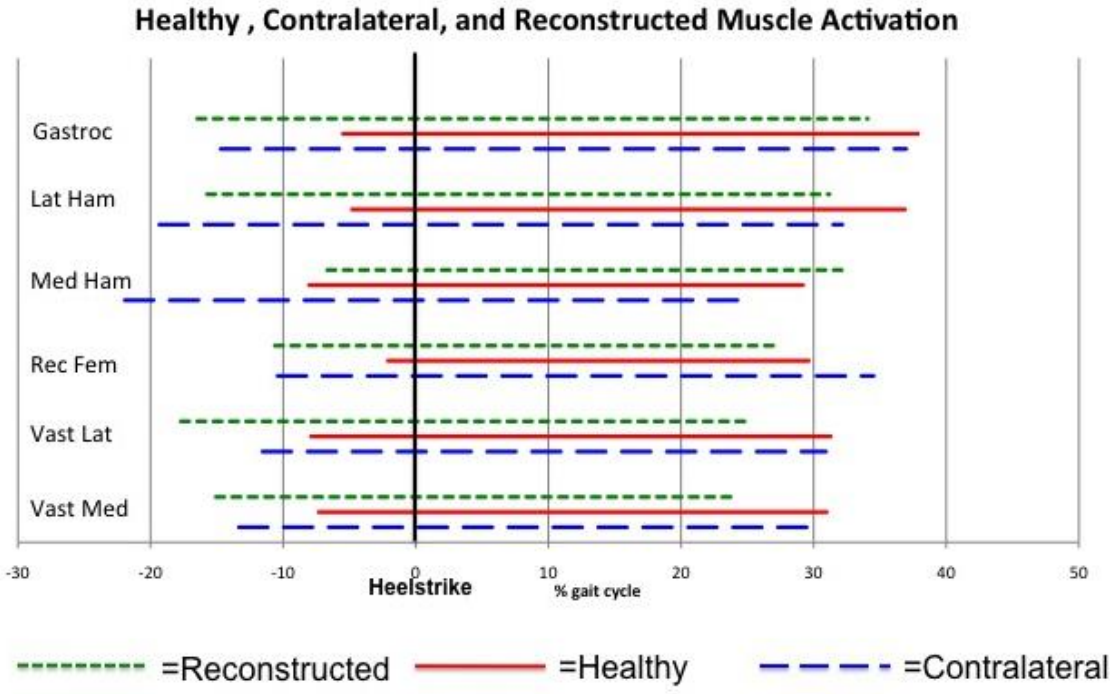

Figure 48. Plot of muscle activation timing patterns in ACL-reconstructed, contralateral, and healthy, uninjured subjects at 5 months after surgery. Green dotted lines represent the muscle activation patterns of the reconstructed limb, while red solid and blue dashed lines again represent the muscle activation patterns of the uninjured healthy subjects and ACLr-contralateral limbs, respectively.

As shown in Figure 4, muscles of both limbs in ACLr patients activate earlier and longer in the gait cycle than uninjured, control subjects. The prolonged activation of antagonistic muscles in the contralateral limb, particularly the rectus femoris, gastrocnemius, and lateral hamstring, could point to increased co-contraction as a potential neuromuscular adaptation to ACLr. Increased co-contraction and tibiofemoral compressive forces are known effects of ACLr in the reconstructed limb [172-175], and may contribute to the increased risk of development of OA after ACLr [43,150,176,177]. These results expand on previous work, suggesting that joint forces and co-contraction may be not only increased in magnitude, but also in duration of the gait cycle. Additionally, these results indicate that the contralateral limb may be experiencing similar

increases in joint forces and co-contraction, thus putting both limbs at risk for OA development after ACL injury.

Results of this study also show that most of the alterations in muscle contraction seen at 5 months post-op are maintained at least one year after ACLr. Thus, contralateral muscles may become trained after injury to activate differently, though the reason for this is unknown. Rehabilitation strategies may contribute to strength deficits after ACLr. Muscle strength and EMG have been shown to decrease after periods of detraining [178,179], which could correlate with contralateral limb weakening after ACL injury and surgery.

It has been postulated that training the injured limb to match the strength of the contralateral limb will leave the patient with both limbs impaired [169], which could explain the similarities between limbs in an ACLr individual. Figure 4 previously showed that comparisons of the muscle activation patterns of the ACL reconstructed and contralateral limbs of the subjects in this study showed no differences. Therefore if health professionals consider the contralateral limb to be the benchmark of health and muscle strength after ACL reconstruction, patients will be left weaker and possibly more vulnerable to future injury. Similarities between the reconstructed and contralateral limbs may also point to compensatory mechanisms after surgery, or the body's attempt to return to symmetry after injury. Gait asymmetries may leave the patient at a greater risk for further injury, and equilibration between the limbs may be the body's attempt to minimize this risk.

There are some limitations to this study, namely variance of the data and non-homogeneity of subject population. The ACL reconstructed patients received ipsilateral hamstring tendon, BPTB, or contralateral BPTB autografts, which could potentially have an effect on the muscle activation patterns of the contralateral limb. Preliminary analysis of this

data, however, showed no effect of graft type on the muscle activation patterns of the reconstructed limb, but this analysis was not sufficiently powered to definitively address this question. Additionally, the ACLr and healthy subject populations include male and female subjects. Preliminary work has found sex-specific neuromuscular adaptations after ACLr, specifically in the vastus lateralis, vastus medialis, and the rectus femoris. Both the healthy and reconstructed groups have similar sex breakdowns, however, which should account for these sex-specific differences. Finally, 25 patients initially participated at 5 months post-op, and this sample size dropped to 15 subjects at the 1-year mark. A larger sample size at the longer timepoint may further elucidate differences in the variables that are trending toward significance.

Future work will link the EMG data with kinematics data acquired with a dynamic stereo X-ray (DSX) system [131,180], in order to link alterations in muscle contraction in the contralateral limb with kinematic adaptations. Our lab has previously reported alterations in gait kinematics as a result of ACLr [66,138], and linking muscle activations with kinematic patterns could shed light on correlations between certain muscle contractions and knee kinematics. Additionally, the subject population will be categorized by gender in order to understand any gender-specific neuromuscular adaptations after ACL reconstruction.

B.5 CONCLUSIONS

The contralateral limb in ACL-reconstructed individuals exhibits significantly different muscle activation patterns than the limbs of healthy, uninjured subjects. These activation patterns are very similar to those seen in the reconstructed limb, indicating a possible compensatory or

adaptive mechanism to protect from further injury. Future work will explore these patterns in more subjects, as well as farther out from surgery.

APPENDIX C

VOIGT MODELING COEFFICIENTS FROM MODELING EACH SUBJECT INDIVIDUALLY

In Chapter 5, we modeled the normalized joint displacement of the grade 0 and grade 1 subjects using a Voigt model. The fits and material properties from the subjects averaged by group was reported. In Table 14, the individual fits and material properties are detailed by subject.

Table 14. Material properties from Voigt modeling each subject individually from Chapter 5. Subject number was used internally to identify each subject.

Grade	Subject Number	Stiffness	Viscosity	R^2
0	1093	14.75	0.1963	0.975
0	1107	8.5862	23.8255	0.911
1	1122	13.339	2.1754	0.7256
0	1121	9.5058	0.128	0.635
0	1082	7.557	0.0925	0.7032
1	1104	3.5891	0.065	0.966
0	1136	7.4	7.473	0.997
0	1058	90.996	6.906	0.0078
1	1151	4.591	8.454	0.933
1	1108	2.4597	0.5663	0.992
0	1158	8.28	0.088	0.904
1	1167	3.741	2.04	0.897
1	1159	3.9	1.19	0.999

Modeling each subject individually sheds more light on the patterns that were established in Chapters 4 and 5, where the group with softened cartilage exhibited lower elastic modulus

values than the subjects with the grade 0 cartilage. Examining each subject's material properties indicates that most of the softened subjects have moduli under 5 (5/6 subjects), and all of the grade 0 subjects have moduli above 5. The differences in individual elastic modulus by grade points to the use of Voigt modeling as a filtering tool to quickly determine the cartilage status of patients.

If you've made it this far you must be forced to read this, or genuinely interested in the development of osteoarthritis. In either case, thanks for reading!

BIBLIOGRAPHY

1 Lawrence, R. C. *et al.* Estimates of the prevalence of arthritis and selected musculoskeletal disorders in the United States. *Arthritis and rheumatism* **41**, 778-799, doi:10.1002/1529-0131(199805)41:5<778::AID-ART4>3.0.CO;2-V (1998).

2 Global. Global Economic and Health Care Burden of Musculoskeletal Disease. (2001).

3 Felson, D. T. *et al.* The incidence and natural history of knee osteoarthritis in the elderly. The Framingham Osteoarthritis Study. *Arthritis and rheumatism* **38**, 1500-1505 (1995).

4 Elders, M. J. The increasing impact of arthritis on public health. *The Journal of rheumatology. Supplement* **60**, 6-8 (2000).

5 Oliveria, S. A., Felson, D. T., Reed, J. I., Cirillo, P. A. & Walker, A. M. Incidence of symptomatic hand, hip, and knee osteoarthritis among patients in a health maintenance organization. *Arthritis and rheumatism* **38**, 1134-1141 (1995).

6 Buckwalter, J. A., Saltzman, C. & Brown, T. The impact of osteoarthritis: implications for research. *Clinical orthopaedics and related research*, S6-15 (2004).

7 Felson, D. T. *et al.* The prevalence of knee osteoarthritis in the elderly. The Framingham Osteoarthritis Study. *Arthritis and rheumatism* **30**, 914-918 (1987).

8 Poole, A. R. *et al.* Composition and structure of articular cartilage: a template for tissue repair. *Clinical orthopaedics and related research*, S26-33 (2001).

9 Sophia Fox, A. J., Bedi, A. & Rodeo, S. A. The basic science of articular cartilage: structure, composition, and function. *Sports health* **1**, 461-468, doi:10.1177/1941738109350438 (2009).

10 Mow, V. C., Ratcliffe, A. & Poole, A. R. Cartilage and diarthrodial joints as paradigms for hierarchical materials and structures. *Biomaterials* **13**, 67-97 (1992).

11 Setton, L. A., Elliott, D. M. & Mow, V. C. Altered mechanics of cartilage with osteoarthritis: human osteoarthritis and an experimental model of joint degeneration. *Osteoarthritis and cartilage / OARS, Osteoarthritis Research Society* **7**, 2-14, doi:10.1053/joca.1998.0170 (1999).

12 Alford, J. W. & Cole, B. J. Cartilage restoration, part 1: basic science, historical perspective, patient evaluation, and treatment options. *The American journal of sports medicine* **33**, 295-306 (2005).

13 Kempson, G. E., Muir, H., Pollard, C. & Tuke, M. The tensile properties of the cartilage of human femoral condyles related to the content of collagen and glycosaminoglycans. *Biochimica et biophysica acta* **297**, 456-472 (1973).

14 Akizuki, S. *et al.* Tensile properties of human knee joint cartilage: I. Influence of ionic conditions, weight bearing, and fibrillation on the tensile modulus. *Journal of orthopaedic research : official publication of the Orthopaedic Research Society* **4**, 379-392, doi:10.1002/jor.1100040401 (1986).

15 Arokoski, J. P., Jurvelin, J. S., Vaatainen, U. & Helminen, H. J. Normal and pathological adaptations of articular cartilage to joint loading. *Scandinavian journal of medicine & science in sports* **10**, 186-198 (2000).

16 Venn, M. F. Chemical composition of human femoral and head cartilage: influence of topographical position and fibrillation. *Annals of the rheumatic diseases* **38**, 57-62 (1979).

17 Lai, W. M., Hou, J. S. & Mow, V. C. A triphasic theory for the swelling and deformation behaviors of articular cartilage. *Journal of biomechanical engineering* **113**, 245-258 (1991).

18 Hollander, A. P. *et al.* Damage to type II collagen in aging and osteoarthritis starts at the articular surface, originates around chondrocytes, and extends into the cartilage with progressive degeneration. *The Journal of clinical investigation* **96**, 2859-2869, doi:10.1172/JCI118357 (1995).

19 Tanaka, E. & van Eijden, T. Biomechanical behavior of the temporomandibular joint disc. *Critical reviews in oral biology and medicine : an official publication of the American Association of Oral Biologists* **14**, 138-150 (2003).

20 Mow, V. C., Kuei, S. C., Lai, W. M. & Armstrong, C. G. Biphasic creep and stress relaxation of articular cartilage in compression? Theory and experiments. *Journal of biomechanical engineering* **102**, 73-84 (1980).

21 Bachrach, N. M. *et al.* Changes in proteoglycan synthesis of chondrocytes in articular cartilage are associated with the time-dependent changes in their mechanical environment. *Journal of biomechanics* **28**, 1561-1569 (1995).

22 Mak, A. F., Lai, W. M. & Mow, V. C. Biphasic indentation of articular cartilage--I. Theoretical analysis. *Journal of biomechanics* **20**, 703-714 (1987).

23 Lu, X. L. & Mow, V. C. Biomechanics of articular cartilage and determination of material properties. *Medicine and science in sports and exercise* **40**, 193-199, doi:10.1249/mss.0b013e31815cb1fc (2008).

24 Shirazi, R. & Shirazi-Adl, A. Analysis of partial meniscectomy and ACL reconstruction in knee joint biomechanics under a combined loading. *Clin Biomech (Bristol, Avon)* **24**, 755-761, doi:10.1016/j.clinbiomech.2009.07.005 (2009).

25 Yang, N., Nayeb-Hashemi, H. & Canavan, P. K. The combined effect of frontal plane tibiofemoral knee angle and meniscectomy on the cartilage contact stresses and strains. *Annals of biomedical engineering* **37**, 2360-2372, doi:10.1007/s10439-009-9781-3 (2009).

26 Pena, E., Calvo, B., Martinez, M. A., Palanca, D. & Doblare, M. Why lateral meniscectomy is more dangerous than medial meniscectomy. A finite element study. *Journal of orthopaedic research : official publication of the Orthopaedic Research Society* **24**, 1001-1010, doi:10.1002/jor.20037 (2006).

27 Lei, F. & Szeri, A. Z. Inverse analysis of constitutive models: biological soft tissues. *Journal of biomechanics* **40**, 936-940, doi:10.1016/j.jbiomech.2006.03.014 (2007).

28 Korhonen, R. K. *et al.* Comparison of the equilibrium response of articular cartilage in unconfined compression, confined compression and indentation. *Journal of biomechanics* **35**, 903-909 (2002).

29 Li, L. P., Soulhat, J., Buschmann, M. D. & Shirazi-Adl, A. Nonlinear analysis of cartilage in unconfined ramp compression using a fibril reinforced poroelastic model. *Clin Biomech (Bristol, Avon)* **14**, 673-682 (1999).

30 Buckwalter, J. A. & Mankin, H. J. Articular cartilage: degeneration and osteoarthritis, repair, regeneration, and transplantation. *Instructional course lectures* **47**, 487-504 (1998).

31 Buckwalter, J. A., Heckman, J. D. & Petrie, D. P. An AOA critical issue: aging of the North American population: new challenges for orthopaedics. *The Journal of bone and joint surgery. American volume* **85-A**, 748-758 (2003).

32 Arden, N. & Nevitt, M. C. Osteoarthritis: epidemiology. *Best practice & research. Clinical rheumatology* **20**, 3-25, doi:10.1016/j.berh.2005.09.007 (2006).

33 Kidron, A. & Thein, R. Radial tears associated with cleavage tears of the medial meniscus in athletes. *Arthroscopy : the journal of arthroscopic & related surgery : official publication of the Arthroscopy Association of North America and the International Arthroscopy Association* **18**, 254-256 (2002).

34 Brody, J. M., Lin, H. M., Hulstyn, M. J. & Tung, G. A. Lateral meniscus root tear and meniscus extrusion with anterior cruciate ligament tear. *Radiology* **239**, 805-810, doi:10.1148/radiol.2393050559 (2006).

35 Bylski-Austrow, D. I., Ciarelli, M. J., Kayner, D. C., Matthews, L. S. & Goldstein, S. A. Displacements of the menisci under joint load: an in vitro study in human knees. *Journal of biomechanics* **27**, 421-431 (1994).

36 Ghosh, P., Ingman, A. M. & Taylor, T. K. Variations in collagen, non-collagenous proteins, and hexosamine in menisci derived from osteoarthritic and rheumatoid arthritic knee joints. *The Journal of rheumatology* **2**, 100-107 (1975).

37 Aspden, R. M., Yarker, Y. E. & Hukins, D. W. Collagen orientations in the meniscus of the knee joint. *Journal of anatomy* **140 (Pt 3)**, 371-380 (1985).

38 Adams, M. E. & Ho, Y. A. Localization of glycosaminoglycans in human and canine menisci and their attachments. *Connective tissue research* **16**, 269-279 (1987).

39 Fithian, D. C., Kelly, M. A. & Mow, V. C. Material properties and structure-function relationships in the menisci. *Clinical orthopaedics and related research*, 19-31 (1990).

40 A.M., A. in *Knee meniscus: Basic and clinical foundations* (ed Arnoczky S.P. Mow V.C. , Jackson D.W.) 59-73 (Raven Press, 1992).

41 Vedi, V. *et al.* Meniscal movement. An in-vivo study using dynamic MRI. *The Journal of bone and joint surgery. British volume* **81**, 37-41 (1999).

42 Allen, C. R. *et al.* Importance of the medial meniscus in the anterior cruciate ligament-deficient knee. *Journal of orthopaedic research : official publication of the Orthopaedic Research Society* **18**, 109-115, doi:10.1002/jor.1100180116 (2000).

43 Daniel, D. M. *et al.* Fate of the ACL-injured patient. A prospective outcome study. *The American journal of sports medicine* **22**, 632-644 (1994).

44 Roos, H. *et al.* Knee osteoarthritis after meniscectomy: prevalence of radiographic changes after twenty-one years, compared with matched controls. *Arthritis and rheumatism* **41**, 687-693, doi:10.1002/1529-0131(199804)41:4<687::AID-ART16>3.0.CO;2-2 (1998).

45 Ahn, J. H., Wang, J. H., Yoo, J. C., Noh, H. K. & Park, J. H. A pull out suture for transection of the posterior horn of the medial meniscus: using a posterior trans-septal portal. *Knee surgery, sports traumatology, arthroscopy : official journal of the ESSKA* **15**, 1510-1513, doi:10.1007/s00167-007-0310-3 (2007).

46 Jones, A. O., Houang, M. T., Low, R. S. & Wood, D. G. Medial meniscus posterior root attachment injury and degeneration: MRI findings. *Australasian radiology* **50**, 306-313, doi:10.1111/j.1440-1673.2006.01586.x (2006).

47 Gale, D. R. *et al.* Meniscal subluxation: association with osteoarthritis and joint space narrowing. *Osteoarthritis and cartilage / OARS, Osteoarthritis Research Society* **7**, 526-532, doi:10.1053/joca.1999.0256 (1999).

48 Lerer, D. B., Umans, H. R., Hu, M. X. & Jones, M. H. The role of meniscal root pathology and radial meniscal tear in medial meniscal extrusion. *Skeletal radiology* **33**, 569-574, doi:10.1007/s00256-004-0761-2 (2004).

49 Guermazi, A. *et al.* Medial posterior meniscal root tears are associated with development or worsening of medial tibiofemoral cartilage damage: the multicenter osteoarthritis study. *Radiology* **268**, 814-821, doi:10.1148/radiol.13122544 (2013).

50 Baker, B. E., Peckham, A. C., Pupparo, F. & Sanborn, J. C. Review of meniscal injury and associated sports. *The American journal of sports medicine* **13**, 1-4 (1985).

51 Hede, A., Jensen, D. B., Blyme, P. & Sonne-Holm, S. Epidemiology of meniscal lesions in the knee. 1,215 open operations in Copenhagen 1982-84. *Acta orthopaedica Scandinavica* **61**, 435-437 (1990).

52 Garrett, W. E., Jr. *et al.* American Board of Orthopaedic Surgery Practice of the Orthopaedic Surgeon: Part-II, certification examination case mix. *The Journal of bone and joint surgery. American volume* **88**, 660-667, doi:10.2106/JBJS.E.01208 (2006).

53 Vyas, D. & Harner, C. D. Meniscus root repair. *Sports medicine and arthroscopy review* **20**, 86-94, doi:10.1097/JSA.0b013e31825186ca (2012).

54 Bolano, L. E. & Grana, W. A. Isolated arthroscopic partial meniscectomy. Functional radiographic evaluation at five years. *The American journal of sports medicine* **21**, 432-437 (1993).

55 Duthon, V. B. *et al.* Anatomy of the anterior cruciate ligament. *Knee surgery, sports traumatology, arthroscopy : official journal of the ESSKA* **14**, 204-213, doi:10.1007/s00167-005-0679-9 (2006).

56 Arnoczky, S. P. Anatomy of the anterior cruciate ligament. *Clinical orthopaedics and related research*, 19-25 (1983).

57 Sakane, M. *et al.* In situ forces in the anterior cruciate ligament and its bundles in response to anterior tibial loads. *Journal of orthopaedic research : official publication of the Orthopaedic Research Society* **15**, 285-293, doi:10.1002/jor.1100150219 (1997).

58 Matsumoto, H. *et al.* Roles of the anterior cruciate ligament and the medial collateral ligament in preventing valgus instability. *Journal of orthopaedic science : official journal of the Japanese Orthopaedic Association* **6**, 28-32 (2001).

59 Iriuchishima, T. *et al.* Impingement pressure in the anatomical and nonanatomical anterior cruciate ligament reconstruction: a cadaver study. *The American journal of sports medicine* **38**, 1611-1617, doi:10.1177/0363546510363461 (2010).

60 Baer, G. S. & Harner, C. D. Clinical outcomes of allograft versus autograft in anterior cruciate ligament reconstruction. *Clinics in sports medicine* **26**, 661-681, doi:10.1016/j.csm.2007.06.010 (2007).

61 Pinczewski, L. A. *et al.* A 10-year comparison of anterior cruciate ligament reconstructions with hamstring tendon and patellar tendon autograft: a controlled,

prospective trial. *The American journal of sports medicine* **35**, 564-574, doi:10.1177/0363546506296042 (2007).

62 van der Hart, C. P., van den Bekerom, M. P. & Patt, T. W. The occurrence of osteoarthritis at a minimum of ten years after reconstruction of the anterior cruciate ligament. *Journal of orthopaedic surgery and research* **3**, 24, doi:10.1186/1749-799X-3-24 (2008).

63 Cohen, M. *et al.* Anterior cruciate ligament reconstruction after 10 to 15 years: association between meniscectomy and osteoarthrosis. *Arthroscopy : the journal of arthroscopic & related surgery : official publication of the Arthroscopy Association of North America and the International Arthroscopy Association* **23**, 629-634, doi:10.1016/j.arthro.2007.03.094 (2007).

64 Mihelic, R., Jurdana, H., Jotanovic, Z., Madjarevic, T. & Tudor, A. Long-term results of anterior cruciate ligament reconstruction: a comparison with non-operative treatment with a follow-up of 17-20 years. *International orthopaedics* **35**, 1093-1097, doi:10.1007/s00264-011-1206-x (2011).

65 Chmielewski, T. L., Rudolph, K. S., Fitzgerald, G. K., Axe, M. J. & Snyder-Mackler, L. Biomechanical evidence supporting a differential response to acute ACL injury. *Clin Biomech (Bristol, Avon)* **16**, 586-591 (2001).

66 Tashman, S., Kolowich, P., Collon, D., Anderson, K. & Anderst, W. Dynamic function of the ACL-reconstructed knee during running. *Clinical orthopaedics and related research* **454**, 66-73, doi:10.1097/BLO.0b013e31802bab3e (2007).

67 Chaudhari, A. M., Briant, P. L., Bevill, S. L., Koo, S. & Andriacchi, T. P. Knee kinematics, cartilage morphology, and osteoarthritis after ACL injury. *Medicine and science in sports and exercise* **40**, 215-222, doi:10.1249/mss.0b013e31815cbb0e (2008).

68 Levy, A. S. & Meier, S. W. Approach to cartilage injury in the anterior cruciate ligament-deficient knee. *The Orthopedic clinics of North America* **34**, 149-167 (2003).

69 Noyes, F. R. & Barber-Westin, S. D. Treatment of meniscus tears during anterior cruciate ligament reconstruction. *Arthroscopy : the journal of arthroscopic & related surgery : official publication of the Arthroscopy Association of North America and the International Arthroscopy Association* **28**, 123-130, doi:10.1016/j.arthro.2011.08.292 (2012).

70 Musahl, V. *et al.* Practice patterns for combined anterior cruciate ligament and meniscal surgery in the United States. *The American journal of sports medicine* **38**, 918-923, doi:10.1177/0363546509357900 (2010).

71 Ait Si Selmi, T., Fithian, D. & Neyret, P. The evolution of osteoarthritis in 103 patients with ACL reconstruction at 17 years follow-up. *The Knee* **13**, 353-358, doi:10.1016/j.knee.2006.02.014 (2006).

72 Thein, R. & Eichenblat, M. Concealed knee cartilage lesions: is arthroscopic probing therapeutic? *The American journal of sports medicine* **27**, 495-499 (1999).

73 Brittberg, M. P., L. Introduction to an articular cartilage classification. *ICRS Newsletter* **1**, 8 (1998).

74 Shelbourne, K. D., Barnes, A. F., Urch, S. E. & Gray, T. Evaluation of Joint Space Width and Narrowing After Isolated Partial Medial Meniscectomy for Degenerative Medial Meniscus Tears. *Orthopaedic Journal of Sports Medicine* **1**, doi:10.1177/2325967113507539 (2013).

75 Steadman, J. R., Rodkey, W. G. & Rodrigo, J. J. Microfracture: surgical technique and rehabilitation to treat chondral defects. *Clinical orthopaedics and related research*, S362-369 (2001).

76 Jakob, R. P., Franz, T., Gautier, E. & Mainil-Varlet, P. Autologous osteochondral grafting in the knee: indication, results, and reflections. *Clinical orthopaedics and related research*, 170-184 (2002).

77 Kleemann, R. U., Krocker, D., Cedraro, A., Tuischer, J. & Duda, G. N. Altered cartilage mechanics and histology in knee osteoarthritis: relation to clinical assessment (ICRS Grade). *Osteoarthritis and cartilage / OARS, Osteoarthritis Research Society* **13**, 958-963, doi:10.1016/j.joca.2005.06.008 (2005).

78 Fairbank, T. J. Knee joint changes after meniscectomy. *The Journal of bone and joint surgery. British volume* **30B**, 664-670 (1948).

79 Sherman, M. F., Warren, R. F., Marshall, J. L. & Savatsky, G. J. A clinical and radiographical analysis of 127 anterior cruciate insufficient knees. *Clinical orthopaedics and related research* **227**, 229-237 (1988).

80 Jorgensen, U., Sonne-Holm, S., Lauridsen, F. & Rosenklint, A. Long-term follow-up of meniscectomy in athletes. A prospective longitudinal study. *The Journal of bone and joint surgery. British volume* **69**, 80-83 (1987).

81 Ryu, J. H. *et al.* Measurement of MMP Activity in Synovial Fluid in Cases of Osteoarthritis and Acute Inflammatory Conditions of the Knee Joints Using a Fluorogenic Peptide Probe-Immobilized Diagnostic Kit. *Theranostics* **2**, 198-206, doi:10.7150/thno.3477 (2012).

82 Higuchi, H., Kimura, M., Shirakura, K., Terauchi, M. & Takagishi, K. Factors affecting long-term results after arthroscopic partial meniscectomy. *Clinical orthopaedics and related research*, 161-168 (2000).

83 Loken, S., Heir, S., Holme, I., Engebretsen, L. & Aroen, A. 6-year follow-up of 84 patients with cartilage defects in the knee. Knee scores improved but recovery was incomplete. *Acta orthopaedica* **81**, 611-618, doi:10.3109/17453674.2010.519166 (2010).

84 Chatain, F., Adeleine, P., Chambat, P. & Neyret, P. A comparative study of medial versus lateral arthroscopic partial meniscectomy on stable knees: 10-year minimum follow-up. *Arthroscopy : the journal of arthroscopic & related surgery : official publication of the Arthroscopy Association of North America and the International Arthroscopy Association* **19**, 842-849 (2003).

85 McCauley, T. R., Recht, M. P. & Disler, D. G. Clinical imaging of articular cartilage in the knee. *Seminars in musculoskeletal radiology* **5**, 293-304, doi:10.1055/s-2001-19040 (2001).

86 Cicuttini, F., Forbes, A., Asbeutah, A., Morris, K. & Stuckey, S. Comparison and reproducibility of fast and conventional spoiled gradient-echo magnetic resonance sequences in the determination of knee cartilage volume. *Journal of orthopaedic research : official publication of the Orthopaedic Research Society* **18**, 580-584, doi:10.1002/jor.1100180410 (2000).

87 Glaser, C. *et al.* Optimization and validation of a rapid high-resolution T1-w 3D FLASH water excitation MRI sequence for the quantitative assessment of articular cartilage volume and thickness. *Magnetic resonance imaging* **19**, 177-185 (2001).

88 Eckstein, F., Hudelmaier, M. & Putz, R. The effects of exercise on human articular cartilage. *Journal of anatomy* **208**, 491-512, doi:10.1111/j.1469-7580.2006.00546.x (2006).

89 Lusse, S. *et al.* Evaluation of water content by spatially resolved transverse relaxation times of human articular cartilage. *Magnetic resonance imaging* **18**, 423-430 (2000).

90 Lusse, S., Knauss, R., Werner, A., Grunder, W. & Arnold, K. Action of compression and cations on the proton and deuterium relaxation in cartilage. *Magnetic resonance in medicine : official journal of the Society of Magnetic Resonance in Medicine / Society of Magnetic Resonance in Medicine* **33**, 483-489 (1995).

91 Mosher, T. J., Dardzinski, B. J. & Smith, M. B. Human articular cartilage: influence of aging and early symptomatic degeneration on the spatial variation of T2--preliminary findings at 3 T. *Radiology* **214**, 259-266, doi:10.1148/radiology.214.1.r00ja15259 (2000).

92 Stahl, R. *et al.* MRI-derived T2 relaxation times and cartilage morphometry of the tibio-femoral joint in subjects with and without osteoarthritis during a 1-year follow-up. *Osteoarthritis and cartilage / OARS, Osteoarthritis Research Society* **15**, 1225-1234, doi:10.1016/j.joca.2007.04.018 (2007).

93 Mosher, T. J., Liu, Y. & Torok, C. M. Functional cartilage MRI T2 mapping: evaluating the effect of age and training on knee cartilage response to running. *Osteoarthritis and cartilage / OARS, Osteoarthritis Research Society* **18**, 358-364, doi:10.1016/j.joca.2009.11.011 (2010).

94 Liess, C., Lusse, S., Karger, N., Heller, M. & Gluer, C. C. Detection of changes in cartilage water content using MRI T2-mapping in vivo. *Osteoarthritis and cartilage / OARS, Osteoarthritis Research Society* **10**, 907-913 (2002).

95 Nishioka, H. *et al.* Detecting ICRS grade 1 cartilage lesions in anterior cruciate ligament injury using T1rho and T2 mapping. *European journal of radiology* **82**, 1499-1505, doi:10.1016/j.ejrad.2013.04.038 (2013).

96 Peterfy, C. G. *et al.* MRI protocols for whole-organ assessment of the knee in osteoarthritis. *Osteoarthritis and cartilage / OARS, Osteoarthritis Research Society* **14 Suppl A**, A95-111, doi:10.1016/j.joca.2006.02.029 (2006).

97 Wluka, A. E., Ding, C., Jones, G. & Cicuttini, F. M. The clinical correlates of articular cartilage defects in symptomatic knee osteoarthritis: a prospective study. *Rheumatology (Oxford)* **44**, 1311-1316, doi:10.1093/rheumatology/kei018 (2005).

98 Sharma, L. *et al.* Varus and valgus alignment and incident and progressive knee osteoarthritis. *Annals of the rheumatic diseases* **69**, 1940-1945, doi:10.1136/ard.2010.129742 (2010).

99 Astephen, J. L., Deluzio, K. J., Caldwell, G. E. & Dunbar, M. J. Biomechanical changes at the hip, knee, and ankle joints during gait are associated with knee osteoarthritis severity. *Journal of orthopaedic research : official publication of the Orthopaedic Research Society* **26**, 332-341, doi:10.1002/jor.20496 (2008).

100 Heiden, T. L., Lloyd, D. G. & Ackland, T. R. Knee joint kinematics, kinetics and muscle co-contraction in knee osteoarthritis patient gait. *Clin Biomech (Bristol, Avon)* **24**, 833-841, doi:10.1016/j.clinbiomech.2009.08.005 (2009).

101 McKean, K. A. *et al.* Gender differences exist in osteoarthritic gait. *Clin Biomech (Bristol, Avon)* **22**, 400-409, doi:10.1016/j.clinbiomech.2006.11.006 (2007).

102 Davies-Tuck, M. L. *et al.* Association between meniscal tears and the peak external knee adduction moment and foot rotation during level walking in postmenopausal women without knee osteoarthritis: a cross-sectional study. *Arthritis research & therapy* **10**, R58, doi:10.1186/ar2428 (2008).

103 Drynda, S. *et al.* Proteome analysis reveals disease-associated marker proteins to differentiate RA patients from other inflammatory joint diseases with the potential to monitor anti-TNFalpha therapy. *Pathology, research and practice* **200**, 165-171 (2004).

104 Rousseau, J. C. *et al.* Serum levels of type IIA procollagen amino terminal propeptide (PIIANP) are decreased in patients with knee osteoarthritis and rheumatoid arthritis. *Osteoarthritis and cartilage / OARS, Osteoarthritis Research Society* **12**, 440-447, doi:10.1016/j.joca.2004.02.004 (2004).

105 Charni, N., Juillet, F. & Garnero, P. Urinary type II collagen helical peptide (HELIX-II) as a new biochemical marker of cartilage degradation in patients with osteoarthritis and

rheumatoid arthritis. *Arthritis and rheumatism* **52**, 1081-1090, doi:10.1002/art.20930 (2005).

106 Kraus, V. B. Biomarkers in osteoarthritis. *Current opinion in rheumatology* **17**, 641-646 (2005).

107 Lawrence, R. C. *et al.* Estimates of the prevalence of arthritis and other rheumatic conditions in the United States. Part II. *Arthritis and rheumatism* **58**, 26-35, doi:10.1002/art.23176 (2008).

108 Buckwalter, J. A. Articular cartilage injuries. *Clinical orthopaedics and related research*, 21-37 (2002).

109 Drexler, W. *et al.* Correlation of collagen organization with polarization sensitive imaging of in vitro cartilage: implications for osteoarthritis. *The Journal of rheumatology* **28**, 1311-1318 (2001).

110 Li, G. *et al.* The cartilage thickness distribution in the tibiofemoral joint and its correlation with cartilage-to-cartilage contact. *Clin Biomech (Bristol, Avon)* **20**, 736-744, doi:10.1016/j.clinbiomech.2005.04.001 (2005).

111 Koo, S., Rylander, J. H. & Andriacchi, T. P. Knee joint kinematics during walking influences the spatial cartilage thickness distribution in the knee. *Journal of biomechanics* **44**, 1405-1409, doi:10.1016/j.jbiomech.2010.11.020 (2011).

112 Halonen, K. S. *et al.* Deformation of articular cartilage during static loading of a knee joint - Experimental and finite element analysis. *Journal of biomechanics*, doi:10.1016/j.jbiomech.2014.04.013 (2014).

113 Hosseini, A. *et al.* In-vivo time-dependent articular cartilage contact behavior of the tibiofemoral joint. *Osteoarthritis and cartilage / OARS, Osteoarthritis Research Society* **18**, 909-916, doi:10.1016/j.joca.2010.04.011 (2010).

114 Liu, F. *et al.* In vivo tibiofemoral cartilage deformation during the stance phase of gait. *Journal of biomechanics* **43**, 658-665, doi:10.1016/j.jbiomech.2009.10.028 (2010).

115 Bingham, J. T. *et al.* In vivo cartilage contact deformation in the healthy human tibiofemoral joint. *Rheumatology (Oxford)* **47**, 1622-1627, doi:10.1093/rheumatology/ken345 (2008).

116 Eckstein, F. *et al.* In vivo cartilage deformation after different types of activity and its dependence on physical training status. *Annals of the rheumatic diseases* **64**, 291-295, doi:10.1136/ard.2004.022400 (2005).

117 Cotofana, S. *et al.* In vivo measures of cartilage deformation: patterns in healthy and osteoarthritic female knees using 3T MR imaging. *European radiology* **21**, 1127-1135, doi:10.1007/s00330-011-2057-y (2011).

118 Altman, R. D. *et al.* Radiographic assessment of progression in osteoarthritis. *Arthritis and rheumatism* **30**, 1214-1225 (1987).

119 Eckstein, F., Burstein, D. & Link, T. M. Quantitative MRI of cartilage and bone: degenerative changes in osteoarthritis. *NMR in biomedicine* **19**, 822-854, doi:10.1002/nbm.1063 (2006).

120 Baliunas, A. J. *et al.* Increased knee joint loads during walking are present in subjects with knee osteoarthritis. *Osteoarthritis and cartilage / OARS, Osteoarthritis Research Society* **10**, 573-579 (2002).

121 Wright, R. W. *et al.* Radiographs are not useful in detecting arthroscopically confirmed mild chondral damage. *Clinical orthopaedics and related research* **442**, 245-251 (2006).

122 Tourville, T. W., Johnson, R. J., Slauterbeck, J. R., Naud, S. & Beynnon, B. D. Assessment of early tibiofemoral joint space width changes after anterior cruciate ligament injury and reconstruction: a matched case-control study. *The American journal of sports medicine* **41**, 769-778, doi:10.1177/0363546513477838 (2013).

123 Boocock, M., McNair, P., Cicuttini, F., Stuart, A. & Sinclair, T. The short-term effects of running on the deformation of knee articular cartilage and its relationship to biomechanical loads at the knee. *Osteoarthritis and cartilage / OARS, Osteoarthritis Research Society* **17**, 883-890, doi:10.1016/j.joca.2008.12.010 (2009).

124 Souza, R. B. *et al.* The effects of acute loading on T1rho and T2 relaxation times of tibiofemoral articular cartilage. *Osteoarthritis and cartilage / OARS, Osteoarthritis Research Society* **18**, 1557-1563, doi:10.1016/j.joca.2010.10.001 (2010).

125 Coleman, J. L. *et al.* Diurnal variations in articular cartilage thickness and strain in the human knee. *Journal of biomechanics* **46**, 541-547, doi:10.1016/j.jbiomech.2012.09.013 (2013).

126 Measurements, U. N. C. o. R. P. a. in *NCRP Report No. 93* 53-55 (NCRP, 1987).

127 Tashman, S. & Anderst, W. In-vivo measurement of dynamic joint motion using high speed biplane radiography and CT: application to canine ACL deficiency. *Journal of biomechanical engineering* **125**, 238-245 (2003).

128 Anderst, W. J. & Tashman, S. A method to estimate in vivo dynamic articular surface interaction. *Journal of biomechanics* **36**, 1291-1299 (2003).

129 Bey, M. J., Zauel, R., Brock, S. K. & Tashman, S. Validation of a new model-based tracking technique for measuring three-dimensional, in vivo glenohumeral joint kinematics. *Journal of biomechanical engineering* **128**, 604-609, doi:10.1115/1.2206199 (2006).

130 Bey, M. J., Kline, S. K., Tashman, S. & Zauel, R. Accuracy of biplane x-ray imaging combined with model-based tracking for measuring in-vivo patellofemoral joint motion. *Journal of orthopaedic surgery and research* **3**, 38, doi:10.1186/1749-799X-3-38 (2008).

131 Anderst, W., Zauel, R., Bishop, J., Demps, E. & Tashman, S. Validation of three-dimensional model-based tibio-femoral tracking during running. *Medical engineering & physics* **31**, 10-16, doi:10.1016/j.medengphy.2008.03.003 (2009).

132 Ronken, S. *et al.* A comparison of healthy human and swine articular cartilage dynamic indentation mechanics. *Biomechanics and modeling in mechanobiology* **11**, 631-639, doi:10.1007/s10237-011-0338-7 (2012).

133 Spahn, G., Klinger, H. M. & Hofmann, G. O. How valid is the arthroscopic diagnosis of cartilage lesions? Results of an opinion survey among highly experienced arthroscopic surgeons. *Archives of orthopaedic and trauma surgery* **129**, 1117-1121, doi:10.1007/s00402-009-0868-y (2009).

134 Spahn, G., Klinger, H. M., Baums, M., Pinkepank, U. & Hofmann, G. O. Reliability in arthroscopic grading of cartilage lesions: results of a prospective blinded study for evaluation of inter-observer reliability. *Archives of orthopaedic and trauma surgery* **131**, 377-381, doi:10.1007/s00402-011-1259-8 (2011).

135 Kim, J. G. *et al.* Tibiofemoral contact mechanics following posterior root of medial meniscus tear, repair, meniscectomy, and allograft transplantation. *Knee surgery, sports traumatology, arthroscopy : official journal of the ESSKA*, doi:10.1007/s00167-012-2182-4 (2012).

136 Marzo, J. M. & Gurske-DePerio, J. Effects of medial meniscus posterior horn avulsion and repair on tibiofemoral contact area and peak contact pressure with clinical implications. *The American journal of sports medicine* **37**, 124-129, doi:10.1177/0363546508323254 (2009).

137 Allaire, R., Muriuki, M., Gilbertson, L. & Harner, C. D. Biomechanical consequences of a tear of the posterior root of the medial meniscus. Similar to total meniscectomy. *The Journal of bone and joint surgery. American volume* **90**, 1922-1931, doi:10.2106/JBJS.G.00748 (2008).

138 Tashman, S., Collon, D., Anderson, K., Kolowich, P. & Anderst, W. Abnormal rotational knee motion during running after anterior cruciate ligament reconstruction. *The American journal of sports medicine* **32**, 975-983 (2004).

139 Holm, S. A simple sequentially rejective multiple test procedure. *Scand J Statist* **6**, 65-70 (1979).

140 Buckwalter, J. A., Mankin, H. J. & Grodzinsky, A. J. Articular cartilage and osteoarthritis. *Instructional course lectures* **54**, 465-480 (2005).

141 Ateshian, G. A., Warden, W. H., Kim, J. J., Grelsamer, R. P. & Mow, V. C. Finite deformation biphasic material properties of bovine articular cartilage from confined compression experiments. *Journal of biomechanics* **30**, 1157-1164 (1997).

142 Korhonen, R. K. *et al.* Fibril reinforced poroelastic model predicts specifically mechanical behavior of normal, proteoglycan depleted and collagen degraded articular cartilage. *Journal of biomechanics* **36**, 1373-1379 (2003).

143 Deneweth, J. M., McLean, S. G. & Arruda, E. M. Evaluation of hyperelastic models for the non-linear and non-uniform high strain-rate mechanics of tibial cartilage. *Journal of biomechanics* **46**, 1604-1610, doi:10.1016/j.jbiomech.2013.04.014 (2013).

144 Keenan, K. E., Pal, S., Lindsey, D. P., Besier, T. F. & Beaupre, G. S. A viscoelastic constitutive model can accurately represent entire creep indentation tests of human patella cartilage. *Journal of applied biomechanics* **29**, 292-302 (2013).

145 Bader, D. L. & Kempson, G. E. The short-term compressive properties of adult human articular cartilage. *Bio-medical materials and engineering* **4**, 245-256 (1994).

146 Leipzig, N. D. & Athanasiou, K. A. Unconfined creep compression of chondrocytes. *Journal of biomechanics* **38**, 77-85, doi:10.1016/j.jbiomech.2004.03.013 (2005).

147 Verbrugge, L. M., Lepkowski, J. M. & Konkol, L. L. Levels of disability among U.S. adults with arthritis. *Journal of gerontology* **46**, S71-83 (1991).

148 Fried, L. P. & Guralnik, J. M. Disability in older adults: evidence regarding significance, etiology, and risk. *Journal of the American Geriatrics Society* **45**, 92-100 (1997).

149 Gelber, A. C. *et al.* Joint injury in young adults and risk for subsequent knee and hip osteoarthritis. *Annals of internal medicine* **133**, 321-328 (2000).

150 Lohmander, L. S., Ostenberg, A., Englund, M. & Roos, H. High prevalence of knee osteoarthritis, pain, and functional limitations in female soccer players twelve years after anterior cruciate ligament injury. *Arthritis and rheumatism* **50**, 3145-3152, doi:10.1002/art.20589 (2004).

151 Menezes, N. M., Gray, M. L., Hartke, J. R. & Burstein, D. T2 and T1rho MRI in articular cartilage systems. *Magnetic resonance in medicine : official journal of the Society of Magnetic Resonance in Medicine / Society of Magnetic Resonance in Medicine* **51**, 503-509, doi:10.1002/mrm.10710 (2004).

152 Regatte, R. R., Akella, S. V., Lonner, J. H., Kneeland, J. B. & Reddy, R. T1rho relaxation mapping in human osteoarthritis (OA) cartilage: comparison of T1rho with T2. *Journal of magnetic resonance imaging : JMRI* **23**, 547-553, doi:10.1002/jmri.20536 (2006).

153 Dragomir, A. D. *et al.* Serum cartilage oligomeric matrix protein and clinical signs and symptoms of potential pre-radiographic hip and knee pathology. *Osteoarthritis and cartilage / OARS, Osteoarthritis Research Society* **10**, 687-691 (2002).

154 Rousseau, J. C. & Delmas, P. D. Biological markers in osteoarthritis. *Nature clinical practice. Rheumatology* **3**, 346-356, doi:10.1038/ncprheum0508 (2007).

155 Kuroki, H. *et al.* Ultrasound has the potential to detect degeneration of articular cartilage clinically, even if the information is obtained from an indirect measurement of intrinsic physical characteristics. *Arthritis research & therapy* **11**, 408, doi:10.1186/ar2727 (2009).

156 Hallgren, K. A. Computing Inter-Rater Reliability for Observational Data: An Overview and Tutorial. *Tutorials in quantitative methods for psychology* **8**, 23-34 (2012).

157 Dupuis, D. E. *et al.* Precision and accuracy of joint space width measurements of the medial compartment of the knee using standardized MTP semi-flexed radiographs. *Osteoarthritis and cartilage / OARS, Osteoarthritis Research Society* **11**, 716-724 (2003).

158 Childs, J. D., Sparto, P. J., Fitzgerald, G. K., Bizzini, M. & Irrgang, J. J. Alterations in lower extremity movement and muscle activation patterns in individuals with knee osteoarthritis. *Clin Biomech (Bristol, Avon)* **19**, 44-49 (2004).

159 Lewek, M. D., Rudolph, K. S. & Snyder-Mackler, L. Quadriceps femoris muscle weakness and activation failure in patients with symptomatic knee osteoarthritis. *Journal of orthopaedic research : official publication of the Orthopaedic Research Society* **22**, 110-115, doi:10.1016/S0736-0266(03)00154-2 (2004).

160 Shelbourne, K. D. & Gray, T. Anterior cruciate ligament reconstruction with autogenous patellar tendon graft followed by accelerated rehabilitation. A two- to nine-year followup. *The American journal of sports medicine* **25**, 786-795 (1997).

161 Kessler, M. A. *et al.* Function, osteoarthritis and activity after ACL-rupture: 11 years follow-up results of conservative versus reconstructive treatment. *Knee surgery, sports traumatology, arthroscopy : official journal of the ESSKA* **16**, 442-448, doi:10.1007/s00167-008-0498-x (2008).

162 Hall, M., Stevermer, C. A. & Gillette, J. C. Gait analysis post anterior cruciate ligament reconstruction: knee osteoarthritis perspective. *Gait & posture* **36**, 56-60, doi:10.1016/j.gaitpost.2012.01.003 (2012).

163 Drechsler, W. I., Cramp, M. C. & Scott, O. M. Changes in muscle strength and EMG median frequency after anterior cruciate ligament reconstruction. *European journal of applied physiology* **98**, 613-623, doi:10.1007/s00421-006-0311-9 (2006).

164 Makihara, Y., Nishino, A., Fukubayashi, T. & Kanamori, A. Decrease of knee flexion torque in patients with ACL reconstruction: combined analysis of the architecture and function of the knee flexor muscles. *Knee surgery, sports traumatology, arthroscopy : official journal of the ESSKA* **14**, 310-317, doi:10.1007/s00167-005-0701-2 (2006).

165 Nakamura, N. *et al.* Evaluation of active knee flexion and hamstring strength after anterior cruciate ligament reconstruction using hamstring tendons. *Arthroscopy : the*

journal of arthroscopic & related surgery : official publication of the Arthroscopy Association of North America and the International Arthroscopy Association **18**, 598-602 (2002).

166 Harter, R. A., Osternig, L. R. & Standifer, L. W. Isokinetic evaluation of quadriceps and hamstrings symmetry following anterior cruciate ligament reconstruction. *Archives of physical medicine and rehabilitation* **71**, 465-468 (1990).

167 Yasuda, K., Ohkoshi, Y., Tanabe, Y. & Kaneda, K. Quantitative evaluation of knee instability and muscle strength after anterior cruciate ligament reconstruction using patellar and quadriceps tendon. *The American journal of sports medicine* **20**, 471-475 (1992).

168 Hiemstra, L. A., Webber, S., MacDonald, P. B. & Kriellaars, D. J. Knee strength deficits after hamstring tendon and patellar tendon anterior cruciate ligament reconstruction. *Medicine and science in sports and exercise* **32**, 1472-1479 (2000).

169 Hiemstra, L. A., Webber, S., MacDonald, P. B. & Kriellaars, D. J. Contralateral limb strength deficits after anterior cruciate ligament reconstruction using a hamstring tendon graft. *Clin Biomech (Bristol, Avon)* **22**, 543-550, doi:10.1016/j.clinbiomech.2007.01.009 (2007).

170 Kalund, S., Sinkjaer, T., Arendt-Nielsen, L. & Simonsen, O. Altered timing of hamstring muscle action in anterior cruciate ligament deficient patients. *The American journal of sports medicine* **18**, 245-248 (1990).

171 Fu, F. H. & Cohen, S. B. 72-73 (SLACK, 2008).

172 Tsai, L. C., McLean, S., Colletti, P. M. & Powers, C. M. Greater muscle co-contraction results in increased tibiofemoral compressive forces in females who have undergone anterior cruciate ligament reconstruction. *Journal of orthopaedic research : official publication of the Orthopaedic Research Society* **30**, 2007-2014, doi:10.1002/jor.22176 (2012).

173 Ferber, R., Osternig, L. R., Woollacott, M. H., Wasielewski, N. J. & Lee, J. H. Gait mechanics in chronic ACL deficiency and subsequent repair. *Clin Biomech (Bristol, Avon)* **17**, 274-285 (2002).

174 Ortiz, A. *et al.* Landing mechanics between noninjured women and women with anterior cruciate ligament reconstruction during 2 jump tasks. *The American journal of sports medicine* **36**, 149-157, doi:10.1177/0363546507307758 (2008).

175 Vairo, G. L. *et al.* Neuromuscular and biomechanical landing performance subsequent to ipsilateral semitendinosus and gracilis autograft anterior cruciate ligament reconstruction. *Knee surgery, sports traumatology, arthroscopy : official journal of the ESSKA* **16**, 2-14, doi:10.1007/s00167-007-0427-4 (2008).

176 Sommerlath, K., Lysholm, J. & Gillquist, J. The long-term course after treatment of acute anterior cruciate ligament ruptures. A 9 to 16 year followup. *The American journal of sports medicine* **19**, 156-162 (1991).

177 Gillquist, J. & Messner, K. Anterior cruciate ligament reconstruction and the long-term incidence of gonarthrosis. *Sports Med* **27**, 143-156 (1999).

178 Hakkinen, K., Alen, M. & Komi, P. V. Changes in isometric force- and relaxation-time, electromyographic and muscle fibre characteristics of human skeletal muscle during strength training and detraining. *Acta physiologica Scandinavica* **125**, 573-585 (1985).

179 Houston, M. E., Froese, E. A., Valeriote, S. P., Green, H. J. & Ranney, D. A. Muscle performance, morphology and metabolic capacity during strength training and detraining: a one leg model. *European journal of applied physiology and occupational physiology* **51**, 25-35 (1983).

180 You, B. M., Siy, P., Anderst, W. & Tashman, S. In vivo measurement of 3-D skeletal kinematics from sequences of biplane radiographs: application to knee kinematics. *IEEE transactions on medical imaging* **20**, 514-525, doi:10.1109/42.929617 (2001).